

# Durham E-Theses

---

## *Resonant cavity method for broadband dielectric measurements*

Makki El-Tayyid Muhammad-Ahmad

### How to cite:

---

Muhammad-Ahmad, Makki El-Tayyid (1987) Resonant cavity method for broadband dielectric measurements. Doctoral thesis, Durham University.

### Use policy

---

The full-text may be used and/or reproduced, and given to third parties in any format or medium, without prior permission or charge, for personal research or study, educational, or not-for-profit purposes provided that:

- a full bibliographic reference is made to the original source
- a <https://etheses.durham.ac.uk/id/eprint/6671/> is made to the metadata record in Durham E-Theses
- the full-text is not changed in any way

The full-text must not be sold in any format or medium without the formal permission of the copyright holders.

Please consult the [full Durham E-Theses policy](#) for further details.

RESONANT CAVITY METHOD  
FOR  
BROADBAND DIELECTRIC MEASUREMENTS

The copyright of this thesis rests with the author.  
No quotation from it should be published without  
his prior written consent and information derived by  
from it should be acknowledged.

**Makki El-Tayyib Muhammad-Ahmad**  
University College

A thesis submitted to the Faculty of Science,  
University of Durham, for the degree of  
Doctor of Philosophy

Department of Applied Physics and Electronics,  
School of Engineering and Applied Science,  
University of Durham, UK.

April 1987



ABSTRACT

The project investigates the Cavity Perturbation Method (CPM) and design of a coaxial resonator covering a wide frequency band from 2.5 to 11.5 GHz. Using the published analyses for coaxial cavities, original theoretical analysis of Cavity Perturbation Method for TEM coaxial cavity was carried out by the author. Using similar approach, the  $H_{011}$  cylindrical cavity was analyzed. The deliberate objective of the method was to produce a wide band technique since there are none available at present. The method then examines the possibility of employing the coaxial cavity as an important and necessary measuring device for dielectric measurements using CPM. It was the aim in the investigations to state clearly what assumptions were made so that the accuracy of the calculated results could be assessed.

A new measurement technique, using a Sweep Generator/Spectrum Analyzer Assembly (SG/SA) was introduced. The technique is based on very precise measurements of the changes in cavity Q and its resonant frequency, displayed on Spectrum Analyzer, when the test sample of the material is inserted. Because the main objective of the project is the method of measurements, the assessment of its validity and accuracy was fully discussed.

### III

Measurements were carried out on fifteen materials of various types of ceramics over the frequency range of interest. These materials were used mainly for the assessment of the validity and accuracy of the new Sweep Generator/Spectrum Analyzer Assembly technique, and also a test of the capability of the constructed broadband coaxial cavity to be used for dielectric measurements. The well-known Bridge and Q-meter methods, were employed initially to provide the low frequency values for the materials as reference. An attempt has also been made to justify the validity of the universal law on those materials.

Additional work not directly related to the main project has been carried out on Curie temperature measurements. The object was to develop a simple and reliable method using the Gouy balance technique.

ACKNOWLEDGEMENTS

With genuine humility, thanks and praise be to God for everything; for keeping me patient, fit and hard working during these most difficult, good, sad and humble years of my life. If this effort is successful it is by His grace and guidance. If, however, it falls short of the readers' expectations, I can only pray and hope that He will forgive any imperfections.

I must not fail to acknowledge the invaluable contribution of the Sudanese People. Without their generosity and financial support this work would not have taken place. They had to starve, suffer and sacrifice to send me abroad hoping that in the future I would be able to help in the development of our country.

I owe special thanks and outstanding appreciation to my supervisors, whose ideas formed the basis of this work; Dr. B.L.J.Kulesza and Dr. J.S.Thorp. Their supervision and discussions are gratefully acknowledged.

Although I am indebted to many others, I must avoid mentioning them all in this acknowledgement. Perhaps I should highlight the technical assistance and help as the most immediate pillars. Technical co-operation most directly supportive of this work came from Mr. W.Mounsey, Mr. P.J.E.Richardson (now employed in Aero-engine Division, Rolls Royce, Derby) and Mr. C.Savage, and for their help and contribution I am grateful.

My thanks and appreciation are also due to Mr. G.Swallow (Hirst Research Centre), Miss K.Cummins, Mrs. J.Smart, Mr. E.Evangelinos (Alvey Research) and to my colleagues and friends, for their co-operation.

Finally, the heart-warming welcome and hospitality I received from Dr. E.C.Salthouse and his wife cannot be adequately described, only deeply felt.

Makki El-Tayyib Muhammad-Ahmad

Durham

April 1987

Sha'ban 1407

CONTENTS**CHAPTER 1: INTRODUCTION**

<b>1.1 General Review</b>	<b>1</b>
1.1.1 Introduction	1
1.1.2 Measurement Methods Employing a Resonant Cavity	2
1.1.3 Cylindrical Cavity Measurements	3
1.1.4 Coaxial Line Techniques	5
1.1.5 Waveguide Measurements	7
1.1.6 Measurements of Biological Substances	8
<b>1.2 The Project</b>	<b>10</b>

**CHAPTER 2: RF & MICROWAVE RESONANT CAVITIES AND APPLICATIONS**

<b>2.1 Introduction</b>	<b>13</b>
<b>2.2 Fundamental Principles</b>	<b>14</b>
<b>2.3 Types &amp; Modes of Oscillations</b>	<b>15</b>
<b>2.4 Coupling in Resonant Cavities</b>	<b>17</b>
2.4.1 Coupling Loops	17
2.4.2 Coupling Probes	18
2.4.3 Coupling Apertures	18
<b>2.5 Resonant Frequency and Quality Factor of a Cavity</b>	<b>19</b>
2.5.1 Introduction	19
2.5.2 TE Rectangular Cavity	22
2.5.3 TE Cylindrical Cavity	23
2.5.4 TEM Coaxial Cavity	24
<b>2.6 Effect of Temperature on Resonant Cavities</b>	<b>25</b>
<b>2.7 Applications.</b>	<b>26</b>

CHAPTER 3: RESONANCE PERTURBATION THEORY AND FORMULAE

3.1 Introduction	28
3.2 Perturbation Formula for a Resonant Cavity	29
3.2.1 General Relations in a Perturbed Field	29
3.2.2 Derivation of the Perturbation Formula	32
3.3 Relationship between the Resonant Frequency and the Q-factor	37
3.4 Dielectric Properties of a Perturbing Sample	41
3.5 Applications of Resonance Perturbation Theory	44
3.5.1 Introduction	44
3.5.2 $H_{101}$ Rectangular Cavity	44
3.5.3 $H_{011}$ Cylindrical Cavity	48
3.5.4 TEM Coaxial Cavity	53

CHAPTER 4: RESONANT COAXIAL CAVITY

4.1 Characteristics of a Transmission Line	57
4.1.1 Introduction	57
4.1.2 Primary Constants of a Transmission Line	57
4.1.3 Secondary Parameters of a Transmission Line	61
4.1.4 Transmission Line as a Resonant Circuit	63
4.2 Design of an Experimental Coaxial Cavity	64
4.3 Quality Factor of a Coaxial Cavity	68
4.3.1 Energy Storage	68
4.3.2 Coupling Considerations	71
4.4 Analysis of a Coaxial Cavity	75
4.5 Deviations from Theoretical Model	78

## VIII

4.5.1 Spurious Responses	78
4.5.2 Fringing Field Effect	79
4.6 Cavity Performance	80
<b>CHAPTER 5: <u>DIELECTRIC MATERIALS FOR VLSI SUBSTRATES</u></b>	
5.1 Introduction	88
5.2 Electrical Properties	89
5.2.1 Fundamental Dielectric Parameters and Definitions	89
5.2.2 Propagation Properties	90
5.3 Molecular Properties of Dielectrics	92
5.4 Frequency and Temperature Dependence of $\epsilon'$ and $\epsilon''$	94
5.5 Dielectric Breakdown	97
5.6 Survey of Substrate Materials	98
5.7 Manufacture and Testing of Substrates	101
5.7.1 Introduction	101
5.7.2 Production Processes and stages	102
5.7.3 Colour in Ceramics	105
5.8 Test Materials.	106
<b>CHAPTER 6: <u>MEASUREMENT METHODS AND TECHNIQUES</u></b>	
6.1 Introduction	108
6.2 Bridge Method	109
6.2.1 Theory	109
6.2.2 Measurement Procedure	113
6.3 Q-meter Method	118
6.3.1 Theory	118
6.3.2 Measurement Procedure	121

6.4 Reflected Power Method	123
6.4.1 Measurement Procedure	124
6.5 Sweep Generator/Spectrum Analyzer Method (SG/SA)	126
6.5.1 Measurement Procedure	131
CHAPTER 7: <u>RESULTS</u>	
7.1 Introduction	134
7.2 Low Frequency Assessment	134
7.3 High Frequency results using CPM	151
CHAPTER 8: <u>CONCLUSIONS AND COMMENTS</u>	
8.1 Coaxial Cavities	174
8.2 Cavity Perturbation Formulae	175
8.3 Assessment of the Measurements	177
8.4 Future Work	179
<u>APPENDIX</u>	182
<u>REFERENCES</u>	194

CHAPTER 1  
INTRODUCTION

1.1 General Review

1.1.1 Introduction

The methods for measuring dielectric properties of materials at microwave frequencies can be broadly classified into two groups, (a) reflection and transmission coaxial or waveguide techniques and (b) the resonance cavity perturbation techniques. The former are suitable when large samples are available as the methods usually require filling the inside of a waveguide section with the material under test. The latter methods avoid this problem, and are therefore most frequently used. The resonance cavity perturbation method, in principle consists of measuring the change in resonant frequency and Q factor of the microwave resonator when it is suitably loaded with a small sample piece. The data may then be related to the properties of the material. During the early years, cylindrical and rectangular waveguide cavities were mostly used for such measurements at cm wavelengths. Presently, cavities of special shapes producing strong field distributions in particular regions are often used for the measurements. In each case, the shape and the dimensions of the sample and its position in the cavity are chosen so that the perturbation formula is applicable. In addition, most



systems have to be experimentally calibrated using samples of known dielectric properties.

### 1.1.2 Measurement Methods Employing a Reentrant Cavity

The reentrant cavity has been used for the measurement of the material dielectric properties by many investigators. The method is well proven and reliable. In the majority of the available publications, the accuracy of the results is affected by the electromagnetic field distribution within the sample cavity also by the apparatus used. Eldumiati and Hadad [1] in 1971 used the reentrant type of the cavity for measurements of the microwave conductivity and dielectric constant of a bulk semiconductor material. This method was different from the conventional approach which normally relies on the Q-factor measurements. It was shown by the authors that the change in the material conductivity as a result of a perturbation can be obtained by measuring the cavity coupling factor prior to the perturbation and the change in the reflected power from the cavity and hence coupling factor as a result of the perturbation.

Milewski and Kaczkowski [2] in 1979 introduced a new mathematical method for calculation of complex electric permittivity of a wide range of materials from the measured parameters of a reentrant cavity containing a sample material. Condition of resonance was obtained based on the analysis of electromagnetic field

distribution in the cavity with the sample. In their experimental work, a reentrant resonator was tunable by means of capacitance and inductance adjustments. The resulting settings of the capacitance and the inductance were then used to calculate the permittivities and dielectric losses. Measurements covering 200 to 1000 MHz frequency range were carried out on many materials with the values of  $\epsilon'$  between 2 and 300 and dielectric losses between  $10^{-5}$  and  $10^{-1}$ .

A new cavity perturbation technique for microwave measurements of dielectric constant was published by Susanta Sen, Saha, and Nag in 1979 [3]. This technique used a modified cylindrical reentrant cavity and seemed to have number of advantages, i.e.

- (a) sample area did not appear in the calculations,
  - (b) only the ratio of frequency shifts due to two samples of the same area and different thickness were involved,
- and (c) calibration of the measuring system with known dielectric was not necessary.

The method, however, was only suitable for low dielectric constants as the accuracy deteriorates for high permittivities.

### 1.1.3 Cylindrical Cavity Measurements

Cylindrical cavity resonator has been used by many workers as the basis of measurement systems for dielec-

tric properties of materials. The major problem incurred in this cavity was the existence of different modes at different frequencies. Rosenberg et al. in 1982 [4] gave a description of two  $TE_{01}$  cylindrical resonators operating at 10 and 35 GHz, respectively. The cavities were used to determine the complex permittivity of low-loss liquids at room temperature. They concluded that the adaptation of the  $TE_{10}$  resonator to the measurement of the dielectric properties of liquids was not easy. The problems encountered when attempting to measure liquids were, first, the likelihood of contamination with consequent change in the properties, and secondly, meniscus effect occurs and the unoccupied portion of the cavity fills with vapour which upsets the measurements.

Parkash, Vaid and Mansingh in 1979 [5] gave the relations for evaluating dielectric parameters from the changes in resonance frequency and Q of cylindrical  $TM_{010}$  mode cavity operating at 3.6986 GHz for thin samples of length less than the height of the cavity. The same authors in 1981 [6] used the same cavity for measuring the conductivity and permittivity of semiconductor spheres.

Hong and Roberts in 1974 [7] carried out method using a resonant cavity as a probe. The method employed consisted of varying the depth of penetration of a continuous cylindrical sample of the material into a cavity operating in the  $TM_{010}$  mode with the resonant frequency

and quality factor determined at each incremental setting of the perturbing sample. The perturbation of the cavity was achieved by advancing the sample into it along the symmetry axis employing the micrometer drive calibrated to give the depth of penetration. A differentiation method was used to obtain the half-power points of the cavity resonance response at each depth of penetration. Then the perturbation formulae for resonant cavities were used to obtain the physical parameters for the samples from the experimental data. The frequency employed was near 10 GHz.

Cylindrical cavity was also used by Mysore et al. in 1979 [8] and Shihe et al. in 1981 [9] for dielectric measurements. The innovation in their method was the shape and positioning of the sample, i.e. it was in the rod form and positioned along the cylindrical axis. The dielectric properties of the sample were then obtained using the perturbation method.

#### 1.1.4 Coaxial Line Techniques

Several microwave measurement techniques for dielectric properties employing coaxial lines have been developed. One of the earliest methods was by Von Hippel in 1978 [10]. It used a coaxial line terminated by a capacitance formed by the gap between the end surfaces of the inner conductor and a conducting plate shorting the cable. The cable was excited from the opposite end, and

the value of the end capacitance was determined from the position of the voltage minimum. The change in the end capacitance, when the gap was loaded with a dielectric sample of known dimensions, could then be directly related to the dielectric constant of the sample. The method is suitable for frequencies below 300 MHz, since the accuracy of determining the position of the voltage minimum as a fraction of the wavelength decreases as the frequency is increased.

Two coaxial line techniques for the determination of complex permittivities of solids and liquids were developed by Kulesza, Thorp and Bakar Ahmad in 1984 [11]. The first, the matched termination method, was essentially a comparison technique using air as the reference dielectric, producing accurate values of  $\epsilon'$ . In the second, the resonant line method, the characteristic impedance termination was replaced by an adjustable short circuit. This method was developed primarily for the purpose of determining the values of  $\tan\delta$  in low loss materials. Both methods can be used for frequencies in the 200 MHz to 9GHz range and normally require only conventional apparatus.

Nelson, Stetson and Schlaphoff in 1974 [12] published a paper describing the principles underlying the short-circuited-waveguide measurement method and a general computer program for calculating dielectric properties of high- or low-loss materials. The program was applicable

to measurements taken on coaxial lines or on rectangular or circular-waveguide systems.

Time-domain techniques for measuring the dielectric properties of materials have been used by many investigators [13] - [17]. In all time-domain methods step voltage is normally applied to a low-loss coaxial line. The shape of the step voltage then remains unchanged as long as the propagation properties of the line are independent of position. When the line contains a section with different propagation characteristics, for example a section with dielectric material enclosed, the voltage step will be reflected. From reflected and transmitted voltage at the interface and from this data the dielectric properties of the material can then be determined.

#### 1.1.5 Waveguide Measurements

Various rectangular waveguide techniques have been developed and used by many researchers. Majority of these techniques are described by Sucher and Fox [18]. The main ones include

(a) a method of measuring the dielectric constant involving the solution of a transcendental equation. This type of measurement depends on the quality of equipment and on the care taken during the experiment. It can be used for low and high values of dielectric constants,

(b) a measurement of dielectric constant involving two reactive terminations. This particular technique depends

on obtaining the short-circuit and open-circuit terminations of the sample at a specific plane by means of a variable short circuiting plunger. It involves the measurements of VSWR and the distance from a minimum to the sample for these two conditions.

#### 1.1.6 Measurements of Biological Substances

Extensive use of microwaves in domestic and industrial food processing and the general problem of electromagnetic pollution have resulted in increasing research into the biological effects of microwave radiation.

Chuo and Guy in 1978 [19] used an S-waveguide system to study the electromagnetic field effect on isolated nerves and muscles. The temperature of the exposed tissues was maintained constant by circulating temperature controlled solution through the waveguide. Specimens were placed in the waveguide either parallel or perpendicular to the electric field of the  $TE_{10}$  mode. Results showed no significant changes in characteristics of nerves or muscles at low-power radiation. The effects were observed during high-power radiation by changing the solution temperature.

Bianco et al. in 1979 [20] developed a method for measuring the complex permittivity of biological liquids at microwave frequencies. The method allows measurements to be made very quickly, using only very small amounts of

material. Measurements were made on human sera (fluids taken from blood) and erythrocytes (red cells) by using slotted line, network analyzer and a sample holder. The quantities measured were the reflection coefficient and the angle for each frequency of interest. The measurements were carried out in the frequency range from 100 to 2000 MHz.

Stuchly, M. and Stuchly, S. in 1980 [21] developed a technique for measuring dielectric properties of biological materials at radio and microwave frequencies using the coaxial line reflection method. Stuchly et al. in 1982 [22] developed a method for the same purpose using an open-ended coaxial line together with a computer-controlled network analyser system. The measurements were carried out in the frequency range from 0.01 to 1GHz.

In agriculture, data on the frequency dependence of dielectric properties of grains and insects were investigated by Nelson and Stetson in 1974 [23]. They presented the possibilities and principles for controlling insects with microwaves and lower frequency energy.

In conclusion, in all the above-mentioned methods and techniques for dielectric properties of materials, no one measuring system can cover the full spectral range and, in fact, several different kinds are in current use. It is thus possible, by the use of several techniques, to achieve a full spectrum coverage and simultaneously obtain estimates of the random and systematic errors in

the measurement techniques. Nevertheless, there is not a technique definitely better than others, and the methods are as yet still not standardized. This is a consequence in part because interest in this field is relatively recent, also of the difficulties arising in such measurements. No method is available at present which overcomes satisfactorily such difficulties of very different types.

### 1.2 The Project

One of the prime interests of the present work was to extend and develop previous techniques for measuring the dielectric properties of materials at microwave frequencies. The work described in this thesis has been primarily directed towards cavities for perturbation techniques. The project was undertaken with three main objectives. Firstly to design and construct a broadband coaxial cavity, secondly to develop and establish the perturbation theory for this particular type and thirdly, to ensure that the cavity as well as the perturbation techniques are of sufficient accuracy to be used as an important and necessary measuring aid in subsequent research applications. To achieve this, a sweep generator/spectrum analyzer combination was developed to enhance accuracy and repeatability.

In Chapter 2 the basic background of RF & microwave cavities and applications is reviewed. Three cavities are

discussed as examples, namely, the TE rectangular, TE cylindrical and TEM coaxial. Types and modes of oscillations, cavity coupling and quality factors are discussed in this chapter.

Chapter 3 is concerned with resonance perturbation theory and formulae. Their derivation together with the assumed approximations are discussed in detail. The relationship between the dielectric properties of a perturbing sample, shift in frequency and change in Q-factor of the cavity are also given for the above-mentioned types.

Considerations regarding the resonant coaxial cavity are outlined and analyzed in chapter 4. As necessary background, the equations and general relations of transmission lines as applied to resonant cavity structures are briefly reviewed. Cavity design considerations and associated parameters such as quality factor and coupling are also described. The performance of the cavity is examined by carrying out a number of tests, results of which are also presented.

Chapter 5 deals with dielectric materials for VLSI substrates. Equations relating the primary and secondary parameters to the dielectric properties are given. Manufacture and testing processes together with a survey of substrates are outlined. A molecular profile on the dielectrics is also included.

In Chapter 6, detailed descriptions and procedures of

the measurement methods and techniques, from low frequency to microwaves, are fully explained.

The accuracy and repeatability of the methods used is reflected in the results obtained for various types of ceramics supplied by Hirst Research Center GEC. These results are presented in the form of tables and graphs given in chapter 7.

Finally, in chapter 8 an assessment of the methods and the coaxial cavity based on the performance achieved is made. The advantages and disadvantages of the perturbation techniques are reviewed and suggestions for future work are proposed.

CHAPTER 2RF & MICROWAVE RESONANT CAVITIES AND APPLICATIONS2.1 Introduction

A cavity resonator is an essential part of many microwave circuits and systems. It is in general, a homogenous or inhomogenous dielectric region of any shape surrounded by conducting walls. At its resonant frequency, the injected energy oscillates back and forth between the walls and as a result, the electric and magnetic fields are set up within the cavity. During each cycle of oscillations the energy is dissipated in the walls. If, however, the conductivity of the walls is infinite and of the dielectric region zero, then there is no energy dissipated and the quality factor of the cavity is infinite.

Resonant circuits are usually discussed in terms of fundamental components, inductance(L), capacitance(C), and equivalent shunt resistance (R). The equations that describe the circuit are usually written using these components, but its behaviour can equally well be described in terms of its impedance( $Z_0$ ), quality factor(Q), and resonant frequency( $f_0$ ).

For circuits used at high frequencies, it is often more convenient to deal with these latter parameters, because at microwave frequencies, the components of a

resonant circuit become small and distributed, losing their meaning as lumped elements.

In microwave practice, cavity resonators are preferred as circuit elements because they are physically large and highly efficient.

## 2.2 Fundamental Principles

The two fundamental features of a microwave resonant cavity normally under consideration are

(i) the physical size, which depends on the wavelength and(ii)the electric and magnetic fields which are totally confined within the conducting walls.

As implied previously, the understanding of the operation of a cavity resonator is complicated by the fact that, the lumped elements of the equivalent low frequency lose their validity. To obtain its resonant frequency, solutions to Maxwell's equations must be found which satisfy the boundary conditions imposed by the resonator. In the analysis, it is usually assumed that the cavity is made of a perfect conductor and therefore, the penetration of the fields into the walls of the resonator is neglected. The boundary conditions which must then be met are that, no tangential electric and no normal magnetic fields at the surface of the cavity walls can exist.

Analytical solutions are only possible for a limited number of cavity shapes, which can simply be defined in terms of one of the standard co-ordinate systems. A number of approximate methods of calculations have been developed and are available which give adequately accurate answers for many cavity shapes that cannot normally be solved by means of analytical methods.

Any cavity resonator has an infinite number of natural frequencies of oscillations, and what is more, it may be excited in more than one mode. If it can be arranged to have only one resonance, however, the analysis of the cavity resonator can be considerably simplified. Because at any one of these resonant modes, the cavity behaves like an ordinary resonant circuit, and its behaviour may be described in terms of  $Z_0$ ,  $Q$  and  $f_0$ . These parameters, in general, will have different values at each of the other modes.

### 2.3 Types & Modes of Oscillations

In order to distinguish between different configurations an accepted mode nomenclature was introduced. The analysis of Maxwell's equations, with boundary conditions imposed at the inner walls of a resonant cavity, leads to a set of different solutions. These solutions are called the normal modes of the cavity, are infinite in number, and they may be represented by three basic types.

The first type is called Transverse Electric and

Magnetic wave, TEM, and contain neither electric nor magnetic field in the direction of propagation. They are found to exist in parallel and coaxial lines and are often referred to as the dominant principal waves.

The second type is called Transverse Electric waves, (TE or H). These waves have a component of magnetic field in the direction of propagation and the electric field is entirely transverse. Most of the parasitic resonances encountered in a coaxial resonator are due to waves of this type.

The third type are called Transverse Magnetic waves, (TM or E). In this wave, a component of electric field is present in the direction of propagation and the magnetic field is entirely transverse. If the diameter of the variable coaxial resonator is sufficiently large (compared with a wavelength), the TM wave will be set up and may produce parasitic resonances that will limit the high-frequency tuning range.

The mode of the wave is denoted by two subscripts "m", "n", i.e.  $H_{mn}$  or  $E_{mn}$ . For rectangular guide, in the American System, "m" indicates the half-period changes of the E field along the wide "a" dimension of the cavity, whilst "n" indicates the half-period changes of the E field along the narrow "b" dimension. A third subscript p or q is added and designates the number of half wavelengths along the cavity length, l. For circular guide, m and n represent the number of antinodes occurring

in the E or H field for a given coordinate direction.

The most important mode in the coaxial cavity is TEM, in the rectangular cavity is  $TE_{101}$  while in the cylindrical cavity  $TM_{010}$ ,  $TE_{011}$ ,  $TE_{111}$  are predominant.

## 2.4 Coupling in Resonant Cavities

An electromagnetic field can exist inside a cavity when a signal is injected from an outside circuit. The excitation element may be a loop, probe or a simple aperture.

For coaxial cavities, power can be extracted via a coupling loop, a capacitive probe or direct connection to the inner conductor.

### 2.4.1 Coupling Loops

An inductive loop is very often utilized as the coaxial cavity coupling. A current flows around the conductor of the loop, generating a magnetic field perpendicular to the plane of the loop. The loop may be placed in any place as long as it links with the magnetic lines of force. The degree of coupling can be altered by rotating the loop plane relative to the direction of the magnetic lines.

The excitation may be maximized by placing the loop plane at right angle to the magnetic lines of the required mode. The magnetic coupling is most effective when positioned near the short-circuit or high current end

because the magnetic field is proportional to the current.

Two distinct coupling loops may be needed, one for the input and the other for the output signal. The two loops should be separated as far as possible so that direct magnetic coupling between them is negligible.

A perfect match at resonant frequency may be obtained if the input and output loops have the same size and shape and are located at points of equal intensity. Usually, the effect of self-inductance of the coupling loops slightly shifts the resonance frequency.

#### 2.4.2 Coupling Probes

The capacitive probe is coupled to the electric field lines parallel to it. The coupling is largest when the probe is located at the maximum electric field of the excited mode.

For the reentrant coaxial cavity, the electric coupling should normally be located at a quarterwavelength from the short circuit end in the region of intense electric field.

#### 2.4.3 Coupling Apertures

In waveguides, a slot or a hole of a required shape is cut through the wall between the cavity and the external circuit, allowing radiation of the signal from one to the other.

To obtain a high quality factor,  $Q$ , a round hole should normally be used as coupling because of an advantageous distribution of the field. In this case the electric field is parallel to the plane of the hole, while the magnetic field is perpendicular to it. Degree of coupling may be modified by introducing inductive or capacitive tuning screws, (Fig.2.1).

Two important factors must be considered in determining the radius of the hole. In the first case, the quality factor of the cavity should be as high as possible. The increase in the radius of the coupling lowers it. Secondly the radius of the hole should not be too small since then the magnitude of the susceptance increases too much. In practice the radius is normally found empirically and the best size recommended at 9.3 GHz is between 3 and 4 mm [24].

In the rectangular cavity constructed, three screws on both sides of the cavity were used as tuners for matching purposes. The quality factor of the cavity was found to be approximately 6000.

## 2.5 Resonant Frequency and Quality Factor of a Cavity

### 2.5.1 Introduction

In order to determine the dielectric loss of a given material using perturbation method, the quality factor ( $Q$ ) of the resonant cavity has to be measured with and without the specimen present and the loss can then be

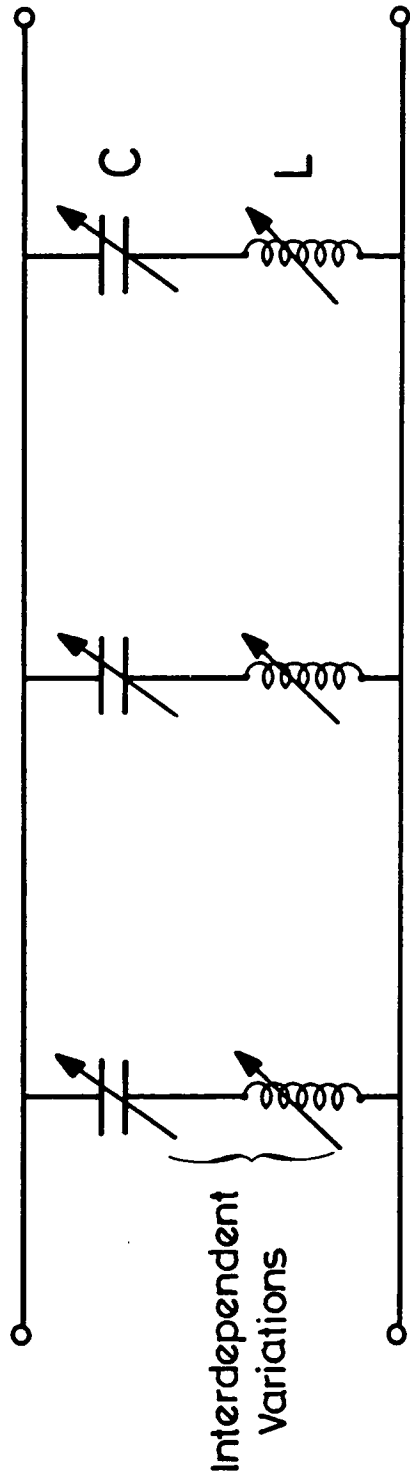


FIG 2.1: Equivalent Circuit of Screws

calculated from the fall in the Q-factor value.

The factor Q is used to determine the quality of an oscillatory system in which the energy storing and dissipative processes occur periodically [25]. It is also found to be a convenient symbol for sharpness of resonance or selectivity of a resonant circuit [18]. It is defined as [26]

$$Q = 2\pi \frac{\text{Energy stored in cavity}}{\text{Energy dissipated per cycle}} \quad (2.1)$$

There are three kinds of quality factor distinguished. The first one is the unloaded quality factor,  $Q_U$ , where only the loss in the cavity is taken into account. The second one is the loaded quality factor,  $Q_L$ , which represents the losses of the cavity and the coupling. The third one is the external quality factor,  $Q_E$ , where only the losses due to an external circuit are considered. These three types of quality factor are related to each other through the equation [18]

$$\frac{1}{Q_L} = \frac{1}{Q_U} + \frac{1}{Q_E} \quad (2.2)$$

which states that the total loss of energy in the cavity system is equal to the sum of the losses due to the cavity and the coupling.

For narrow-band resonant structures or circuits it may be shown that [27]

$$Q_L = \frac{f_o}{f_1 - f_2} \quad (2.3)$$

where  $f_o$  is the resonant frequency, and  $f_1$ ,  $f_2$  are the frequencies at the half-power bandwidth points. This is the relationship which is normally used in determining the loaded Q of a cavity.

The unloaded Q and the resonant Frequency,  $f_o$ , for TE rectangular, TE cylindrical, and TEM coaxial cavities are given by many authors [27] - [30] and these will now be reviewed.

### 2.5.2 TE Rectangular Cavity

Let the cavity dimensions be A, B, and C. The resonant frequency and the unloaded Q are then given by

$$f_o = \frac{c}{2} \left[ \left( \frac{m}{A} \right)^2 + \left( \frac{n}{B} \right)^2 + \left( \frac{p}{C} \right)^2 \right]^{1/2} \quad (2.4)$$

or

$$\lambda = 2 \left[ \left( \frac{m}{A} \right)^2 + \left( \frac{n}{B} \right)^2 + \left( \frac{p}{C} \right)^2 \right]^{-1/2} \quad (2.5)$$

and

$$\frac{Q\delta}{\lambda} = \frac{ABC (a^2+b^2)(a^2+b^2+r^2)^{3/2}}{4 AC(a^2r^2+(a^2+b^2)) + BC(b^2r^2+(a^2+b^2)) + ABr^2(a^2+b^2)} \quad (2.6)$$

where

$$a = \frac{m}{A} \quad b = \frac{n}{B} \quad r = \frac{p}{C}$$

also  $\delta$  = skin depth ,

$m$  = number of half-period variations of  $\bar{E}$  along  $x$  ,

$n$  = number of half-period variations of  $\bar{E}$  along  $y$  ,

and  $p$  = number of half-period variations of  $\bar{E}$  along  $z$  .

### 2.5.3 TE Cylindrical Cavity

These cavities are easier to construct mechanically have a high quality factor and are often used in wavemeters.

Let the cavity dimensions be  $L$  (the length of the cavity) and  $D$  (the diameter of the cavity). Then, for this cavity we have

$$f_o = \frac{c}{D} \left[ \left( \frac{x_{mn}}{TT} \right)^2 + \left( \frac{qD}{2L} \right)^2 \right]^{1/2} \quad (2.7)$$

or

$$\lambda = 2 \left[ \left( \frac{2x_{mn}}{\pi D} \right)^2 + \left( \frac{q}{L} \right)^2 \right]^{-1/2} \quad (2.8)$$

and

$$Q\delta = \frac{\left[ 1 - \left( \frac{m}{x_{mn}} \right)^2 \right] \left[ (x_{mn})^2 + \left( \frac{q\pi D}{2L} \right)^2 \right]^{3/2}}{2\pi \left[ (x_{mn})^2 + \left( \frac{q\pi D}{2L} \right)^2 + \left( \frac{D}{L} \right)^2 + \left( 1 - \frac{D}{L} \right) \left( \frac{q\pi D}{2L} \right) \left( \frac{m}{x_{mn}} \right)^2 \right]} \quad (2.9)$$

where,

$x_{mn}$  = nth root of  $J_m(x) = 0$

$m$  = number of full-period variations of  $\bar{E}_r$  with respect to  $\theta$ ,

$n$  = number of half-period variations of  $\bar{E}_\theta$  with respect to  $r$ ,

and

$q$  = number of half-period variations of  $\bar{E}_z$  with respect to  $z$ .

#### 2.5.4 TEM Coaxial Cavity

These cavities are superior to the other cavities from the point of view of wide operational frequency range. The resonant frequency and the unloaded  $Q$  of a coaxial cavity with outer radius  $b$ , inner radius  $a$ , and length  $L$  are given by

$$f_0 = \frac{c}{\lambda} \quad (2.10)$$

or

$$\lambda = 2\pi Ta \left( \frac{L}{2d} - \ln b/a \right)^2 \text{ approx.} \quad (2.11)$$

and

$$Q\delta = \left[ \frac{1}{L} + \frac{1}{2 \ln b/a} (1/a + 1/b) \right]^{-1} \quad (2.12)$$

where  $d$  is the capacitance gap, i.e., the gap between the inner conductor and the short circuit.

## 2.6 Effect of Temperature on Resonant Cavities

The resonant frequency of a cavity will vary with changing temperature because of dimensional variations. For a cavity constructed of a single metal, the percentage change in resonant wavelength will be equal to the percentage change in linear dimensions, which in turn depends on the expansion coefficient of the material of which the cavity is built.

In addition, if the cavity is not sealed, there will be a change in resonant frequency because of the varying dielectric constant of air with changing temperature and humidity.

## 2.7 Applications

At the higher radio frequencies, coil and capacitor networks become difficult to construct on account of small sizes of the elements and the large effects of the interconnecting windings. There has been a tendency to replace coils by small lengths of transmission lines, and these have been used in many applications.

The most obvious application of a resonant cavity is as a substitute for lumped components. The cavity has the advantages over the lumped components in simplicity, manageable physical size at high frequencies and very low losses. Consequently, cavities play the role of resonators and are utilized in the following microwave circuits:

- (i) **Generators:** The frequency of oscillation of most microwave generators, such as Klystrons and magnetrons is determined by a resonant cavity.
- (ii) **Frequency Meters:** A cavity of adjustable dimensions is used to measure the frequency or frequencies of microwave signals.
- (iii) **Filters:** The frequency-selective properties of resonant cavities are used in the design of filters, most often band-pass or band-stop.

The resonant cavities are also employed in measuring the properties of materials which is the area of interest of this research project. In this case the material

inside the cavity interacts with the field and modifies the resonance characteristics. Information about the material may then be obtained from the modified characteristics and the actual position of the sample in the field distribution is of importance.

The cavities also play a role in heating applications. In microwave ovens, the electromagnetic energy produced by a magnetron using resonant cavities to heat up, cook, or dry a material placed inside a container. This was discovered in 1945 when a manufacturer of radar magnetrons found out that microwaves can generate heat. This effect was rapidly applied in the design of ovens, and other heating processes.

There are endless usable physical forms of a cavity resonator and the choice is usually made by the application required. Practical examples of these can be divided into two groups. The first uses geometric shapes such as cylinders, prisms, spheres or ellipsoids. The second may utilise transmission lines as resonant structures.

CHAPTER 3RESONANCE PERTURBATION THEORY AND FORMULAE3.1 Introduction

The resonance perturbation method is one of the most important techniques that has been devised for determining the dielectric properties of materials.

The purpose of this chapter is to present detailed derivations of the "perturbation formulas" for the frequency shift and the reduction in the Q-factor of a resonant system when a sample of dielectric material is introduced. It is the aim in the derivations to state clearly what assumptions are made so that the accuracy of the calculated results can be assessed and hence better experimental methods developed.

When a sample of dielectric material is introduced into a resonant system, its frequency of resonance is altered by a small amount (perturbed) and its selectivity, represented by a Q-factor is lowered. These effects are related to the dielectric properties of the sample.

As the name "perturbation" implies the system without and with the sample presents two very close situations in behaviour. The relation between the changes in frequency and selectivity and the dielectric properties can be derived using the so called "perturbation theory". The theory has been formulated by several authors and the earliest treatment by Bethe and Schwinger [31] considered

perturbation as being a small deformation of the boundary surface of the cavity. Casimir [32] has applied the theory to the case of a cavity where a small body is introduced. The relation between frequency shift and deformation is now well known from the above analyses, however, none of them presented the derivations in any great detail and consequently the assumptions on which the theory is based were not apparent. Waldron [33] at a later date published a paper on the derivation of the perturbation formula discussing the assumed approximations.

### 3.2 Perturbation Formula for a Resonant Cavity

#### 3.2.1 General Relations in a Perturbed Field

The cavity perturbation methods employed for measurements of dielectric constant involve approximations in their formulation which lead to acceptable results only under very restricted conditions. First, the sample must be very small as compared with the cavity dimensions so that the frequency shift produced by the insertion of the sample is small as compared with the resonant frequency of the empty cavity. Second, the fields in the sample are assumed to be static if the sample is small as compared to the wavelength, or the field in the region where the sample is introduced must be uniform.

Let the electric and magnetic fields in the unperturbed cavity be

$$E = E_0 e^{j\omega t} \quad (3.1)$$

and

$$H = H_0 e^{j\omega t} \quad (3.2)$$

where  $E_0$  and  $H_0$  are functions of position. The field magnitudes should not be so large as to cause dielectric breakdown in the cavity or appreciable heating of the wall by induced currents. On introducing a small dielectric sample, the fields and the resonant frequency are altered as follows:

$$E' = (E_0 + E_1) e^{j(\omega + \delta\omega)t} \quad (3.3)$$

and

$$H' = (H_0 + H_1) e^{j(\omega + \delta\omega)t} \quad (3.4)$$

where it is assumed that the fields in the perturbed situation can be represented as the sums of the unperturbed fields  $E_0$  or  $H_0$  and additional small field components  $E_1$  or  $H_1$  accompanied by a frequency change.

Substituting eqns.(3.1) and (3.3) into Maxwell's curl equation for the E field yields

$$\nabla \times E_0 = \frac{-\partial B_0}{\partial t} = -j\omega B_0 \quad (3.5)$$

and

$$\nabla \times (E_0 + E_1) = -j(\omega + \delta \omega)(B_0 + B_1) \quad (3.6)$$

which on subtraction gives

$$\nabla \times E_1 = -j[\omega B_1 + \delta \omega (B_0 + B_1)] \quad (3.7)$$

Similarly, using Maxwell's curl equations for the H field results in

$$\nabla \times H_1 = j[\omega D_1 + \delta \omega (D_0 + D_1)] \quad (3.8)$$

Now, adding scalar products

$E_0 \cdot \nabla \times H_1$  and  $H_0 \cdot \nabla \times E_1$  gives

$$\begin{aligned} E_0 \cdot \nabla \times H_1 + H_0 \cdot \nabla \times E_1 &= j\omega [E_0 \cdot D_1 - H_0 \cdot B_1] \\ &\quad + j\delta \omega [(E_0 \cdot D_0 - H_0 \cdot B_0) + (E_0 \cdot D_1 - H_0 \cdot B_1)] \end{aligned} \quad (3.9)$$

and using the vector identity [34]

$$\nabla \cdot [(H_0 \times E_1) + (E_0 \times H_1)] = E_1 \cdot \nabla \times H_0 - H_0 \cdot \nabla \times E_1 + H_1 \cdot \nabla \times E_0 - E_0 \cdot \nabla \times H_1 \quad (3.10)$$

results in

$$H_0 \cdot \nabla \times E_1 + E_0 \cdot \nabla \times H_1 = j\omega(E_1 \cdot D_0 - H_1 \cdot B_0) - \nabla \cdot [(H_0 \times E_1) + (E_0 \times H_1)] \quad (3.11)$$

On substitution into eqn. (3.9) gives finally,

$$\begin{aligned} & j\omega(E_1 \cdot D_0 - H_1 \cdot B_0) - \nabla \cdot [(H_0 \times E_1) + (E_0 \times H_1)] \\ & = j\omega(E_0 \cdot D_1 - H_0 \cdot B_1) + j\delta\omega[(E_0 \cdot D_0 - H_0 \cdot B_0) + (E_0 \cdot D_1 - H_0 \cdot B_1)] \quad (3.12) \end{aligned}$$

### 3.2.2 Derivation of the Perturbation Formula

If we wish to use the relations derived in the preceding paragraphs for a cavity containing a sample then the dimensions of both must be included in any integration over the field regions.

Let  $V_0$  be the volume of the cavity and  $V_s$  the volume of the sample in Fig. 3.1 .

Integrating equation (3.12) over the volume  $V_0$  gives

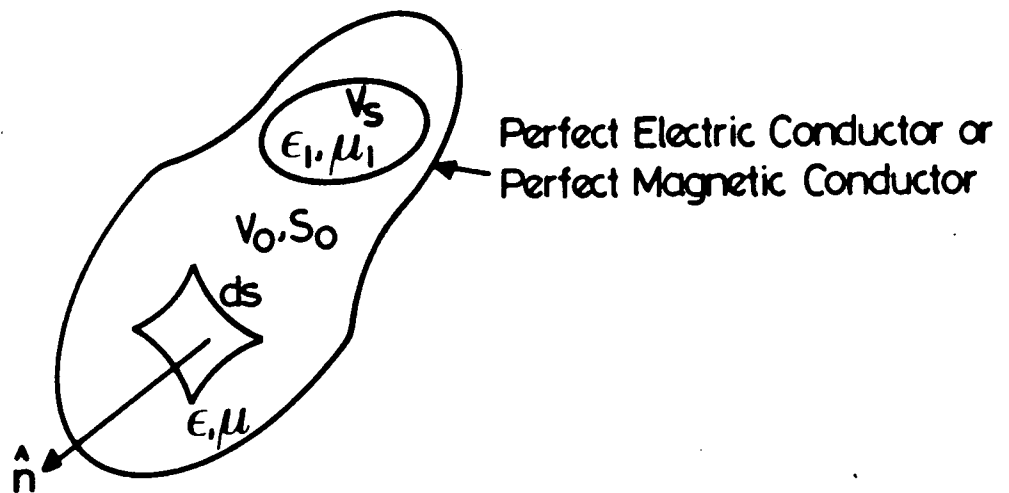


FIG 3.1: Homogeneous Cavity and Sample of Arbitrary Shapes

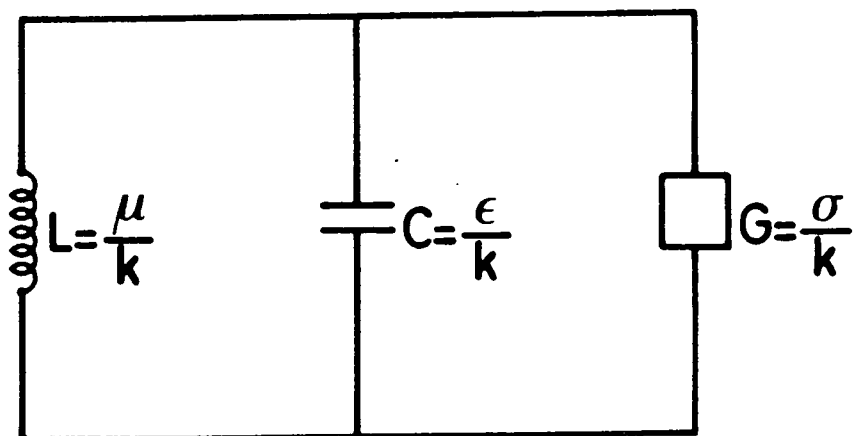


FIG 3.2: Equivalent Circuit of a Resonant Cavity

$$\begin{aligned}
& j\omega \int_{V_0} (E_1 \cdot D_0 - H_1 \cdot B_0) dv - \int_{V_0} \nabla \cdot [(H_0 \times E_1) + (E_0 \times H_1)] dv \\
& = j\omega \int_{V_0} (E_0 \cdot D_1 - H_0 \cdot B_1) dv + j\delta\omega \int_{V_0} [(E_0 \cdot D_0 - H_0 \cdot B_0) + (E_0 \cdot D_1 - H_0 \cdot B_1)] dv
\end{aligned} \tag{3.13}$$

The divergence integral over the cavity volume may be represented using Green's Theorem [34] as the integral over the cavity surface, i.e.

$$\int_{V_0} \nabla \cdot (H_0 \times E_1 + E_0 \times H_1) dv = \int_{S_0} (H_0 \times E_1 + E_0 \times H_1) \cdot \hat{n} ds \tag{3.14}$$

where  $S_0$  is the surface of the cavity and  $\hat{n}$  is the unity vector normal to the element surface  $ds$ , (see Fig.3.1). As the cavity walls are assumed to be perfect conducting surfaces, and  $H_0 \times E_1$  and  $E_0 \times H_1$  are tangential to the walls, the two scalar products with  $\hat{n}$  are zero and the divergence integral vanishes, i.e.

$$(H_0 \times E_1) \cdot \hat{n} = (E_0 \times H_1) \cdot \hat{n} = 0$$

since

$$|E_0 \times H_1| |\hat{n}| \cos\theta = 0 \quad \text{where } \theta = 90^\circ$$

In addition, assuming that when the frequency shift,  $\delta \omega$ , is very small,

$$D_1 \ll D_0 \text{ and } B_1 \ll B_0$$

which finally reduces eqn.(3.13) to

$$j\omega \int_{V_0} (E_1 \cdot D_0 - H_1 \cdot B_0) dv = j\omega \int_{V_0} (E_0 \cdot D_1 - H_0 \cdot B_1) dv + j\delta\omega \int_{V_0} (E_0 \cdot D_0 - H_0 \cdot B_0) dv \quad (3.15)$$

Now, outside the sample, i.e.  $V_0 - V_s$  volume

$$B_0 = \mu_0 H_0, \quad D_0 = \epsilon_0 E_0, \quad D_1 = \epsilon_0 E_1, \quad B_1 = \mu_0 H_1$$

and inside the sample, i.e.  $V_s$  volume

$$B_1 = \mu_1 H_1, \quad \text{and} \quad D_1 = \epsilon_1 E_1$$

Therefore, since  $E_1$ ,  $H_1$ ,  $D_1$ , and  $B_1$  only have values inside the sample, the integration is over the  $V_s$  volume; hence eqn. (3.15) now becomes

$$j\omega \int_{V_S} (E_1 \cdot D_0 - H_1 \cdot B_0) dv = j\omega \int_{V_S} (E_0 \cdot D_1 - H_0 \cdot B_1) dv + j\delta\omega \int_{V_S} (E_0 \cdot D_0 - H_0 \cdot B_0) dv \quad (3.16)$$

resulting in the Cavity Perturbation Formula, i.e.

$$\frac{\delta\omega_0}{\omega_0} = \frac{\int_{V_S} [(\mu_1 - \mu_0)H_0 \cdot H_1 - (\epsilon_1 - \epsilon_0)E_0 \cdot E_1] dv}{\int_{V_0} [\epsilon_0 E_0 \cdot E_0 - \mu_0 H_0 \cdot H_0] dv} \quad (3.17)$$

where field densities  $D$  &  $B$  are replaced by  $E$  &  $H$  field intensities.

The sample may be considered to be homogeneous, in which case  $\epsilon_1$  and  $\mu_1$  are constants and since maximum energies stored in electric and magnetic fields are also equal

$$\int_{V_0} \epsilon_0 |E_0|^2 dv = \int_{V_0} \mu_0 |H_0|^2 dv$$

where  $\epsilon_1 = \epsilon_r \epsilon_0$  and  $\mu_1 = \mu_r \mu_0$

Eqn. (3.17) now becomes

$$\frac{\delta \omega_0}{\omega_0} = \frac{(\mu_r \mu_0 - \mu_0) \int_{V_s} H_0 \cdot H_1 dv - (\epsilon_r \epsilon_0 - \epsilon_0) \int_{V_s} E_0 \cdot E_1 dv}{2\epsilon_0 \int_{V_0} |E_0|^2 dv} \quad (3.18)$$

and since  $\mu_1 = \mu_0$  or  $\mu_r = 1$  for the sample which is nonmagnetic, finally results in

$$\frac{\delta \omega_0}{\omega_0} = - \frac{\epsilon_r - 1}{2} \frac{\int_{V_s} E_0 \cdot E_1 dv}{\int_{V_0} |E_0|^2 dv} \quad (3.19)$$

where  $\epsilon_r$  is the relative dielectric constant of the material sample.

### 3.3 Relationship between the Resonant Frequency and the Q-factor

The relations for the fields within the cavity may be expressed by wave equations

$$\nabla^2 E + k^2 E = 0$$

and

$$\nabla^2 H + k^2 H = 0$$

The two expressions are the three-dimensional Helmholtz's equations where,

$$k^2 = -j\omega\mu (j\omega\epsilon + \sigma)$$

from which on solving the quadratic in  $\omega$  gives positive root as

$$\omega = j\frac{\sigma}{2\epsilon} + \sqrt{\frac{k^2}{\mu\epsilon} - \left(\frac{\sigma}{2\epsilon}\right)^2}$$

or in general

$$\omega = \omega_r + j\omega_1$$

where

$$\omega_0 = \frac{k}{\sqrt{\mu\epsilon}}, \quad \omega_r = \sqrt{\frac{k^2}{\mu\epsilon} - \left(\frac{\sigma}{2\epsilon}\right)^2} \approx \omega_0 \quad \text{and} \quad \omega_1 = \frac{\sigma}{2\epsilon}, \quad (3.20)$$

The equivalent circuit of a resonant cavity may be represented by the diagram in Fig.3.2 .

The Q-factor of the circuit is defined as [18,26]

$$Q_o = \frac{\omega_o \times \text{maximum energy stored}}{\text{average power dissipated}}$$

which leads to

$$Q_o = \frac{\omega_o C}{G} = \frac{\omega_o \epsilon}{\sigma}$$

Substituting eqn.(3.20) into above results in

$$Q_o = \frac{\omega_r}{2\omega_1} \approx \frac{\omega_o}{2\omega_1} \quad (3.21)$$

Expanding the expression

$$\frac{\delta \omega_o}{\omega_o} = \frac{\omega_1 - \omega_o}{\omega_o}$$

results in [18]

$$\begin{aligned} \frac{\delta \omega_o}{\omega_o} &= \frac{\Delta \omega_{ro} + j \Delta \omega_{io}}{\omega_{ro} + j \omega_{io}} \\ &= \frac{\Delta \omega_{ro} + j \Delta \omega_{io}}{\omega_{ro} (1 - j \frac{\omega_{io}}{\omega_{ro}})} \left( 1 - j \frac{\omega_{io}}{\omega_{ro}} \right) \end{aligned} \quad (3.22)$$

where

$$\begin{aligned} \omega_1 &= \omega_{r1} + j \omega_{i1} , \\ \omega_o &= \omega_{ro} + j \omega_{io} , \\ \Delta \omega_{ro} &= \omega_{r1} - \omega_{ro} , \\ \Delta \omega_{io} &= \omega_{i1} - \omega_{io} , \end{aligned}$$

Since  $\left( \frac{\omega_{io}}{\omega_{ro}} \right)^2 \ll 1$ , eqn. (3.22) now becomes

$$\frac{\delta \omega_o}{\omega_o} \approx \frac{\Delta \omega_{ro}}{\omega_{ro}} + j \left( \frac{\omega_{i1}}{\omega_{ro}} - \frac{\omega_{io}}{\omega_{ro}} \right) \left( 1 - j \frac{\omega_{io}}{\omega_{ro}} \right) \quad (3.23)$$

Substituting eqn. (3.21) in eqn. (3.23) gives

$$\frac{\delta \omega_o}{\omega_o} \approx \frac{\Delta \omega_{ro}}{\omega_{ro}} + \frac{j}{2} \left( \frac{1}{Q_1} - \frac{1}{Q_o} \right) \left( 1 - j \frac{1}{2Q_o} \right) \quad (3.24)$$

Since  $\frac{1}{2Q_0} \ll 1$ , eqn.(3.24) resulting in

$$\frac{\delta \omega_0}{\omega_0} \approx \frac{\Delta f_0}{f_0} + \frac{j}{2} \left( \frac{1}{Q_1} - \frac{1}{Q_0} \right) \quad (3.25)$$

which is a useful practical equation relating the change in Q-factor to the shift in frequency  $\Delta f_0 = f_1 - f_0$ .

#### 3.4 Dielectric Properties of a Perturbing Sample

When a material sample is introduced in a cavity, the resonance frequency and the Q-factor of the cavity will change. The dielectric properties of the material sample may then be written in terms of frequency shift and change in Q-factor of the cavity.

Equation (3.25) provides the link between the measured quantities ( $f_0, f_1, Q_0, Q_1$ ) and the theoretical expressions involving  $\delta \omega/\omega$  in eqn.(3.19). Equating both equations, the relative dielectric constant must eventually be

$$\frac{\Delta f_0}{f_0} + \frac{j}{2} \left( \frac{1}{Q_1} - \frac{1}{Q_0} \right) = \frac{\epsilon_r - 1}{2} \frac{\int_{V_s} E_0 \cdot E_1 dv}{\int_{V_0} |E_0|^2 dv} \quad (3.26)$$

Here the field  $E_0$  in the empty cavity is presumed to be known and only the perturbed field  $E_1$  in the sample volume  $V_B$  remains unknown.  $E_1$  is found only with the knowledge of sample geometry and  $E_0$ .

Since  $\epsilon_r = \epsilon' - j\epsilon''$  where  $\epsilon'$  is the permittivity and  $\epsilon''$  the dielectric loss and by separating real and imaginary parts, eqn.(3.26) yields

$$\epsilon' = 1 + 2 \frac{\Delta f_0}{f_0} \frac{\int_{V_0} |E_0|^2 dv}{\int_{V_B} E_0 \cdot E_1 dv} \quad (3.27)$$

$$\epsilon'' = \left( \frac{1}{Q_1} - \frac{1}{Q_0} \right) \frac{\int_{V_0} |E_0|^2 dv}{\int_{V_B} E_0 \cdot E_1 dv} \quad (3.28)$$

but

$$\frac{\int_{V_0} |E_0|^2 dv}{\int_{V_B} E_0 \cdot E_1 dv} \propto \frac{V_0}{V_B}$$

which leads to

$$\frac{\int_{V_0} |E_0|^2 dv}{\int_{V_S} E_0 \cdot E_1 dv} = F(x, y, z) \frac{V_0}{V_S}$$

where  $F(x, y, z)$  is the function of the cavity and specimen determined by the proportion of  $E$  appearing in the specimen and is given by

$$F(x, y, z) = \frac{V_S}{V_0} \frac{\int_{V_0} |E_0|^2 dv}{\int_{V_S} E_0 \cdot E_1 dv} \quad (3.29)$$

Eqns. (3.27) and (3.28) now become

$$\epsilon' = 1 + 2 \frac{\Delta f_0}{f_0} \frac{V_0}{V_S} F(x, y, x) \quad (3.30)$$

$$\epsilon^* = \left( \frac{1}{Q_1} - \frac{1}{Q_0} \right) \frac{V_0}{V_s} F(x,y,z) \quad (3.31)$$

which is the general cavity perturbation formula giving the specimen properties.

### 3.5 Applications of Resonance Perturbation Theory

#### 3.5.1 Introduction

The perturbation formulae, i.e, eqns. (3.30) and (3.31), can be applied to resonant cavities of different shapes. The purpose of this para. is to present the applications of the perturbation formulae to

$H_{101}$  mode rectangular,

$H_{011}$  mode circular,

and TEM coaxial cavities.

#### 3.5.2 $H_{101}$ Rectangular Cavity

As the first example of the application of the perturbation formulae, let us consider a rectangular cavity in the  $H_{101}$  mode with dimensions A,B,C as shown in Fig.3.3 .

The normalized field in a rectangular cavity are easily found and can be expressed in a trigonometrical form. For the TE modes the fields are given by [28].

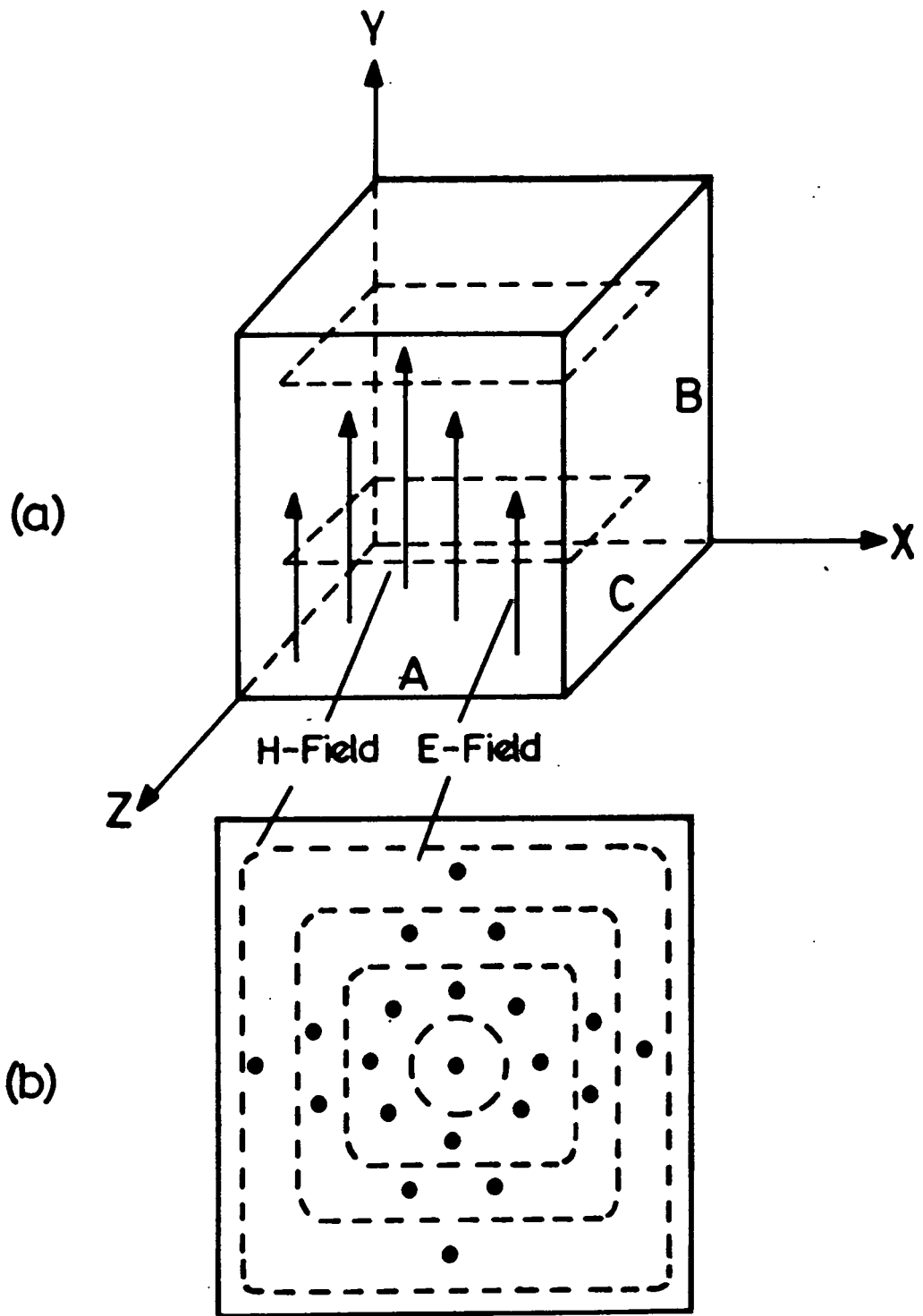


FIG 3.3: (a)  $H_{101}$  Mode Rectangular Cavity  
 (b) Top View of  $\vec{E}$  and  $\vec{H}$  Fields

$$\begin{aligned}
 E_x &= -\frac{k_2}{k} \cos(k_1 x) \sin(k_2 y) \sin(k_3 z) \\
 E_y &= \frac{k_1}{k} \sin(k_1 x) \cos(k_2 y) \sin(k_3 z) \\
 E_z &= 0
 \end{aligned}
 \tag{3.32}$$

where

$$k_1 = \frac{m\pi}{A}, \quad k_2 = \frac{n\pi}{B}, \quad k_3 = \frac{p\pi}{C}, \quad \lambda = \frac{2\pi}{k}$$

and

$$k^2 = k_1^2 + k_2^2 + k_3^2$$

The restriction is that  $m, n, \text{ or } p > 0$  where,

$m$  = number of half-period variations of  $E$  along  $x$ ,

$n$  = number of half-period variations of  $E$  along  $y$ ,

$p$  = number of half-period variations of  $E$  along  $z$ .

The general expression for the fields of an  $H_{101}$  mode in a rectangular cavity can now be obtained from the above equations giving

$$E_x = E_z = 0$$

$$E_y = \frac{C}{\sqrt{A^2 + C^2}} \sin \frac{\pi x}{A} \sin \frac{\pi z}{C}$$

resulting in,

$$E_v = E_{\max.} \sin \frac{\pi x}{A} \sin \frac{\pi z}{C} \quad (3.33)$$

Integration of  $E_v$  over the volume of the cavity gives ,

$$\begin{aligned} \int_{V_0} |E_v|^2 dv &= E_{\max.}^2 \int_0^A \int_0^B \int_0^C \left( \sin^2 \frac{\pi x}{A} \sin^2 \frac{\pi z}{C} \right) dx dy dz \\ &= E_{\max.}^2 \frac{ABC}{4} = \frac{1}{4} E_{\max.}^2 V_0 \quad (3.34) \end{aligned}$$

assuming that the sample with a volume  $V_s$  is located in an essentially uniform field, i.e., at the centre of the cavity where  $x = A/2$  and  $z = C/2$ . This is in fact the maximum field,  $E_{\max.}$

The integral over  $V_s$ , therefore, can be written

$$\int_{V_s} |E_v|^2 dv = E_{\max.}^2 V_s \quad (3.35)$$

Now, the function  $F(x,y,z)$  can be found for this case by combining eqns.(3.29),(3.34) and (3.35) resulting in

$$\begin{aligned}
 F(x, y, z) &= \frac{V_s}{V_o} \frac{\int |E_o|^2 dv}{\int_{V_s} E_o \cdot E_1 dv} \\
 &= \frac{V_s}{V_o} \frac{1}{4} \frac{E_{\max}^2 \cdot V_o}{E_{\max}^2 \cdot V_s} = \frac{1}{4}
 \end{aligned} \tag{3.36}$$

For a rectangular cavity in the  $H_{101}$  mode, the specimen properties are now given by

$$\epsilon' = 1 + \frac{1}{2} \frac{\Delta f_o}{f_o} \frac{V_o}{V_s} \tag{3.37}$$

$$\epsilon'' = \frac{1}{4} \left( \frac{1}{Q_1} - \frac{1}{Q_2} \right) \frac{V_o}{V_s} \tag{3.38}$$

### 3.5.3 $H_{011}$ Cylindrical Cavity

For the second example of the formula application, let us consider a right circular cylindrical cavity in  $H_{011}$  mode with dimensions  $L$  and  $D$  as shown in Fig.3.4 .

The normalized fields for the TE-modes cylindrical cavity, as given by Montgomery [28] are

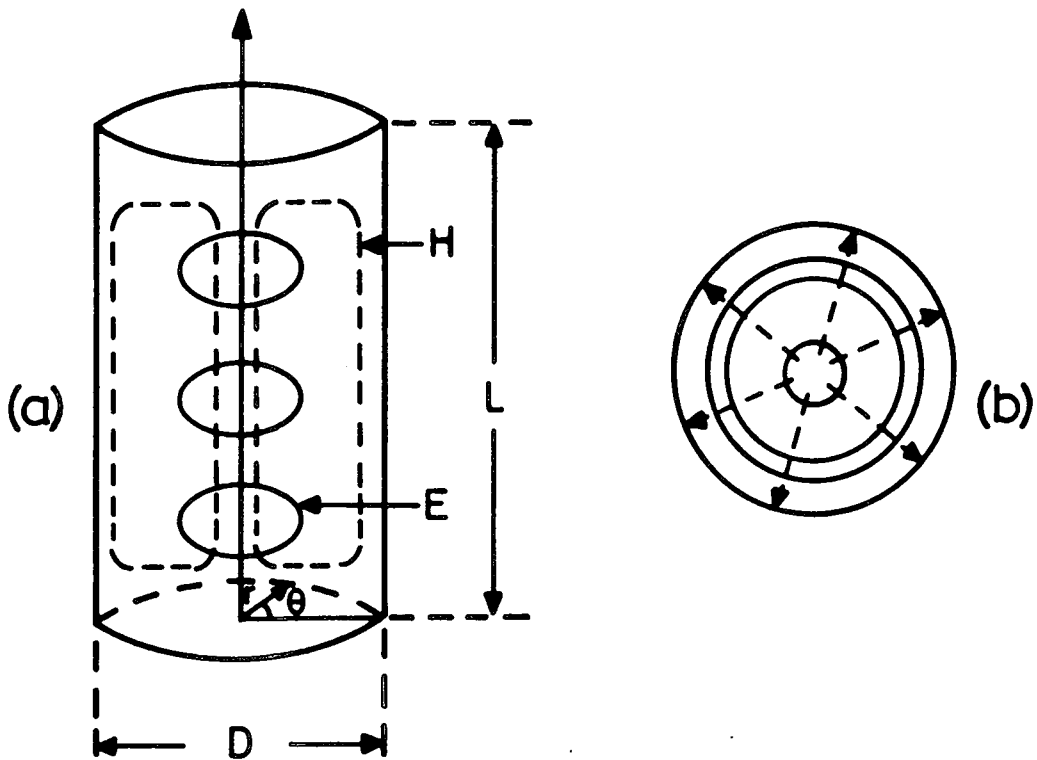


FIG 3.4: (a)  $H_{011}$  Mode Cylindrical Cavity  
(b) Top View of  $\vec{E}$  and  $\vec{H}$  Fields

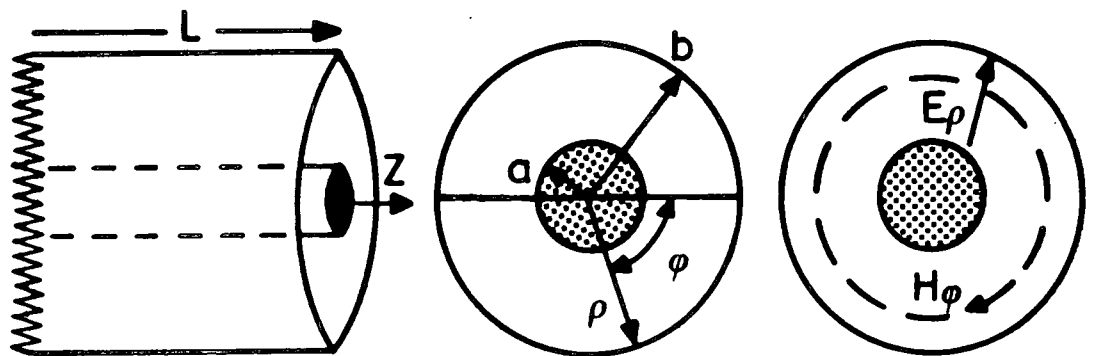


FIG 3.5: Variables Involved in Coaxial Cavity

$$\begin{aligned}
 E_r &= -m \frac{J_m(k_1 r)}{k_1 r} \sin(m\theta) \sin(k_3 z) \\
 E_\theta &= -J'_m(k_1 r) \cos(m\theta) \sin(k_3 z) \\
 E_z &= 0
 \end{aligned}
 \tag{3.39}$$

where,

$$k_1 = \frac{2X_{mn}}{D}, \quad k_3 = \frac{q\pi}{L}, \quad k_1^2 = k_2^2 + k_3^2, \quad \lambda = \frac{2\pi}{k}$$

and  $X_{mn}$  = Roots of  $J_m(x)$  and  $J'_m(x)$

The restrictions are that  $n > 0$  and  $q > 0$

where,  $m$  = number of full-period variations of  $E_r$  with respect to  $\theta$ .

$n$  = number of half-period variations of  $E_\theta$  with respect to  $r$ .

$q$  = number of half-period variations of  $E_r$  with respect to  $z$ .

From the above equations, the general expression for the fields of  $H_{011}$  mode in a cylindrical cavity can now be obtained, i.e.

$$E_r = E_z = 0$$

$$E_\theta = -3.832 \sin \frac{\pi z}{L}$$

i.e.

$$E_{\theta} = E_{\max.} \sin \frac{\pi z}{L} \quad (3.40)$$

To determine the function  $F(x,y,z)$ , a suggested solution is presented below.

Integrating over the volume of the cavity gives ,

$$\begin{aligned} \int_{V_0} |E_{\theta}|^2 dv &= E_{\max.}^2 \int_0^{D/2} \int_0^{2\pi} \int_0^L \sin^2 \frac{\pi z}{L} r dr d\theta dz \\ &= E_{\max.}^2 \cdot 2\pi \frac{D^2}{8} \left[ \frac{1}{2} z - \frac{L}{4\pi} \sin \frac{2\pi}{L} z \right]_0^L \\ &= \frac{\pi}{8} E_{\max.}^2 D^2 L \\ \int_{V_0} |E_{\theta}|^2 dv &= \frac{1}{2} E_{\max.}^2 V_0 \quad (3.41) \end{aligned}$$

If a sample of small volume  $V_0$  is placed at  $z = L/2$ , the field in that sample will be

$$E_{\theta s} = E_{\max.} \sin \frac{\pi}{L} (L/2) = E_{\max.}$$

Integrating over  $V_s$  yields ,

$$\int_{V_s} E_o \cdot E_o s dv = E_{max}^2 \cdot V_s \quad (3.42)$$

Now, the function  $F(x,y,z)$  can be obtained by combining eqns. (3.29), (3.41), and (3.42), i.e.,

$$F(x,y,z) = \frac{V_s}{V_o} \frac{\int_{V_o} |E_o|^2 dv}{\int_{V_s} E_o \cdot E_o s dv}$$

$$= \frac{V_s}{V_o} \frac{V_o \cdot E_{max}^2 / 2}{V_s \cdot E_{max}^2} = 1/2 \quad (3.43)$$

Therefore, for the specimen of the material inserted in an  $H_{011}$  mode cylindrical cavity the relative dielectric constant and loss are given by

$$\epsilon' = 1 + \frac{\Delta f_o}{f_o} \frac{V_o}{V_s} \quad (3.44)$$

$$\epsilon'' = \frac{1}{2} \left( \frac{1}{Q_1} - \frac{1}{Q_o} \right) \frac{V_o}{V_s} \quad (3.45)$$

### 3.5.4 TEM Coaxial Cavity

Equations (3.30) & (3.31) are also applicable to the measurements in a coaxial cavity. The only problem arises is how to determine the function  $F(x,y,z)$  for this case.

At the lower range of frequency, where the inner conductor is almost close to the plate, a theoretical solution for  $F(x,y,z)$  is suggested below.

Sander and Reed [35] have represented the electric field in the TEM coaxial cavity by

$$E_{\rho} = \frac{\psi_0}{\rho \ln b/a} \exp.(-j \beta z) \quad (3.46)$$

where  $\psi_0$  is a constant and the other symbols are defined as shown in Fig.3.5.

Integration of (3.46) over the volume of the cavity gives,

$$\begin{aligned} \int_{V_0} |E_{\rho}|^2 dv &= \int_{V_0} \left| \frac{\psi_0}{\rho \ln b/a} \right|^2 dv \\ &= \frac{\psi_0^2}{(\ln b/a)^2} \int_{z=0}^L \int_{\phi=0}^{2\pi} \int_{\rho=a}^b \frac{1}{\rho^2} \rho d\rho d\phi dz \\ &= \frac{\psi_0^2}{(\ln b/a)^2} \cdot 2\pi \cdot L \cdot \ln b/a \end{aligned}$$

i.e.

$$\int_{V_0} |E_\rho|^2 dv = \frac{2}{\ln b/a} \cdot \frac{\psi_0^2}{b^2 - a^2} \cdot V_0 \quad (3.47)$$

since

$$V_0 \approx \pi L(b^2 - a^2)$$

Suppose now the sample is located in the region half way between  $\rho = a$  and  $\rho = b$ . Integrating next over the sample volume,  $V_s$ , leads to

$$\begin{aligned} \int_{V_s} E_\rho \cdot E_{\rho_s} dv &= \int_{V_s} \left| \frac{\psi_0}{\frac{(b-a) \cdot \ln b/a}{2}} \right|^2 dv \\ &= \frac{4 \psi^2}{(\ln b/a)^2} \frac{V_s}{(b-a)^2} \end{aligned} \quad (3.48)$$

assuming that the sample is very small and the cavity without and with the sample is only slightly perturbed. Combining eqns. (3.29), (3.47) and (3.48) gives, therefore, the required factor

i.e.

$$F(x, y, z) = \frac{1}{2} \frac{(b-a)}{(b+a)} \ln b/a \quad (3.49)$$

In the practical cavity constructed, where  $2a = 4.75\text{mm}$ ,  $2b = 15.2\text{mm}$ , the function  $F(x, y, z)$  was found to be

$$F(x,y,z) \approx 1/3.28 \quad (3.50)$$

and eqns. (3.30) and (3.31) become, therefore ,

$$\epsilon' = 1 + \frac{2}{3.28} \frac{\Delta f_0}{f_0} \frac{V_0}{V_E} \quad (3.51)$$

$$\epsilon'' = \frac{1}{3.28} \left( \frac{1}{Q_1} - \frac{1}{Q_0} \right) \frac{V_0}{V_E} \quad (3.52)$$

According to Hansen [36], Lamont and Glazier [27], the electric field pattern in a coaxial cavity behaves as shown in Fig.3.6 and Fig.3.7 , respectively. Therefore, eqns. (3.51) and (3.52) will still be approximately valid for coaxial cavities in which the capacitance gap is small because the electric field is uniform and concentrated within the gap region.

At the upper end of the frequency range the capacitance gap is wide ,i.e., low capacitance, which may lead to the nonuniformity of the electric field. In this case a theoretical solution for the function  $F(x,y,z)$  might not be easy to find

To overcome this problem , a known material with known  $\epsilon'$  and  $\epsilon''$  has to be used to determine the function  $F(x,y,z)$  experimentally.

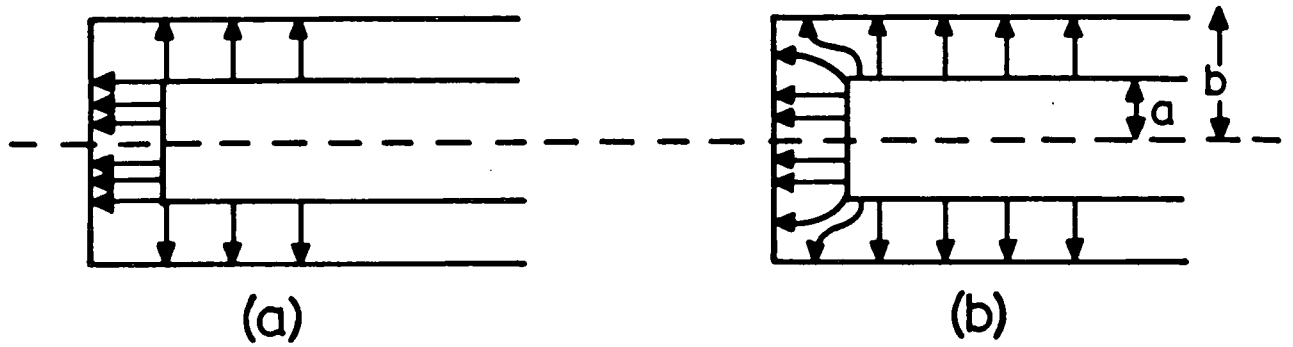


FIG 3.6: Qualitative Drawings  
of an Assumed Field  
Distribution

Another, and Better  
Field Distribution

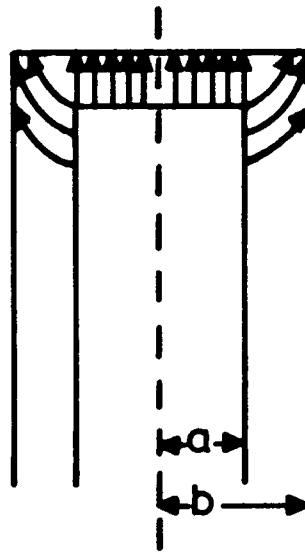


FIG 3.7: Electric Field Pattern in a Resonant Cavity

CHAPTER 4  
RESONANT COAXIAL CAVITY

4.1 Characteristics of a Transmission Line

4.1.1 Introduction

Transmission line is the preferred term to describe a transmission system with two or more metallic conductors electrically insulated from one another, for instance the two-wire line and the coaxial line.

When the length of an electrical conductor is of the same order of magnitude as the wavelength, the transit time of a signal is comparable to its period, and can not be neglected. The length and size of the conductors and their geometrical setting, therefore, become important parameters at high frequencies.

To facilitate an understanding of the following chapter, the equations and general relations of a transmission line as they apply to resonant cavity structures will be briefly reviewed first.

4.1.2 Primary Constants of a Transmission Line

In defining the primary constants of a transmission line, it is necessary to develop a representative equivalent circuit. Such a circuit is shown in Fig.4.1 and it contains the four primary elements of the line, resistance, conductance, inductance and capacitance ( $R$ ,  $G$ ,  $L$  and  $C$ ) which are expressed as the values per unit

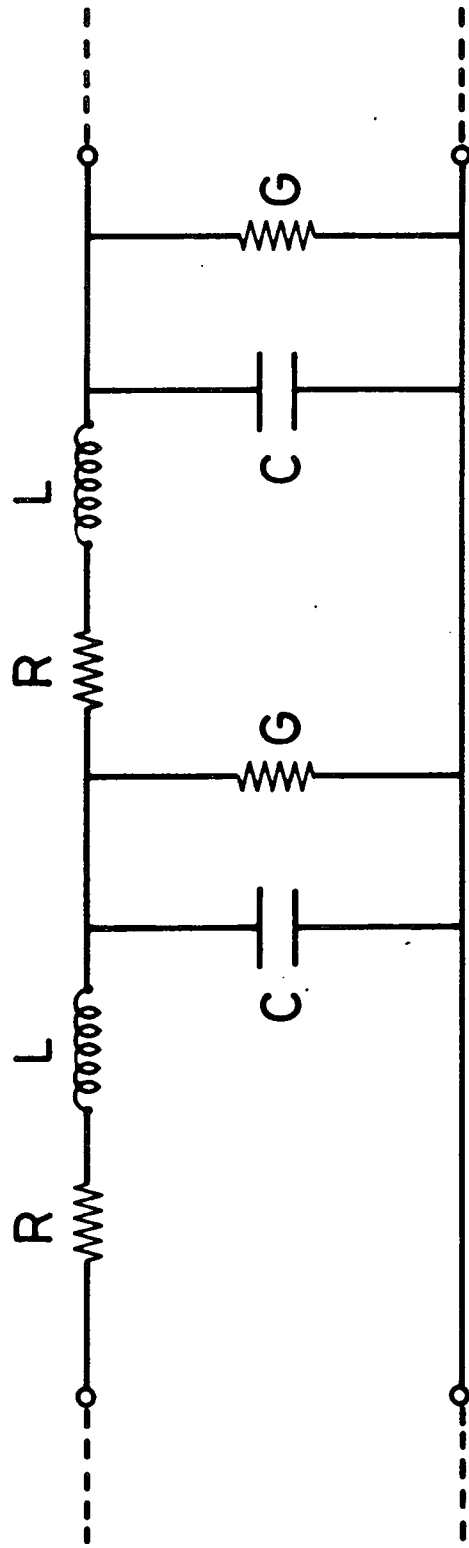


FIG 4.1: Distribution of Impedance and Admittance Along a Transmission Line

length distributed uniformly along the line [37]. Therefore, a small length of line  $\delta x$  will have a series impedance  $(R+j\omega L)\delta x$  and a shunt admittance  $(G+j\omega C)\delta x$ .

At high frequencies the a.c resistance per unit length is of importance and is given by [27]

$$R_{a.c} = \frac{1}{2\pi} \left( \frac{\omega\mu\rho}{2} \right)^{\frac{1}{2}} \left( \frac{1}{a} + \frac{1}{b} \right) \quad (4.1)$$

where,

$\omega$  = angular frequency,

$\mu$  = conductor permeability,

$\rho$  = conductor resistivity,

$a$  = radius of the inner conductor,

$b$  = radius of the outer conductor.

Consequently, the primary constant,  $R$ , is the total resistance of the line per unit length and is given by

$$R = R_{a.c} + R_{d.c}$$

where,

$$R_{d.c} = \rho \left( \frac{1}{\pi a^2} + \frac{1}{\pi b^2} \right)$$

The line inductance is the result of the magnetic field established around the conductors as the current

flows through them and is effectively in series with line resistance. It is substantially dependent on the total flux in the dielectric space and, to a lesser extent, on the flux leakages within the conductors. For a coaxial line the inductance per unit length is given by [38]

$$L = \frac{\mu}{2\pi} \ln(b/a) \quad (4.2)$$

where

$\mu$  applies to the dielectric medium between conductors.

Capacitance between the two conductors will also be present. They can be thought of as plates of a capacitor, with a voltage existing across them. The capacitance per unit length  $C$ , will depend on the line configuration and relative permittivity of the dielectric, and can be expressed as [38]

$$C = \frac{2\pi\epsilon}{\ln(b/a)} \quad (4.3)$$

where

$\epsilon$  applies to the dielectric medium between conductors.

Finally, due to the imperfections of the dielectric medium some leakage current will flow between the conduc-

tors. This conduction, or leakage path, may be represented by a shunt resistance or, more conveniently, by a conductance  $G$  per unit length between the conductors whose value can be calculated from the following equation [27].

$$G = \omega C \tan \delta \quad (4.4)$$

where

$\delta$  is the loss angle which varies with frequency.

#### 4.1.3 Secondary Parameters of a Transmission Line

The primary characteristics of a transmission line lead to secondary parameters, namely, the characteristic impedance,  $Z_0$ , attenuation,  $\alpha$ , and phase,  $\beta$ . They all depend on and can be expressed in terms of distributed primary constants.

The characteristic impedance  $Z_0$ , defined as the voltage to current ratio at any point along the line, is given by

$$Z_0 = \sqrt{\frac{R + j\omega L}{G + j\omega C}} \quad (4.5)$$

This impedance is in general complex but it was found that [27] at very high frequencies for a lossless line,

it is a pure resistance given by

$$Z_0 = \sqrt{\frac{L}{C}} \quad (4.6)$$

For a coaxial line, the corresponding formula for  $Z_0$  can be developed by the use of eqns. (4.2) & (4.3), leading to

$$\begin{aligned} Z_0 &= \sqrt{\frac{L}{C}} = \frac{1}{2\pi} \sqrt{\frac{\mu}{\epsilon}} \log(b/a) \\ &= 138 \sqrt{\frac{\mu_r}{\epsilon_r}} \log(b/a) \end{aligned} \quad (4.7)$$

where

$\epsilon_r$  = relative permittivity of the dielectric medium,

$\mu_r$  = relative permeability of the dielectric medium.

The coaxial line performance may be assessed by the manner the signal is attenuated and delayed during transmission. It has been shown that the line contains impedance  $Z$  and admittance  $Y$  distributed along its entire length. The quantity  $\sqrt{ZY}$  dictates how the voltages and currents vary along the line; it governs the way in which the waves propagate. It is known as the propagation constant  $\gamma$  and is given by [27]

$$\gamma = \sqrt{ZY} = \sqrt{(R + j\omega L)(G + j\omega C)} = \alpha + j\beta \quad (4.8)$$

The real part of the solution of the above equation, known as the attenuation factor or coefficient  $\alpha$ , determines the way in which the waves are attenuated as they travel along the line. The imaginary part  $\beta$  is known as the phase shift constant and indicates the delay of the propagating waves.

#### 4.1.4 Transmission Line as a Resonant Circuit

At sufficiently high frequencies, a short section of a transmission line with completely reflecting terminations acts as an inductor if it is less than quarterwavelength long. It can be shown that for a line of fixed length, short-circuited at its terminal the impedance is given by [39].

$$Z_s = jZ_0 \tan\beta l \quad (4.9)$$

it also shows how the sending impedance  $Z_s$  varies with frequency.

For a short-circuited line of length  $l$  meters, at zero frequency the impedance is zero, but as the frequency is raised it behaves as an increasing inductive reactance,

On the other hand, as the frequency is raised higher,

the tangent function becomes negative, indicating that  $Z_0$  is capacitive and its reactance decreases.

At the point where  $Z_0$  passes from plus infinity to minus infinity the line behaves like a parallel resonant circuit, i.e., anti-resonance. When the frequency reaches the value where the angle is  $\pi$  radians, corresponding to  $l = \lambda/2$ , the value  $Z_0$  becomes zero. At that instance the line behaves like a series resonant circuit. Just beyond this frequency  $Z_0$  becomes a positive reactance and so on, as shown in Fig.4.2. The same figure can be made to apply to the open-circuited case by moving the length scale to the right until its zero coincides with the first anti-resonance, as illustrated in the Fig.4.2 by a dotted line.

The above theory can be applied to a coaxial cavity in which case the inductance created by the line length of less than  $\lambda/4$  can resonate with either a lumped capacitance or a capacitance due to the gap between the inner conductor and the lower short circuiting wall.

#### 4.2 Design of an Experimental Coaxial Cavity

In order to have a coaxial resonant cavity of high performance many points must be taken into account. To decrease the losses of the electromagnetic wave inside the cavity the inner surface must be made as smooth as possible. Also the inner and outer conductor dimensions

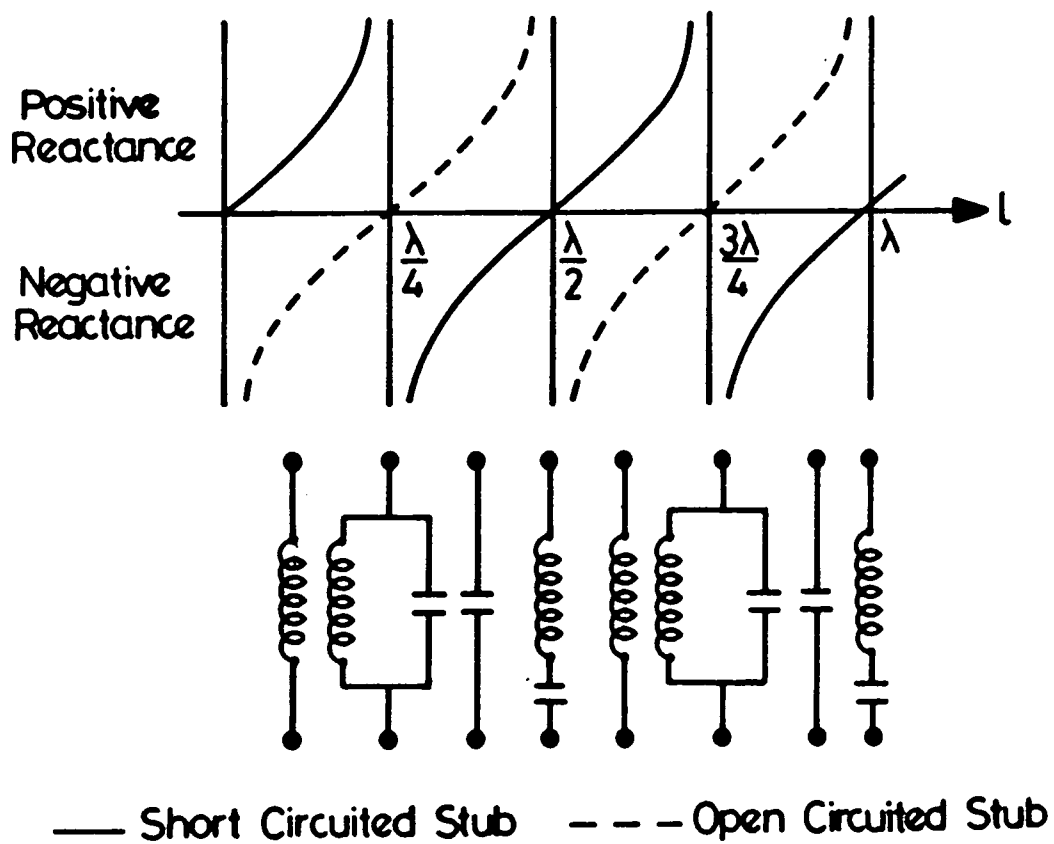


FIG 4.2: Variation of Input Impedance With Frequency for a Short-Circuited and an Open-Circuited Lines

have to be chosen to give high quality factor and low losses. A good short circuit between the inner and outer conductors is very important at one or both ends of the cavity.

The loaded quality factor must be high and transmission loss low to provide a sharp resonance at the frequency of the signal transmitted through the cavity. This may be achieved by careful tuning of the micrometer attached to the inner conductor and further improved by loose coupling if the unloaded quality factor is high.

The performance of the resonance cavity may be improved by matching to the external circuit by means of adjustable stubs screws or attenuators. It is also important to keep the cavity under constant environmental conditions.

The ratio  $b/a$  for optimum quality factor of a coaxial cavity can be found as follows: the a.c resistance  $R$  of the line is proportional to

$$(1/d - 1/D) \quad (4.10)$$

where,

$d$  and  $D$  are the diameters of the inner and outer conductors, respectively.

The attenuation coefficient  $\alpha$  is given by [40]

$$\alpha = \frac{R}{2Z_0} \quad (4.11)$$

Combining eqns.(4.10) & (4.11) yields

$$\alpha = \frac{K(1/d + 1/D)}{\log(D/d)} \quad (4.12)$$

where K is a constant of proportionality.

Differentiating eqn.(4.12) with respect to D/d and equating to zero gives an optimum value of  $Z_0$  of approximately 77 ohms which corresponds to  $D/d = 3.592$ . Therefore, for optimum quality factor of a coaxial cavity, the ratio b/a should be 3.6.

In designing a coaxial cavity the ratio b/a chosen will depend on considerations other than attaining slight increase in the quality factor. Consequently, the ratio b/a was chosen to be 3.2 in order to avoid any resonant modes other than TEM. To compensate for any losses that might exist, the cavity was silver plated with a layer 12 microns thick.

To have a good electrical short circuit, a radial choke was created with a clearance of 0.1 mm all around the inner conductor. This produced a low impedance between the inner and the outer conductor and a short circuit at a particular frequency. A teflon ring was inserted in a groove of 1.5 mm wide and 1 mm away from

the short circuit to avoid contact between the inner and the outer conductors.

The coupling loops were made from a length of Radiall RG401/U semi-rigid, PTFE-filled cable. The inner conductor of the cable was connected to the outer by forming a loop of 7 to 8 mm in length and soldered to ensure good electrical contact. The inner and the outer diameters of the semi-rigid cable are 1.67 and 5.46 mm, respectively, from which the characteristic impedance was calculated to be approximately 50 ohms. The other end of the semi-rigid cable was connected to the inner conductor of a 50 ohms N-type connector. Fig.4.3 shows a cross-sectional view and dimensions of the cavity.

In summary, to achieve a high performance, a standard cavity design should provide a broad tuning range, a high loaded quality factor, low transmission loss, small coupling to external load, a simple tuning mechanism and freedom from the effects of other modes and temperature.

### 4.3 Quality Factor of a Coaxial Cavity

#### 4.3.1 Energy Storage

In general, the electromagnetic energy in a cavity at resonance is stored in the electric and magnetic fields. The amount stored in each field will vary during the cycle, but their summation is always equal to the total energy content of the cavity. If the loaded quality factor of the cavity is reasonably high, the rate of the

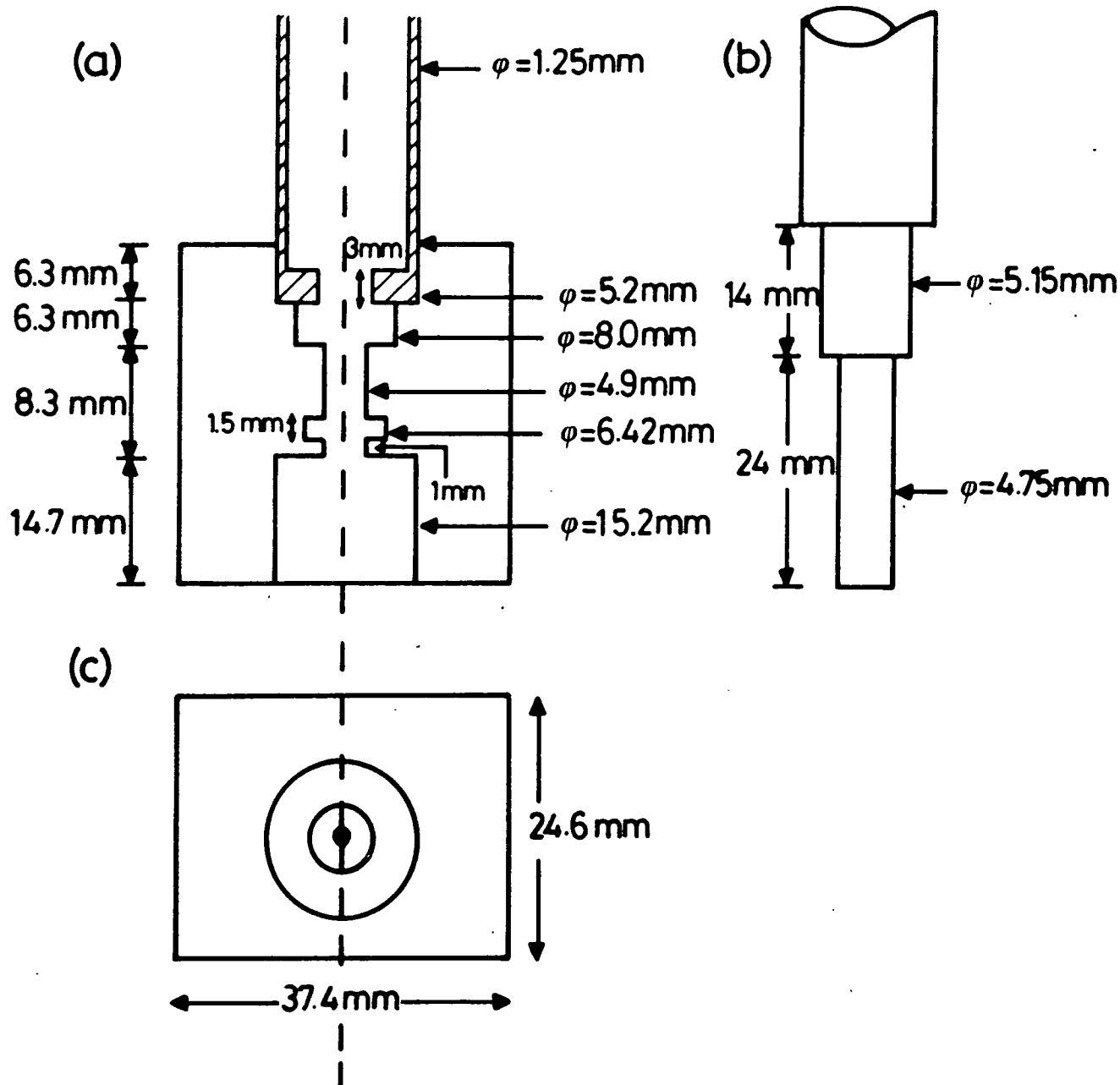


FIG 4.3 : Schematic Representation of Cavity Dimensions  
 (a) Cross-sectional View of the Cavity  
 (b) Cross-sectional View of the Inner Conductor  
 (c) Under View of the Cavity

stored-to-dissipated energy is high, and the average magnetic field density is equal to the average electric field density over a cycle.

At some instants in the cycle the energy will be entirely in the magnetic field, and at other instants the energy will be entirely in the electric field. With this knowledge we may calculate the total energy stored by finding the peak magnetic or electric field energy.

In a coaxial cavity, the magnetic field is created by the oscillatory currents flowing in the centre conductor, and if these currents can be calculated, the energy stored may also be found.

If we consider a resonant coaxial line of length  $l$ , the energy stored in a segment is

$$E = (L \delta L) I^2 / 2$$

where,

$L$  = inductance per unit length,

$I$  = current flowing in the segment.

Therefore, the total energy stored in a length  $l$  is

$$E = \frac{1}{2} LI_0^2 \int_0^l \cos^2\left(\frac{2\pi}{\lambda} \cdot l\right) dl$$

$$= \frac{1}{4} LI_0^2 \frac{\lambda}{2\pi} \left( \theta + \frac{1}{2} \sin 2\theta \right)$$

where,

$\lambda$  = line wavelength,

$\theta$  = electrical length.

But,

$$L = \frac{Z_0}{\lambda f_0}$$

Therefore,

$$E = \frac{1}{4} \frac{Z_0}{2\pi f_0} I_0^2 \left( \theta + \frac{1}{2} \sin 2\theta \right)$$

Normally under resonant conditions  $\theta$  is near  $n\pi/2$  where  $n$  is an integer. Hence the total energy in a coaxial cavity may be expressed as

$$E \approx \frac{nZ_0 i_0^2}{8f_0} \quad (4.13)$$

where  $i_0$  is the root mean square value of  $I_\theta$ .

#### 4.3.2 Coupling Considerations

It has been mentioned earlier in chapter 2 that, for coaxial cavities, power can be extracted via a coupling loop, a capacitive probe or direct connection to the inner conductor. The coaxial cavity may be loaded in many ways, some of which are shown in Fig.4.4. In the constructed coaxial cavity, two coupling loops are used, one for the input signal and the other for the output

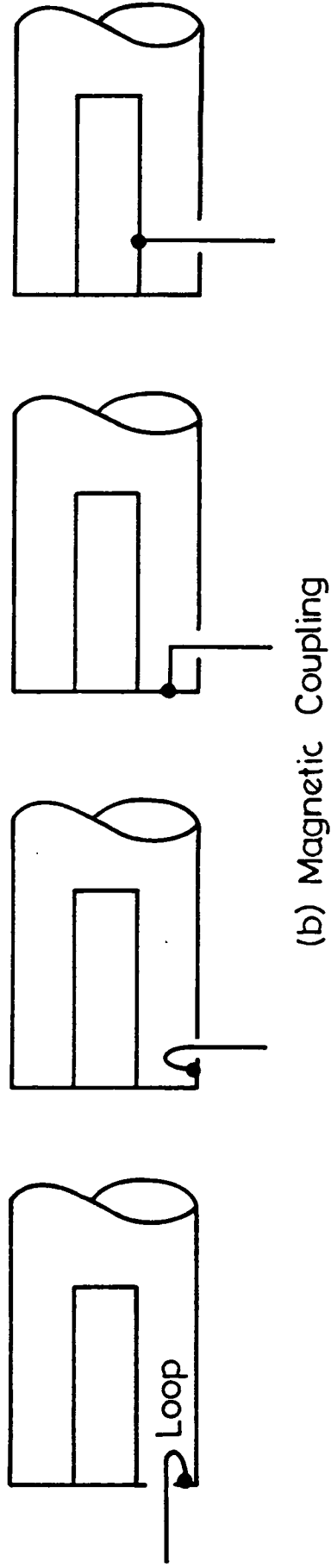
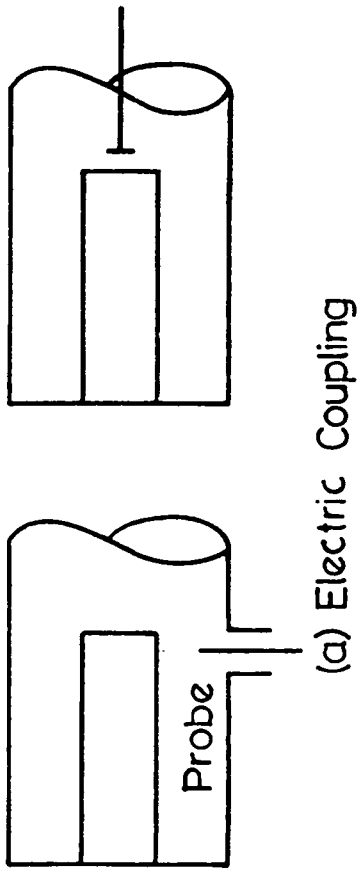


FIG 4.4: Coupling Devices to a Coaxial Cavity

signal. The coupling loops were positioned near the short circuit because the magnetic coupling is most effective in that region. The input and the output loops were separated as far as possible so that direct magnetic coupling is negligible. A perfect match at resonant frequency may always be obtained if the input and output loops have the same size and shape and are located at points of equal intensity.

In practice, a certain amount of electric coupling will be combined with the magnetic coupling of the loop. This is due to the fact that the loops project into the cavity and some electric field lines will terminate at the loop. If the loop is large, the amount of electric coupling may be quite appreciable. If the loop is small, however, and is located at the short-circuit point in the cavity, there will be negligible electric field near the loop and hence negligible electric coupling.

From the definition of quality factor of a resonant cavity and eqn.(4.13) given in the previous section, the quality factor can be written as

$$Q = \frac{2\pi f_0 i_0^2 Z_0 n / 8f_0}{\text{average power dissipated}} \quad (4.14)$$

Since the loading may be assumed to be anywhere in the cavity, it will be convenient to assume it to be concentrated at the short-circuited end and to consist of

a resistance  $R_L$  (load resistance), offered to the current  $i$ . Hence, eqn.(4.14) now becomes

$$Q = \frac{TTZ_0 n}{4R_L} \quad (4.15)$$

which is a useful relationship between the Q-factor and the load resistance. This formula assumes the unloaded  $Q_U$  to be infinite and was obtained from the following exact equation [41] i.e.

$$Q = \frac{(TTZ_0 n / 4R_L) Q_U}{(TTZ_0 n / 4R_L) + Q_U} \quad (4.16)$$

A number of valuable conclusions may be deduced from this equation, i.e.

- (i) the loaded Q is proportional to the number of quarter wavelength in the cavity,
- (ii) the loaded Q is proportional to the characteristic impedance of the cavity, and
- (iii) the loaded Q is inversely proportional to the equivalent load resistance.

All these parameters may be used, therefore, in obtaining the desired Q and, hence, the desired bandwidth.

#### 4.4 Analysis of a Coaxial Cavity

The coaxial cavity is defined here as a length of short circuited transmission line terminated with a capacitive reactance formed by the gap between the inner conductor and the end plate short circuit. The transmission line is of length just less than a quarter wavelength so that its input impedance is an inductive reactance. The frequency of resonance is given by

$$f_0 = 3 \times 10^{10} n / 4l$$

where  $n$  is the number of quarter wavelengths along the line at the resonant frequency  $f_0$ , and  $l$  is the length in centimetres.

To simplify the analysis we assumed the transmission line to be lossless. The parameters of importance are the length of the cavity, the position of the probe, the value of the capacitance and the characteristic impedance (see Fig.4.5).

The input impedance  $Z_{in}$  of a transmission line terminated in an impedance  $Z_R$  ohms is given by [39]

$$Z_{in} = Z_0 \frac{Z_R + jZ_0 \tan \beta l}{Z_0 + jZ_R \tan \beta l}$$

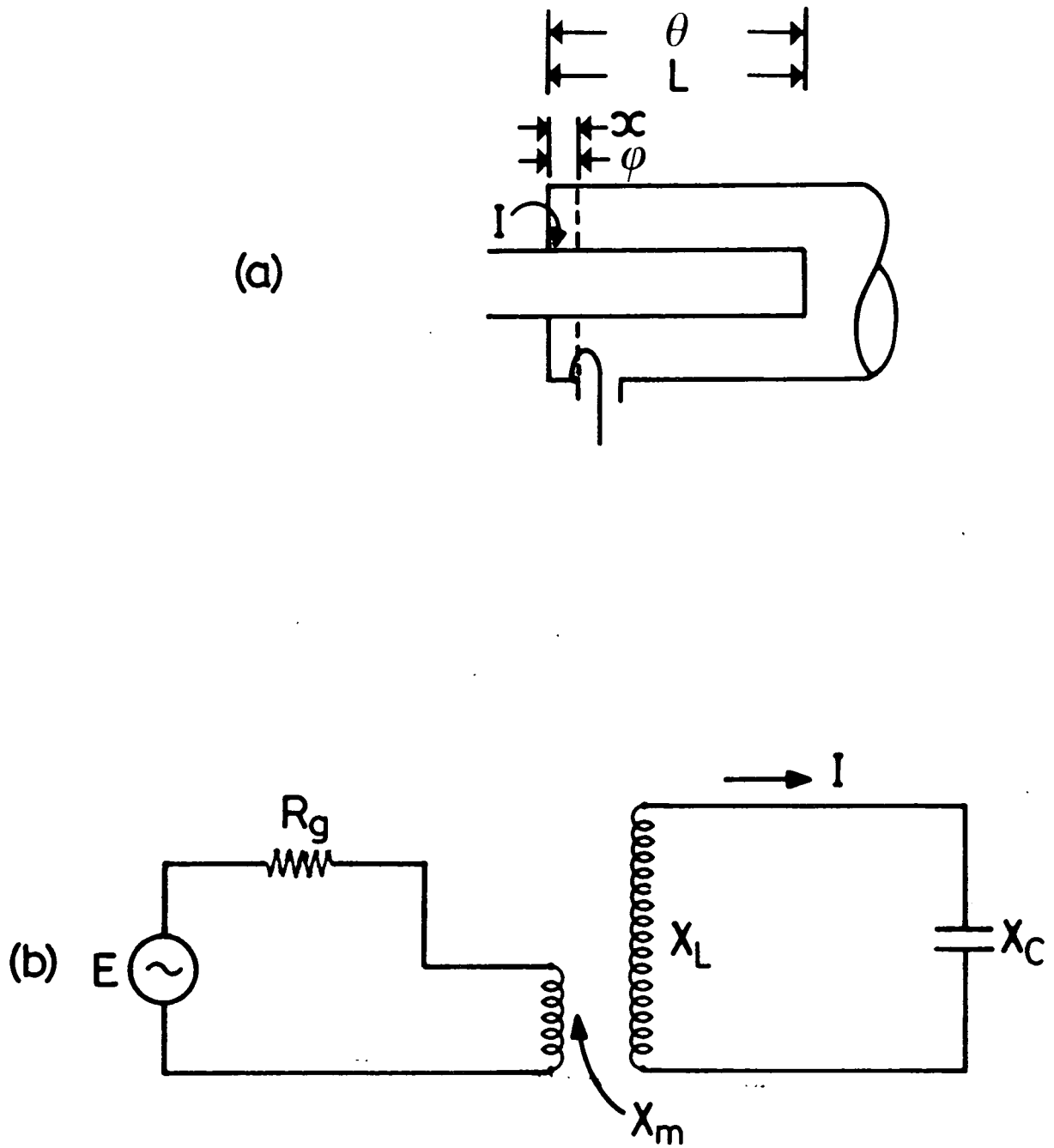


FIG 4.5: A Coaxial Cavity Load by a Single Loop  
 (a) General View  
 (b) Equivalent Circuit

where  $\beta$  is the phase change constant in radians per meter of the transmission line which has zero attenuation per unit length as it was assumed.

When the transmission line is terminated in a short circuit the impedance is reactive and is given by

$$Z_{s/c} = jZ_0 \tan \beta l$$

The electrical length of the cavity measured in radians of phase change is given by

$$\theta = \beta l$$

and  $\beta$  can be written in terms of the inductance and capacitance per unit length of the line,  $L$  and  $C$  as

$$\beta = 2\pi f_0 \sqrt{LC}$$

or for an air dielectric line as

$$\beta = 2\pi f_0 / c$$

where  $c$  is the velocity of light in free space.

If the frequency at which the cavity is a quarter wavelength long will be called  $f_{cav.}$ , then

$$c / f_{cav.} = \lambda = 4l$$

$$\text{or } l = c / 4f_{\text{cav.}}$$

Therefore,

$$\theta = \beta l = (2\pi f_0 / c)(c / 4f_{\text{cav.}}) = (\pi/2)(f_0 / f_{\text{cav.}})$$

At resonance the capacitive reactance should be equal to the inductive reactance, i.e.,

$$X_c = X_L$$

or

$$1 / 2\pi f_0 C = Z_0 \tan(\pi/2)(f_0 / f_{\text{cav.}})$$

which leads to

$$C = \frac{1}{2\pi f_0 Z_0 \tan(\pi/2)(f_0 / f_{\text{cav.}})}$$

The above mentioned analysis is the ideal case of a coaxial cavity, but it was suggested by the Radio Research Lab. staff [41] that, some of inductive and capacitive reactances may exist due to the imperfections inside the cavity.

#### 4.5 Deviations from Theoretical Model

##### 4.5.1 Spurious Responses

It was pointed out in the previous chapters that a

quarter-wave resonant cavity will have higher resonances at odd multiples of the fundamental frequency. Besides these usual responses, a coaxial cavity can also have waveguide-mode resonances which can cause spurious tuning responses.

If the transverse dimensions of the coaxial cavity are comparable to the wavelength, resonant modes other than TEM-type may exist in the cavity. The cut off frequency of the lowest possible waveguide mode occurs very nearly at the frequency at which the average circumference in the coaxial cavity is equal to the free space wavelength, i.e., at which the free space wavelength in centimeters is equal to  $2\pi(a+b)$ , where "a" and "b" are the radii of the inner and the outer conductors in centimetres, respectively. Spurious responses of these higher order transmission modes will therefore not occur below this frequency, and it is important to avoid them.

#### 4.5.2 Fringing Field Effect

When a material sample, whose permittivity is to be determined, is inserted in a coaxial cavity not only the capacitance ( $C_0$ ), due to air gap occupied by the sample is considered, but the capacitance ( $C_F$ ) due to fringing field should also be taken into account. This is because as the fields extend slightly beyond the end of the inner conductor, fringing capacitive reactances will exist and consequently affect the measurements.

Theoretical analysis of the effect of the fringing field in permittivity measurements using the lumped capacitance was studied by Iskander & Stuchly [42]. It included both the shunt and series capacitor methods. In both cases it was shown that the measured values of  $\epsilon'$  are larger than the true values by a factor  $C_F/C_0$ , while the measured values of the imaginary part,  $\epsilon''$ , are not affected by the fringing field.

The effect of additional inductance and capacitance occurring between the tip of the inner conductor and the adjacent cavity wall (Fig.4.6), should also be considered if a more accurate electrical circuit of the cavity is to be established.

#### 4.6 Cavity Performance

On completion of the design and construction, various tests were carried out to establish the quality of the cavity performance.

Frequency range, was the first quality to be measured. The frequency of the sweeper was accurately set to the desired value by calibrating it against the spectrum analyzer. The input and the output of the coaxial cavity were then connected to the sweeper and the spectrum analyzer respectively, via a 3dB attenuator on either side so that any possible mismatches were eliminated. Then by tuning the cavity to different frequencies, it was found that it operated in the frequency range

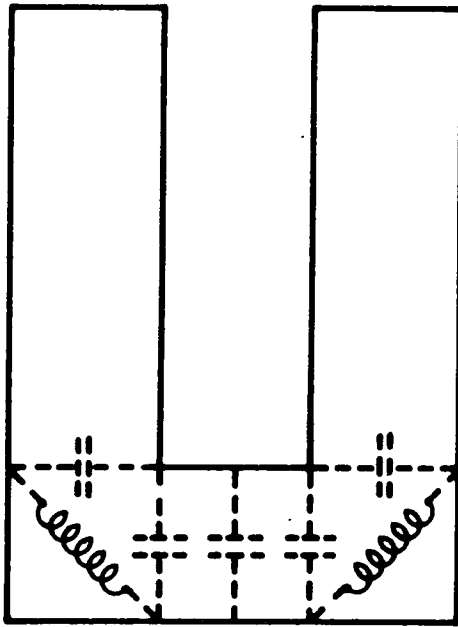


FIG 4.6: Distribution of Additional Inductance and Capacitance  
in the Coaxial Cavity

between 2.5GHz to 11.5 GHz which may be considered as a broad band application. Fig.4.7 shows the variations of the attached micrometer setting with frequency.

Another parameter measured was the capacitive gap between the end plate short circuit and the inner conductor which influences the value of the capacitance in the cavity. For comparison, theoretical values of the capacitive gap were obtained from eqn. (2.11) as shown in Fig.4.8 . The discrepancies observed in the measured and calculated values are suggested to be caused by either or both the reasons mentioned earlier, i.e. the fringing field effect and the additional capacitive and inductive reactances created inside the cavity.

Another important parameter measured was the quality factor of the cavity. The technique employed the use of a spectrum analyzer and a sweep generator. The details of this method will be discussed later in chapter 6 . The highest quality factor attained was 1885 at 4.25 GHz and the lowest was 300 at 11.5GHz. It is clear from Fig. 4.9 that, the nearer the inner conductor gets to the coupling apertures the lower the quality factor becomes. The values of the unloaded quality factor were obtained from eqn.(2.12) and are presented on the same Fig.4.9 . The discrepancies in the respective plots may be explained as being due to the nonideal nature of the cavity, the losses due to couplings, and moreover, due to the fact that the cavity walls were assumed to be perfect

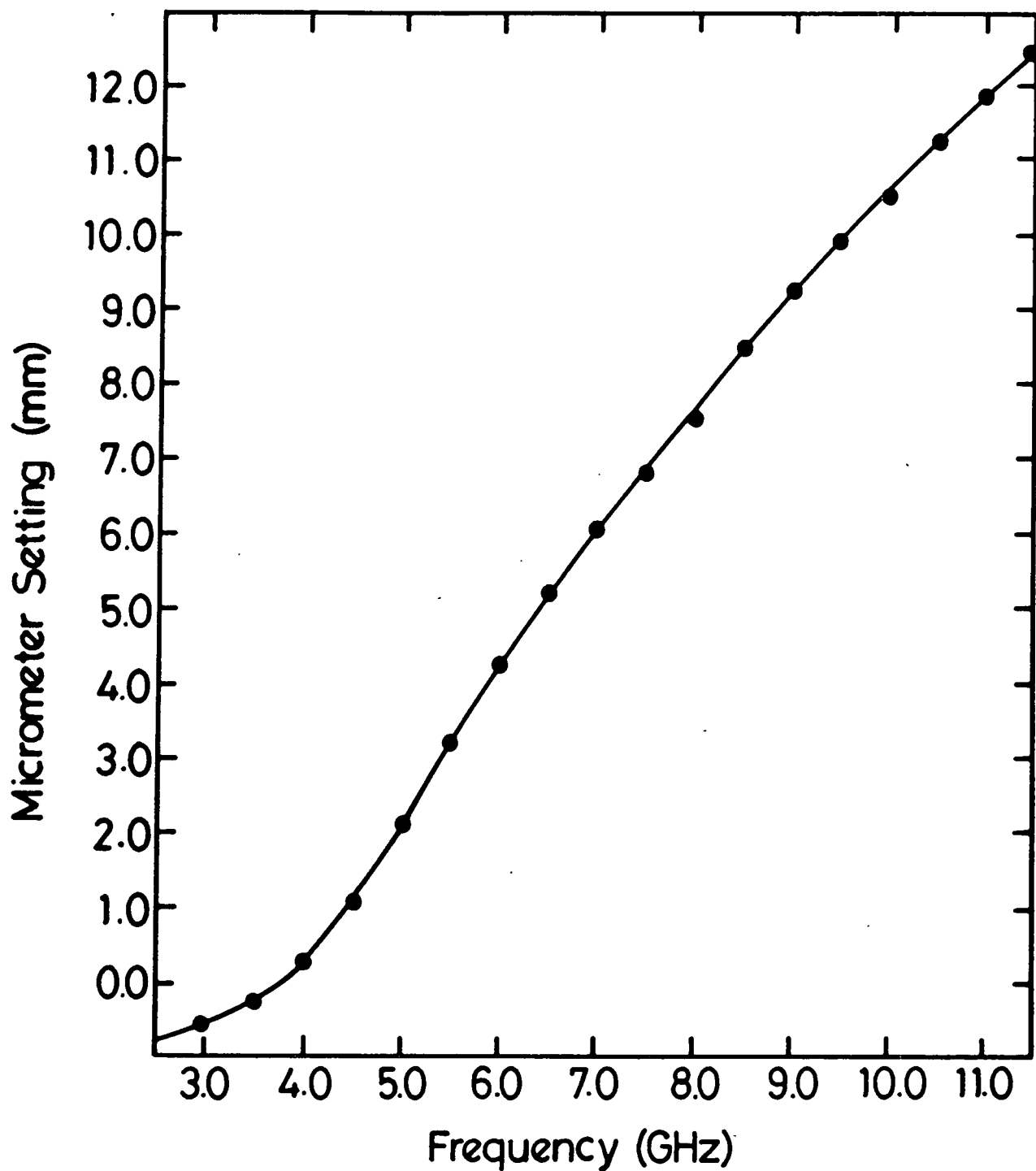


FIG 4.7: Variations of Micrometer Setting With Frequency for the Coaxial Cavity

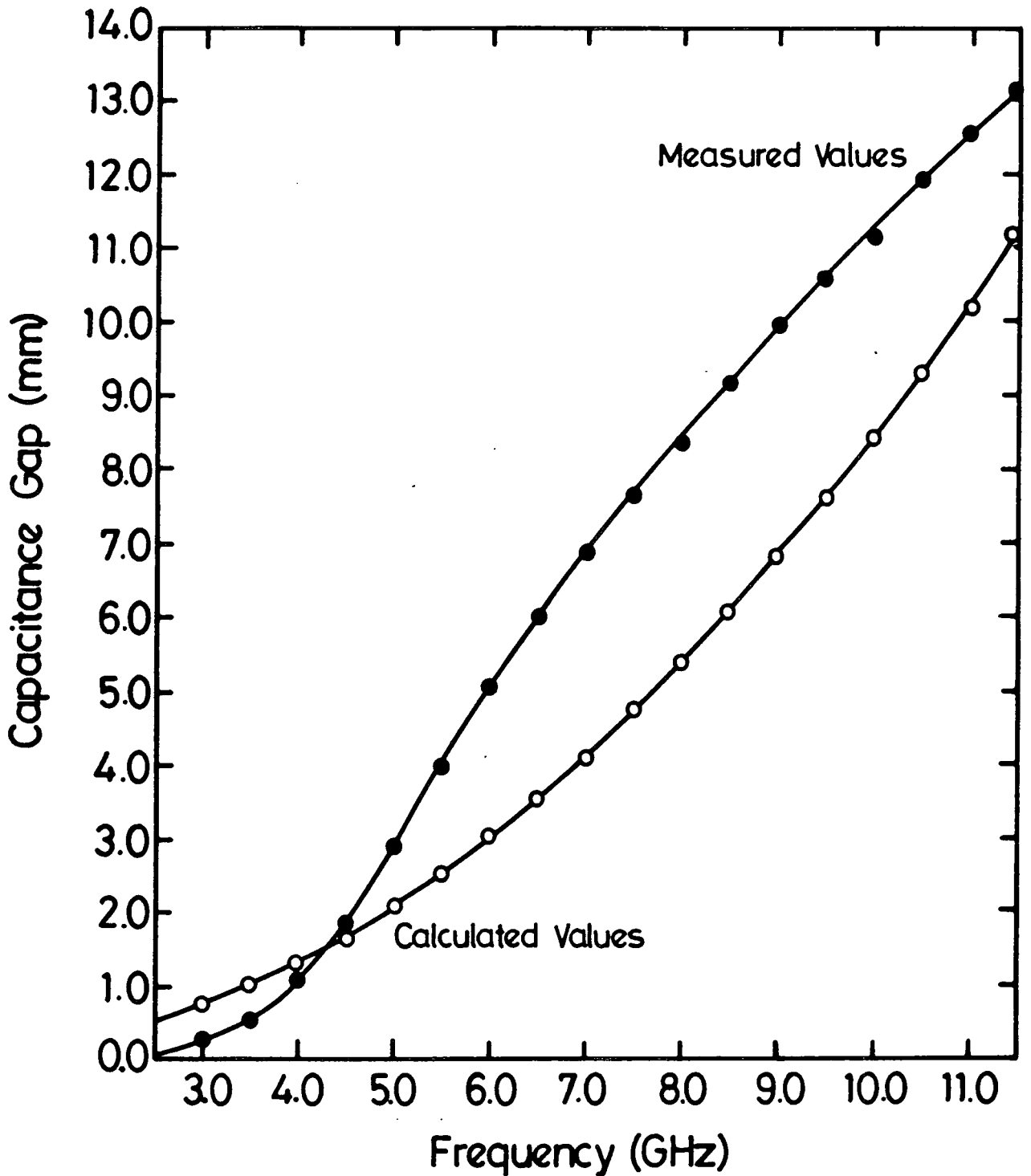


FIG 4.8: Comparison Between the Measured and Calculated Capacitance Gaps for the Coaxial Cavity at Different Frequencies

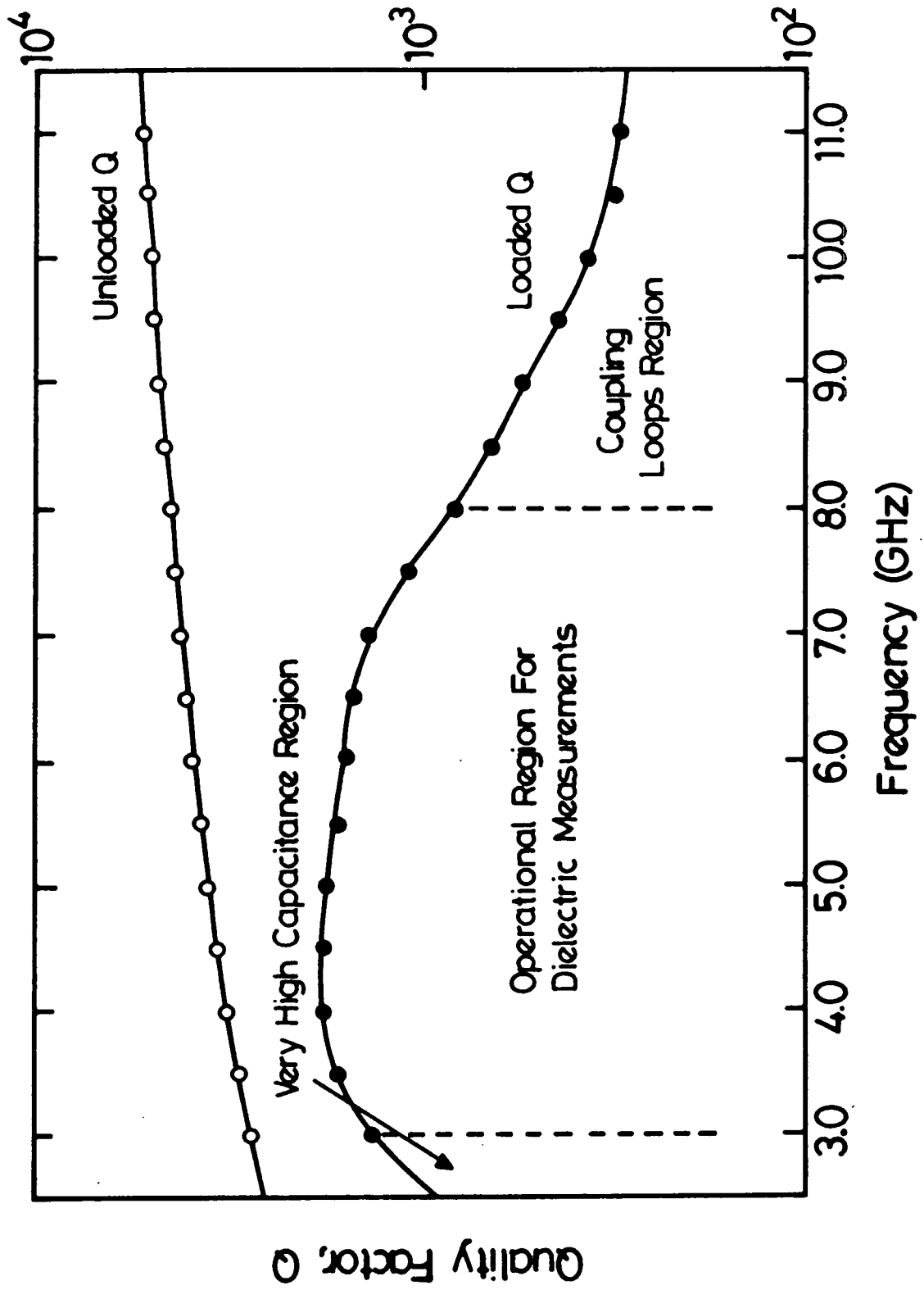


FIG 4.9: The Loaded and Unloaded  $Q$  of the Coaxial Cavity

conducting surfaces when the quality factors were calculated (eqn.2.12). It was also found that dielectric measurements could only be carried out accurately in the frequency range between 3 GHz and 8 GHz.

The length of the inner conductor, which tuned with the capacitive reactance formed by the gap between itself and the bottom wall of the coaxial cavity was also measured at different frequencies. For an ideal case the transmission line should be of length just less than a quarter wavelength with an electrical length of  $\pi/2$  in the constructed coaxial cavity. The length was found to be less than a quarter wavelength which meant its input impedance was still an inductive reactance which can resonate with the capacitive reactance present in the cavity. The corresponding electrical length of 52 (min.) and 71 (max.) were found at 3 GHz and 5 GHz respectively, indicating that the coupling performance is frequency dependent. The above details are shown in Fig.4.10 .

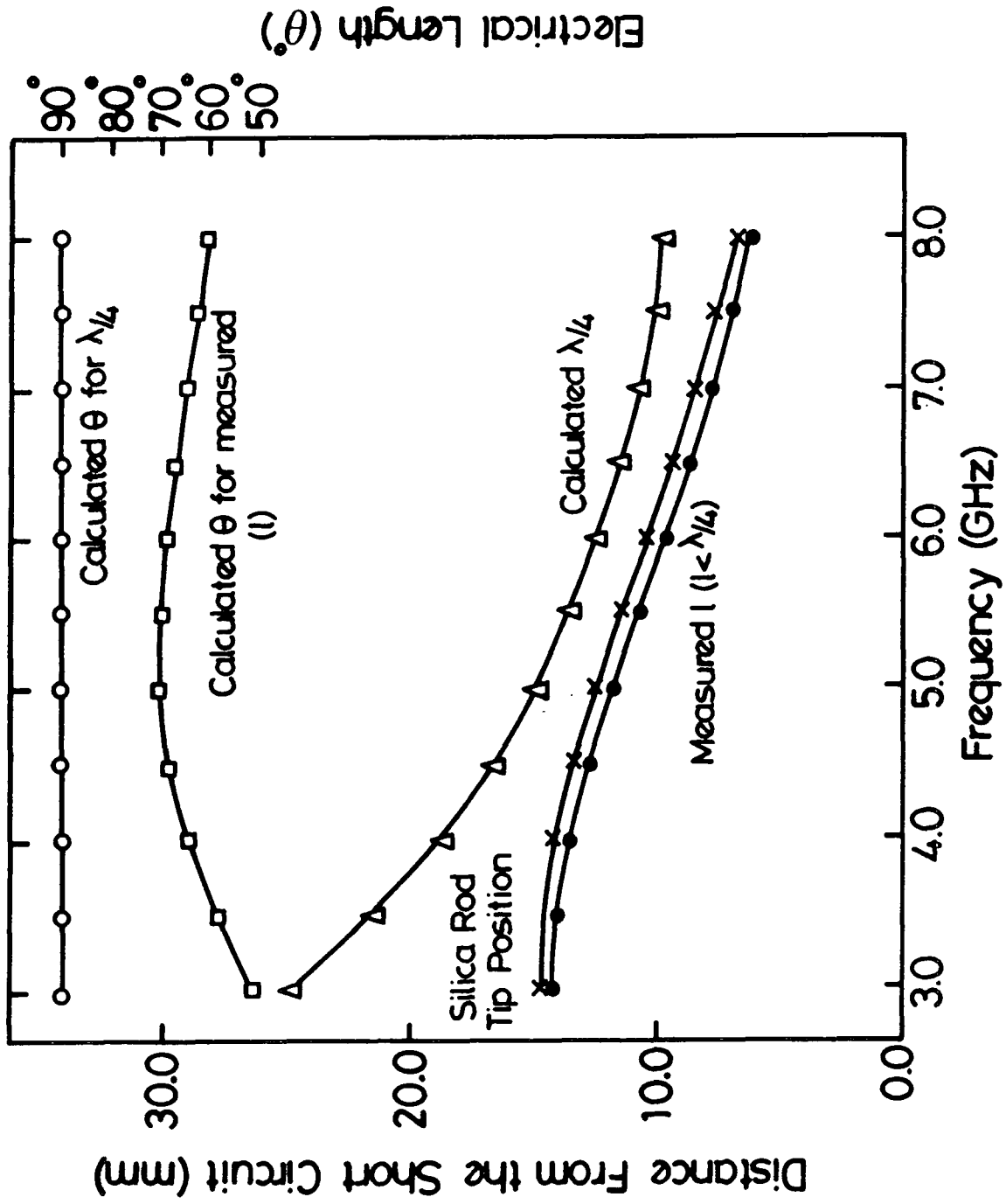


FIG 4.10: The Relationship Between the Electrical and Physical Length of the Coaxial Cavity Inner Conductor

CHAPTER 5DIELECTRIC MATERIALS FOR VLSI\* SUBSTRATES5.1 Introduction

The need for careful selection and evaluation of substrate materials for multiple-line, microstrip packaging should be apparent under any circumstances. An electrical operation within the claimed specification and hence higher yields in quantity production could be the main benefit. In order to achieve such aims it is necessary to become aware of the difficulties that may be encountered before the assembly of the final package. In carrying out precision measurements of the material properties beforehand may expose possible problems in processes which at an early stage can still be modified or corrected.

Many reasons may be responsible for the inadequacy or excellence of a completed package performance and the characteristics of the substrate used will certainly make an important contribution. The properties of substrates that may be of interest to VLSI package designers can be grouped under three general headings:-

- (i) electrical mainly dielectric
- (ii) thermal
- and (iii) mechanical

\*[VLSI]: Very Large Scale Integration.

Electrical or specifically dielectric properties is the subject of this chapter and the importance of substrate fabrication and the factors that might control its properties are examined and discussed in para. 5.7.

Changes in the substrate dielectric properties will, in turn, have an effect on the line secondary constants, i.e. characteristic impedance,  $Z_0$ , and propagation constant,  $\gamma$ . These line parameters directly affect transmission of signals to and from the line especially, attenuation,  $\alpha$ , and phase shift,  $\beta$ , the real and imaginary parts of the propagation constant, respectively.

## 5.2 Electrical Properties

### 5.2.1 Fundamental Dielectric Parameters and Definitions

The electrical properties of insulating and semiconducting materials are primarily determined by the dielectric constant or permittivity and the dielectric loss combined into a single complex expression

$$\epsilon = \epsilon' - j\epsilon'' = \epsilon_0(\epsilon_r' - j\epsilon_r'')$$

The former, the dielectric constant,  $\epsilon_r'$ , represents a change in the velocity of signal transmission due to the medium giving the velocity in the substrate as

$$v = \frac{c}{\sqrt{\epsilon_r}}$$

where  $c$  is the velocity of signal in air or vacuum and  $\epsilon_r$  is the relative dielectric constant. This in turn is used to determine the effective relative dielectric constant sometimes called permittivity  $\epsilon_{re}$ , applicable in the case of semi-TEM lines such as microstrip, and hence the characteristic impedance and transmission properties of the line. The latter, the dielectric loss parameter  $\epsilon_r^*$  represents the energy loss and is a function of conductivity or resistivity of the material. The ratio of energy dissipated to energy stored termed "the tangent of the loss angle" or simply "loss tangent" of the material is expressed as

$$\tan\delta = \frac{\epsilon_r^*}{\epsilon_r}$$

It is also known as the dissipation factor.

### 5.2.2 Propagation Properties

The complex propagation constant for signals transmission through a homogeneous medium comprises  $\alpha$  the attenuation and  $\beta$  the phase shift coefficients, and is usually expressed as

$$\gamma = \alpha + j\beta$$

where

$\alpha$  is in nepers (or dB) per unit length and  $\beta$  is in radians per unit length.

The propagation constant depends on the dielectric properties of the medium, the permittivity,  $\epsilon'$ , dielectric loss,  $\epsilon''$ , and hence the phase velocity at a particular frequency.

The connection between the propagation constant and the complex relative permittivity may be derived from the fundamental relationship for a homogeneous dielectric space, i.e.

$$\gamma = j \frac{2\pi}{c} f \sqrt{\epsilon' - j\epsilon''}$$

resulting in equations for  $\alpha$  and  $\beta$  in terms of permittivity and dielectric loss [43], i.e.

$$\frac{\alpha}{\beta} = \left( \frac{2\pi}{\lambda} \right) \left( \frac{\epsilon'}{2} \right)^{1/2} \left\{ \left[ 1 + \left( \frac{\epsilon''}{\epsilon'} \right)^2 \right]^{1/2} \mp 1 \right\}^{1/2} \quad (5.1)$$

Alternatively,  $\epsilon'$  and  $\epsilon''$  may be expressed as function of  $\alpha$  and  $\beta$  i.e.

$$\epsilon_r' = \left( \frac{\lambda \beta}{2\pi} \right)^2 \left[ 1 - \left( \frac{\alpha}{\beta} \right)^2 \right]$$

and

$$\epsilon_r'' = \left( \frac{\lambda \beta}{2\pi} \right)^2 \frac{2\alpha}{\beta}$$

Above equations will assume modified versions if we consider, for example, a rectangular dielectric-filled waveguide or a microstrip transmission line etc..

The first set of equations will normally be used to predict the effect of permittivity and dielectric loss ( $\epsilon'$  &  $\epsilon''$ ) on the signal in transmission. The second set of equations, on the other hand, may be used to determine dielectric properties of a substrate from the attenuation and phase shift or phase velocity measurements.

### 5.3 Molecular Properties of Dielectrics

The polarization mechanisms which can take place in materials are related to the definition of complex dielectric constant and its resulting electrical properties.

There are no free charges in an ideal dielectric material. The atoms of a dielectric are normally affected by the applied electric field. The result of this field is a force which is exerted on each charged particle. Therefore, the particles with positive

electric charge are being attracted in the direction of the field, and those with negative charge in the opposite direction. As a result, the positive and negative charged ions of each atom are displaced from their equilibrium positions in opposite directions.

This condition of a dielectric is called polarization which depends on the total electric field in the material. It is also defined as electric dipole moment per unit volume .

The degree of polarization depends on the electric field and the properties of atoms which make the material. There are four mechanisms of polarization [44]

- (i) Electronic Polarization,
- (ii) Ionic Polarization,
- (iii) Dipole Polarization,
- and (iv) Space-charge Polarization.

In the first mechanism , the electrons are slightly displaced relative to the nucleus as a result of applying an external electric field to the dielectric. This creates an electric dipole moment causing an electronic polarization to occur in the system . This is shown in Fig.5.1(a).

In the second mechanism , ionic polarization , the positive and negative ions in a partially ionic solid are displaced from their equilibrium positions when an

external electric field is applied . This is shown in Fig.5.2(b).

In the third mechanism, dipole orientation , atoms with displaced positive and negative charges of the dipole, tend to orientate themselves in a direction opposite to that of the applied electric field. This is shown in 5.1(c).





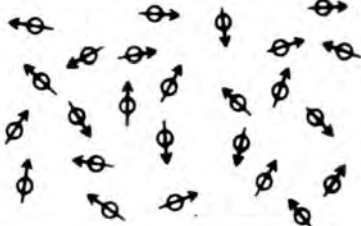
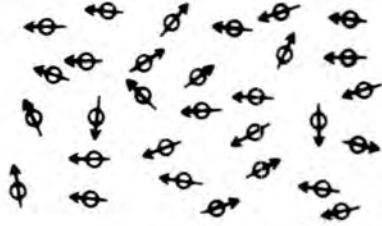
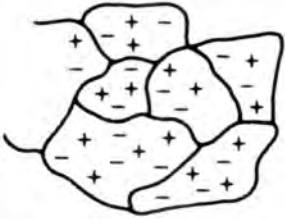

The last mechanism, space-charge polarization, generally only occurs in solids, multiphase dielectrics in which the various phases or components have different dielectric constants. (see Fig.5.1(d)).

It is known that the direction of the electric field is from positive to negative charges but the orientation of dipoles in the dielectrics is in opposition to the direction of the electric field. This condition results in the reduction of the electric component with the applied field.

Each type of polarization is characterized by a relaxation time  $\tau$  , which represents the time taken for the polarization to respond to the removal of the applied electric field.

#### 5.4 Frequency and Temperature Dependence of $\epsilon'$ and $\epsilon''$

The dielectric response of a solid medium reflects the various polarizing contributions present - permanent and induced dipoles, electrons and ions, each of which is characterized by the specific dependence of its

Type of polarisation mechanism	Condition with no electric field $E = 0$	Condition with electric field $\vec{E}$
(a) Electronic polarisation		
(b) Ionic polarisation		
(c) Orientation or dipolar polarisation		
(d) Space-charge polarisation		

**FIG 5.1: Schematic Representation of the Different Types of Polarisation Mechanisms**

complex dielectric permittivity, on the temperature, and on the frequency.

When an electric field of frequency,  $f$ , is applied to the dielectric, each type of polarization can only make its full contribution to the total polarization as long as the period of oscillation,  $T$ , of the field is much greater than the relaxation time,  $\tau$ . The time required for electronic or ionic polarization to be established is very small compared with the period of the applied field. For this case, there is no reason to expect that any frequency dependence should appear in such dielectrics.

In the case of the dipole polarization mechanism, the value of  $\epsilon'$  of the dielectric begins to drop when the frequency begins to increase because the relaxation time of the dipole orientation is comparable to the period of oscillation.

In general, as the frequency is increased it is reasonable to expect that the total polarization will decrease and hence  $\epsilon'$  will decrease. Some of the energy will be lost in the dielectric as a result of the random thermal motion that exist in any substance and therefore as  $\epsilon'$  decreases,  $\epsilon''$  increases.

In practice, both  $\epsilon'$  and  $\epsilon''$  may vary with frequency and this will depend on the type of the dielectric polarization involved.

The responses of the individual polarizing contributions are undoubtedly dominated by many-body interact-

ions, resulting in a characteristic "universal" form [45] of frequency dependence of dielectric constant and loss, i.e.

$$(\epsilon' - \epsilon'_\infty) \propto \omega^{-(n-1)}$$

$$\text{and } \epsilon'' \propto \omega^{-(n-1)}$$
(5.2)

where

$\epsilon'_\infty$  is the high frequency value of  $\epsilon'$  and the exponent  $n$ , lies in the range  $0 < n < 1$ .

The nature of the dependence of dielectric properties on temperature may be determined by a number of factors. In most cases when the temperature increases, the ionic process of polarization increases and hence  $\epsilon'$  will increase. In contrast, the increase of temperature does not affect the electronic polarization because the temperature affects the nuclei and electrons by the same degree. But since thermal energy increases the rate of vibration of atoms, the dipole or orientation polarization does vary with temperature. In practice, both  $\epsilon'$  and  $\epsilon''$  may increase with temperature.

### 5.5 Dielectric Breakdown

The failure of dielectrics under sufficiently high electric field is referred to as "breakdown". The "breakdown" field depends, on the nature and composition

of the sample, its shape, its environment, and on the method by which the external field is applied (d.c, a.c, square pulse, etc ...).

Two basic mechanisms of "breakdown" can be distinguished. The first of these is termed as "intrinsic breakdown". In this case as the applied voltage is increased from zero, a small current will begin to flow reaching quickly a saturation value. As the voltage continues to rise, this current remains constant until a certain critical voltage,  $V_b$ , is attained. At this point the current suddenly rises rapidly resulting in dielectric breakdown.

The second mechanism is known "thermal breakdown". This occurs whenever the Joule heating in the sample cannot be extracted fast enough resulting in a permanent damage to the sample because of temperature rise.

### 5.6 Survey of Substrate Materials

Materials may be grouped according to the predominant component present in their composition. In practice, purity is not normally maintained, as additions are deliberately introduced to improve particular properties or make the material less sensitive to fabrication processes or environmental conditions. However, in general, for substrate applications, we can distinguish three families of materials under the names, polymers,

ceramics, and glasses.

Historically, polymers as substrates were first on the scene, when low permittivity plastics were employed in early microstrip assemblies and experiments of the 1950's. These were not very successful and were eventually replaced by PTFE (Teflon)/glass laminates in the 1960's. Further developments and compounding with cloth, microfibre, glass and ceramic-filled displaced predominantly polystyrene products in many applications, with their problems of cracking and softening due to temperature. Many of teflon based materials are still used today offering a wide range of substrates and laminates with low dielectric constants and acceptable dissipation factors. Higher values of dielectric constants between 6 and 10, are also available with ceramic-filled PTFE/Glass composites.

Characteristic properties of stability and hardness found in the majority of ceramics makes them very popular substrate materials. The ceramic group includes a large number of compounds of metallic and nonmetallic elements available in nature. Majority of them are based on silicate structures (similar to those found in clay, cement, fired earthenware and china) resulting from reactions of silica (or silicon oxide,  $\text{SiO}_2$ ) with oxides of various elements. The most widely used nonsilicate material, in pure form or with other oxides, for production of ceramics is alumina (corundum) or

aluminium oxides ( $\text{Al}_2\text{O}_3$ ). Structures containing various percentages of alumina and other oxides are known as mullite or spinels and are used where heat-resistant or refractory materials are needed. Nitrides, such as boron nitride (BN) and silicon nitride ( $\text{Si}_3\text{N}_4$ ) of high density which are inert and oxidation-resistant up to high temperature ( $\sim 1500^\circ\text{C}$ ) are also used for new composite ceramics.

Ceramic substrates may be categorised according to the availability or abundance of the materials for their fabrication, costs and hazards involved in manufacturing processes, reproducibility and applications.

The reason for including glasses in the survey of possible substrates were to emphasize some of the more unusual characteristics in comparison to ceramics and polymers, their usage in the reinforcement of other materials and enhancement of particular properties. Glasses are basically supercooled liquids and most of them, known as silicate glasses are composed of silicon oxide (>50%) and other oxides added to obtain a wide range of different properties. If cooled over a long period of time and heat-treated they are transformed by recrystallisation into what is known as devitrified glass ceramic with its low coefficient of thermal expansion and absence of porosity. Although, usual applications at high frequencies are mainly for lumped elements and, in a limited way, microwave integrated

circuits, their properties are comparable with other substrate materials except for the thermal conductivity which may be too low for packaging.

A wide range of dielectric materials is available for substrate use. It may be also apparent that each material can usually be found a specific application or a number of applications for which its properties are adequate. The requirement of some packages may not be as stringent as it appears and less expensive materials, possibly of polymeric type, could be completely satisfactory in performance.

## 5.7 Manufacture and Testing of Substrate Materials

### 5.7.1 Introduction

There are many processes involved in the manufacture of substrate materials and therefore to maintain high yield in reproducibility will normally be a difficult task. The selection of ingredient minerals and compounds for the intended composition and ultimate dielectric properties will initially demand preliminary measurements to establish permissible tolerances in the purity of the components. Most of the processes that follow are mainly concerned with the accomplishing a well blended, often under high temperatures, composition into required shapes.

Production of a material, in general, will incorporate four fundamental stages, namely, crushing, wet



mixing, shaping and sintering (or drying and firing) . The measurements of dielectric constant and dissipation factor may be advisable between these processes as intermediate quality checks and certainly during the first few production runs. It is possible that such tests may expose any problems in the mixing processes and timing of various stages. At the end of the fabrication the measurements of dielectric properties will have additional objectives to determine, for example, the degree of dielectric inhomogeneity and anisotropy of the final samples.

Apart from the need to satisfy the required dielectric qualities, substrates will have to possess physical properties such as stickiness, structural strength, high thermal conductivity, machinability etc. These are normally achieved by introducing various additives to impart the desirable characteristics. The effect of these additives on dielectric properties will normally have to be monitored and recorded.

#### 5.7.2 Production Processes and Stages

After the essential components have been prepared and tested for impurities the objective next is to crush or grind the raw materials and the special additives into a powder. The granularity or the size of particles of individual constituents is of some importance, the finer it is the better mixture is obtained leading to a more

homogeneous and isotropic result. The materials of the grinding tools could at this point contribute to the composition which may be detectable when measurements of the substrate powder are carried out, e.g. iron impurities.

In the second stage, dry powder has a lubricant added to reduce friction between particles and avoid clotting, also melting and binding agents to make the mixture semifluid formable mass. Other additives may also be included here for the final sample to acquire particular physical properties such as adhesiveness, elasticity, mechanical strength etc. ... There may be a process of drying next if the mixture is found to contain too much moisture which could make the following step of shaping difficult to achieve.

Checks on the properties at the end of this process will possibly produce widely-varying results in addition to creating problems in the contrivance of the measurement methods. The information obtained may not be correct and not of much use and consequently testing outlay will not be justified at this stage.

The shaping stage involved a number of different processes depending on the geometry of the final product and applications. Among the method casting, injection moulding or extraction, compaction and hot pressing are self explanatory and recognised as the main shaping techniques. The first two, casting and injection

moulding, are the methods for which the material should have sufficient fluidity and low viscosity to allow an easy flow. For the other two, the moisture content will have to be reduced to below 4% unless wet pressing method is used which allows between 10 and 15% moisture content, making the latter in fact a plastic forming process. In hot pressing, the pressure and temperature are applied at the same time resulting in low porosity and denser materials. This latter method is possibly the one which will be used in the case of substrate materials and being a penultimate process may require a measurement check on the properties.

The final bonding or sintering process, also known as drying and firing, is carried out at high temperatures to give the material its proper strength. It is a very critical stage since an unwelcome cracking and/or warping may occur unless the environmental conditions and the applied temperatures are strictly controlled. Movement of moisture to the surface and its loss by evaporation, even under humid conditions, can result in unequal rates of shrinking creating as a consequence tensile or stress forces within the sample. Localised higher temperature areas can also produce glassy bond (crystallisation) adding to the inhomogeneity of the material properties. During the process physical properties such as porosity, the strength and hardness, also adhesion property of metal

deposition are significantly affected by the manner in which individual operations are timed and sequenced. After firing, additional machining may be necessary to eliminate any imperfections in order to improve surface finish which may also include chemical means.

### 5.7.3 Colour in Ceramics

Colour in oxide ceramics and glasses is produced by impurity atoms in the lattice. Particular frequencies are absorbed by the electronic structure associated with the impurity site, and this gives reduced transmission in parts of the spectrum. Transition metals, particularly V, Cr, Mn, Fe, Co, Ni, and Cu and combination of these, are most effective in producing colour. The colour may also be dependent on the atmosphere used in firing or melting because the valency state of many of those listed above may be altered, and this changes the electronic configuration and hence the absorption spectrum.

Iron is a very common impurity in all raw materials, and produces coloration from slight creaminess through to orange in otherwise white products. "Whiteness" is often preferred because products tends to sell better, but this requires more expensive processing, purer raw materials, and perhaps even reduction firing, to keep iron in the ferrous state in which it tends to cause a dead white rather than a yellow colour. Brown or black

aluminas contains ingredients necessary for the fabrication process.

Although the colour of oxide-based technical and engineering ceramics can be changed deliberately by the addition of secondary oxides of various types, this usually done for commercial reasons. Deliberate coloration gives some identity to a product. In some instances, dark-coloured oxide ceramics are advantageous in the end use, e.g. substrates for photo-electronic devices.

#### 5.8 Test Materials

As it has been mentioned, the VLSI materials used in this project were mainly for the assessment of the validity and accuracy of the new Sweep Generator/Spectrum Analyzer Assembly technique, and also a test of the capability of the constructed broadband coaxial cavity to be used for dielectric measurements.

Some of these materials are known very often only by their trade names with composition and ingredients not been freely available as information to the customer. They are mainly oxide and glass ceramics and are summarized in Table (1).

Although dielectric properties of materials used in VLSI applications played an important role, the requirements of the microelectronic circuits are not restrictive. Most of the circuits can accept dielectric constant and dielectric loss of very wide ranging values.

Table (1): List of Ceramic Materials Used

- 1- Coors ADS 995 (polycrystalline alumina, 99.5%  $Al_2O_3$ )
- 2- Coors ADS 96R (polycrystalline alumina, 99%  $Al_2O_3$ )
- 3- Coors ADO 90 (polycrystalline alumina, black, 90%  $Al_2O_3$ )
- 4- Vitox (high density  $Al_2O_3$ )
- 5- NK2/3447 (glass ceramics cordierite based)
- 6- NK2/3802 (glass ceramics cordierite based)
- 7- Glass Ceramics
- 8- MRC
- 9- NTK
- 10- Rosenthal
- 11- Alsimag
- 12- Thomson
- 13- Deranox
- 14- Hoechst
- 15- Kyocera

CHAPTER 6MEASUREMENT METHODS AND TECHNIQUES6.1 Introduction

In order to determine the dielectric properties of a material over a wide range of frequencies, it is usually necessary to use different measurement methods.

At low frequencies, the dielectric properties of materials are normally determined by measuring the capacitance and conductance of a sample using the bridge method or by measuring the capacitance and the quality factor due to the sample using the Q-meter technique.

The sample is normally placed between a pair of micrometer electrodes and the entire system is contained in a metal shielding box to eliminate undesirable effects of stray fields.

At high frequencies, there are several methods available for obtaining the dielectric properties of materials. Two methods will be described in this chapter. The first, called the reflectometer method, involves the ratio of reflected to incident powers, while the second method uses a spectrum analyzer to display the response of the cavity with and without the material sample whose dielectric properties are to be determined.

## 6.2. Bridge Method

### 6.2.1 Theory

The components of the complex dielectric constant ( $\epsilon'$ ), and the loss tangent ( $\tan\delta$ ) of a sample can be deduced from the following equations [46,47],

$$\epsilon' = \frac{C}{C_0} \quad (6.1)$$

$$\tan\delta = \frac{G}{\omega C} = \frac{\epsilon''}{\epsilon'} \quad (6.2)$$

$$C_0 = \frac{\epsilon_0 A}{d} \quad (6.3)$$

where

$C$  = capacitance of sample,

$C_0$  = capacitance between electrodes (air),

$G$  = conductance of sample,

$\omega$  = angular frequency,

$d$  = thickness of sample,

$A$  = cross-sectional area of electrodes,

and  $\epsilon_0$  = permittivity of free space =  $8.85 \times 10^{-12}$  (Fcm<sup>-1</sup>).

However, the final equation must include the correction factor for the edge effects capacitance  $C_e$  with circular electrodes of the same diameter  $D$  given by

[48].

$$C_{\infty} = \frac{1.113D}{8TT} \left( \ln \frac{8TTD}{d} - 3 \right) \quad \text{in (pF)} \quad (6.4)$$

leading to

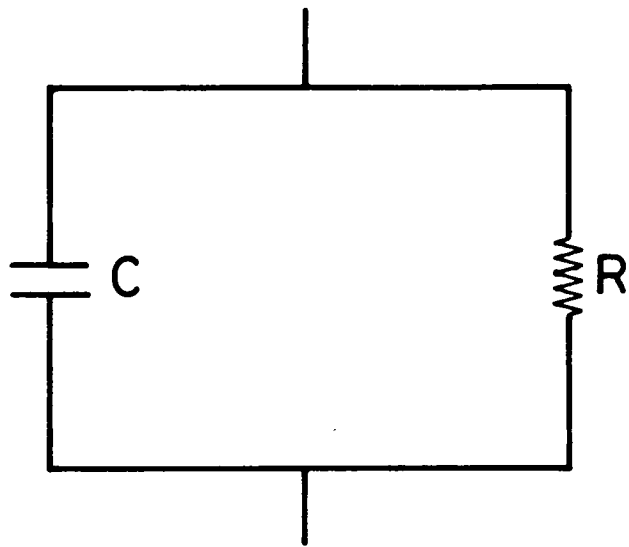
$$\epsilon' = \frac{C}{C_0 + C_{\infty}} \quad (6.5)$$

Since the stray capacitance due to the electrodes is included in the measured value of  $C$ , another correction factor may be needed before the true capacitance of the sample can be determined.

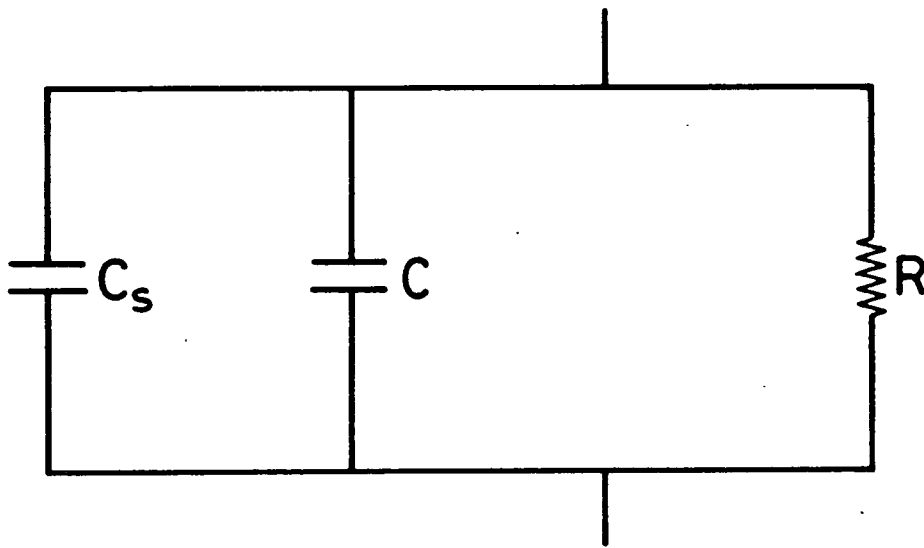
The equivalent circuit of the sample is shown in Fig.6.1.a. In this circuit the sample is represented by a capacitance,  $C$ , shunted by the resistance,  $R$ , representing the loss. These quantities are the true values of capacitance and resistance of the sample and can be calculated from the measured results.

Let  $C_0$  be the stray capacitance associated with the electrodes and connecting cables. It is assumed to be in parallel with  $C$  as shown in Fig.6.1.b.

The conductance has been omitted since the performance is being measured at low frequency and its effect is considered insignificant. It is intended that the leakage admittance effect is included by using the correction



(a)



(b)

FIG 6.1: Equivalent Circuits of Dielectric Sample

factor.

Accordingly, the total capacitance,  $C_t$ , measured on the bridge, when the sample is placed between the electrodes, can be written as.

$$C_t = C + C_s \quad (6.6)$$

When the sample is removed, the capacitance due to the air gap can be written as

$$C_a = C_o + C_s \quad (6.7)$$

On substitution for  $C_s$  from eqns. (6.6) & (6.7), the capacitance,  $C$ , of the sample now can be expressed as

$$C = C_t - C_a + C_o \quad (6.8)$$

Finally, combining eqns. (6.2), (6.5) & (6.8) yields

$$\epsilon' = \frac{C_t - C_a + C_o}{C_o + C_s} \quad (6.9)$$

$$\tan \delta = \frac{G}{\omega(C_t - C_a + C_o)} \quad (6.10)$$

In the above equations  $C_t$ ,  $C_a$  &  $G$  are measurable quantities and  $C_o$  can be found from eqn. (6.3).

### 6.2.2 Measurement Procedure

The Universal Bridge to be used should be calibrated (trimmed) before taking any measurements because the capacitance of the measurement cables and the coupling between them and the test jig would give rise to false zero readings. The TRIM potentiometer enables these effects to be balanced out.

Initially, the measurements cables to be used were connected to the UNKNOWN sockets E and I of the Bridge and the LINK-NEUTRALS switch was set to the ON position. Then the RANGE 4 was selected and all the decade controls were set to zero. The C and G buttons were depressed to reading 1. Finally, TRIM C and TRIM G were adjusted to obtain minimum indication on the NULL indicating meter (see Fig.6.2).

Although the trimming conditions established on RANGE 4 will be approximately correct on RANGE 4-10, it is desirable always to check the trim on the RANGE finally selected for measurement, with the setting of the MULTIPLIER switches determined for any special jigs connected [47].

The balance of the Bridge was obtained to minimize the effect of any residual capacitance and conductance. The material sample was then inserted between the electrodes of the test jig and the Bridge was rebalanced. The capacitance and the conductance of the sample were



FIG 6.2: Indicators and Connectors of Wayne Kerr Universal Bridge B224

measured directly. The corresponding capacitance and conductance of the air gap were similarly measured. Finally, from the above information the dielectric constant and the loss tangent of the material were calculated solving eqns. (6.9) & (6.10).

Gough and Isard [49] have mentioned errors up to about 10% in  $\epsilon'$  and  $\tan\delta$  can arise in the cases when dielectric measurement are made without metallic coatings. It is found necessary for elimination of any air gaps between the main electrodes and the sample to use gold contacts. Circular gold electrodes of 7mm diameter were evaporated on the opposite surfaces of the sample ( $1 \times 1 \text{cm}^2$ ) to ensure a good electrical contact over a well defined area between the sample and the electrodes of the dielectric test jig shown in Fig.6.3 .

The measuring jig is usually assembled in a metal box to eliminate undesirable effects due to external stray fields and to provide the sample with a high degree of electrical shielding. Fig.6.4 shows the effect of the stray capacitance due to the fringing effect.

In the present measurements, the dielectric constant and the loss tangent of various ceramics were determined with and without gold contacts on the sample and the results are presented in the next chapter.

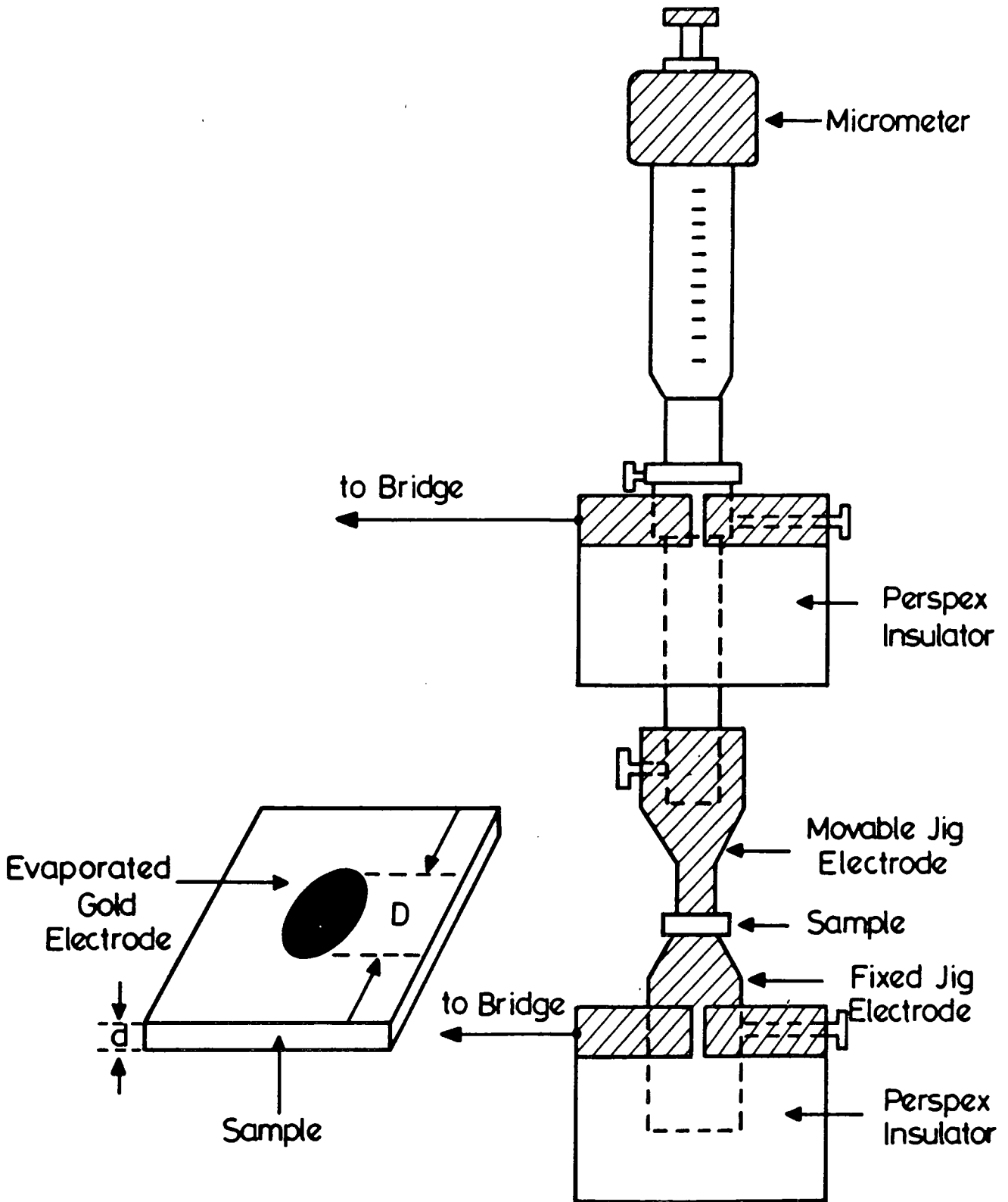


FIG 6.3: General Form of Specimen and Dielectric Testing Jig

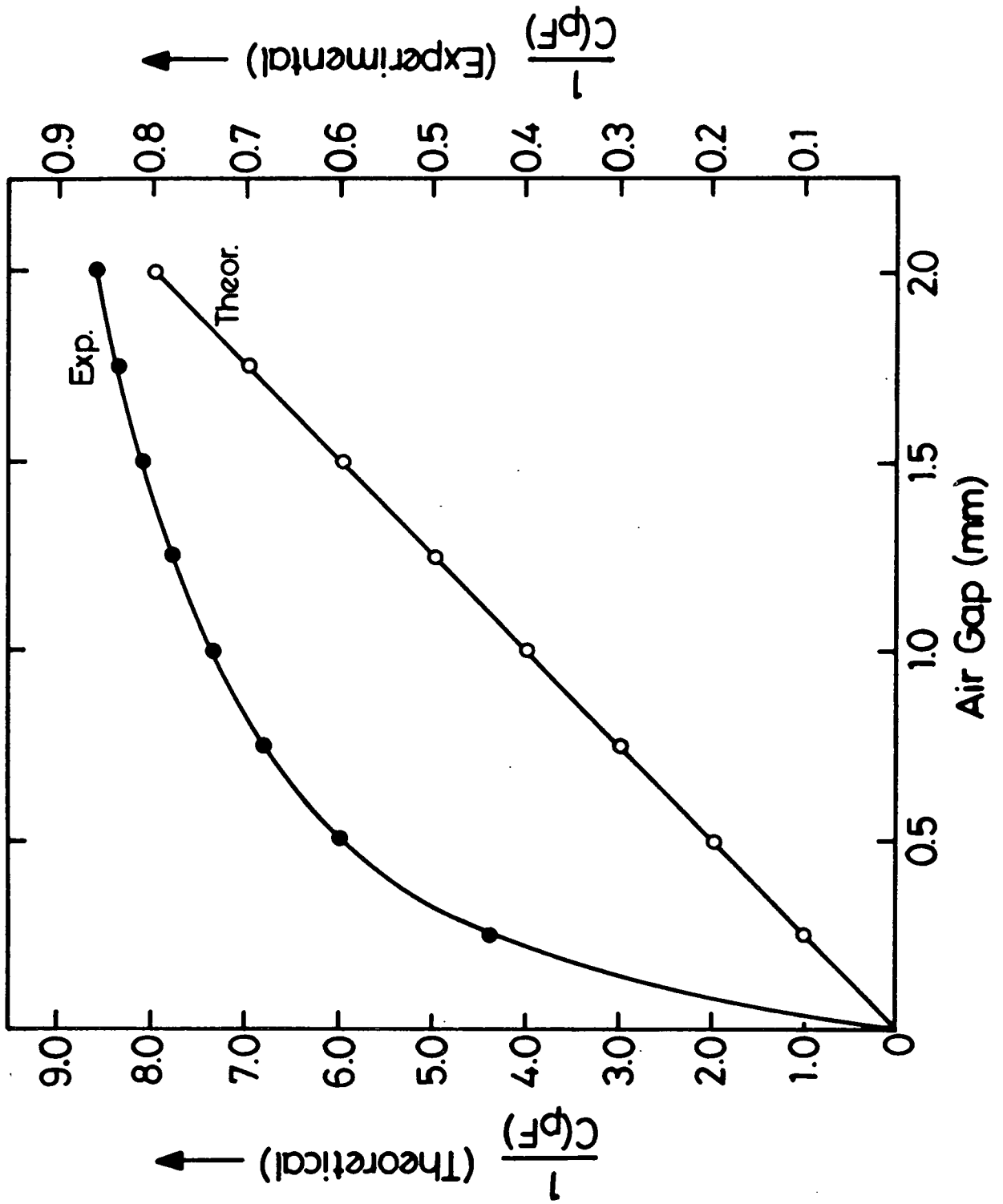


FIG 6.4: Effect of the Stray Capacitance Due to Fringing Effect

### 6.3. Q-Meter Method

#### 6.3.1 Theory

The principle of the Q-meter circuit is based on the series resonant circuit. Its equivalent circuit is shown in Fig.6.5 . It consists of resistor, R, which represents the internal resistance of the circuit, inductor, L , and capacitor, C , all in series and connected to a variable signal source. Taking L and C as the total inductance and capacitance we have the resonant frequency

$$f_0 = \frac{1}{2\pi\sqrt{LC}} \quad (6.11)$$

At resonance, the total capacitance,  $C_T$ , of the circuit without the sample can be written as

$$C_T = C_1 + C_0 + C_H + C_L \quad (6.12)$$

where

$C_1$  = the variable capacitance of the Q-meter,

$C_H$  = capacitance of the sample holder,

$C_L$  = capacitance of the connecting cables,

$C_0$  = capacitance due to the air gap.

By inserting the sample between the electrodes,  $C_1$  changes to  $C_2$  and therefore  $C_T$  will now become

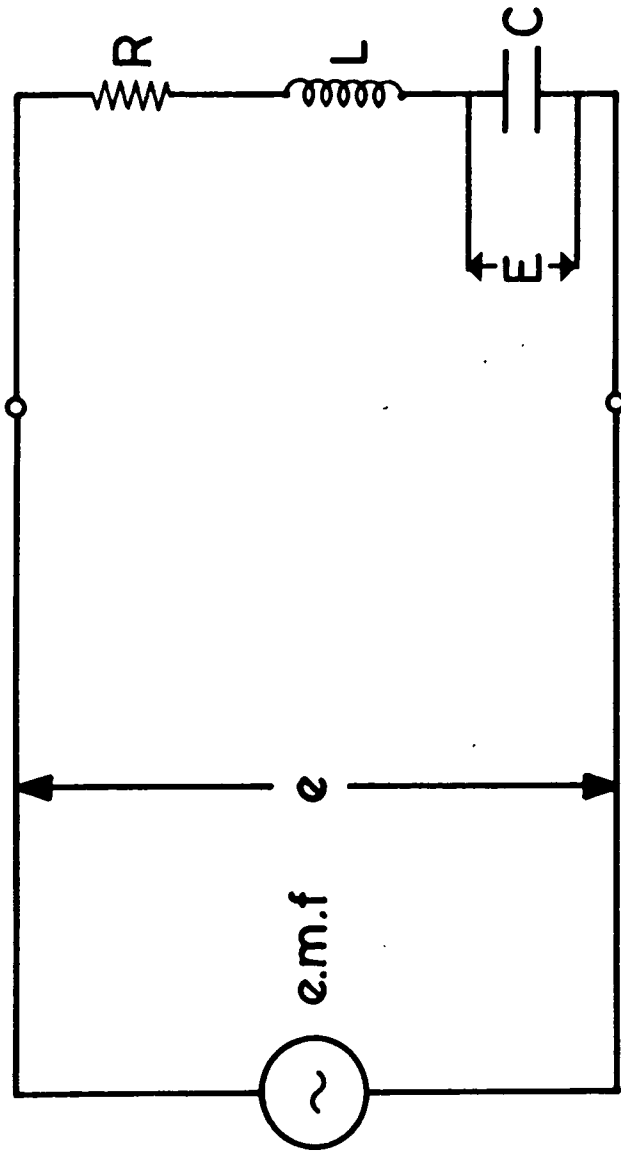


FIG 6.5: Equivalent Resonant Circuit of the Q-Meter

$$C_T = C_2 + C + C_H + C_L \quad (6.13)$$

where

$C$  is the sample capacitance.

Equating eqn. (6.12) and (6.13) yields

$$C_1 - C_2 = C - C_0 \quad (6.14)$$

Substituting this in eqn. (6.1) and adding the edge effects, i.e.  $C_0$ , we finally get

$$\epsilon' = \frac{C_1 - C_2}{C_0 - C_0} + 1 \quad (6.15)$$

The loss tangent of the sample can also be calculated [50] from

$$\tan \delta = \frac{Q_1 - Q_2}{Q_1 Q_2} \frac{C_1}{C_1 - C_2} = \frac{\epsilon''}{\epsilon'} \quad (6.16)$$

where

$Q_1$  and  $Q_2$  are the  $Q$ -values of the circuit without and with the sample, respectively.

In practice, knowledge of the effective capacitances ( $C_e$ ) of  $C_1$  and  $C_2$  are required and it is given by [50]

$$C_E = C_{ind} \frac{1}{1 - \omega^2 LC_{ind}} \quad (6.17)$$

where

$C_{ind}$  is equal to the indicated measured capacitances  $C_1$ ,  $C_2$  and  $L$  is the inductor used in the resonant circuit.

In general, it is sufficient to use the value indicated on the tuning capacitance dial.

### 6.3.2 Measurement Procedure

The Q-meter was set to zero and this must be checked immediately before taking any measurement. The measurement may be carried out at any frequency within the range but it must be remembered that the effective capacitance varies with frequency because of the residual self inductance of the system under test.

Initially, the test jig with the sample was connected to the test circuit terminal, and the oscillator frequency was set to the required resonant frequency. A suitable resonating inductor was connected to the H1 and L0 terminals of the Q-meter and the tuning-capacitor dial was adjusted so that an indication of maximum value of  $Q$  was obtained (see Fig.6.6). Let this capacitance be  $C_2$  and the corresponding quality factor be  $Q_2$ .

Next, the sample was removed and the tuning-capacit-

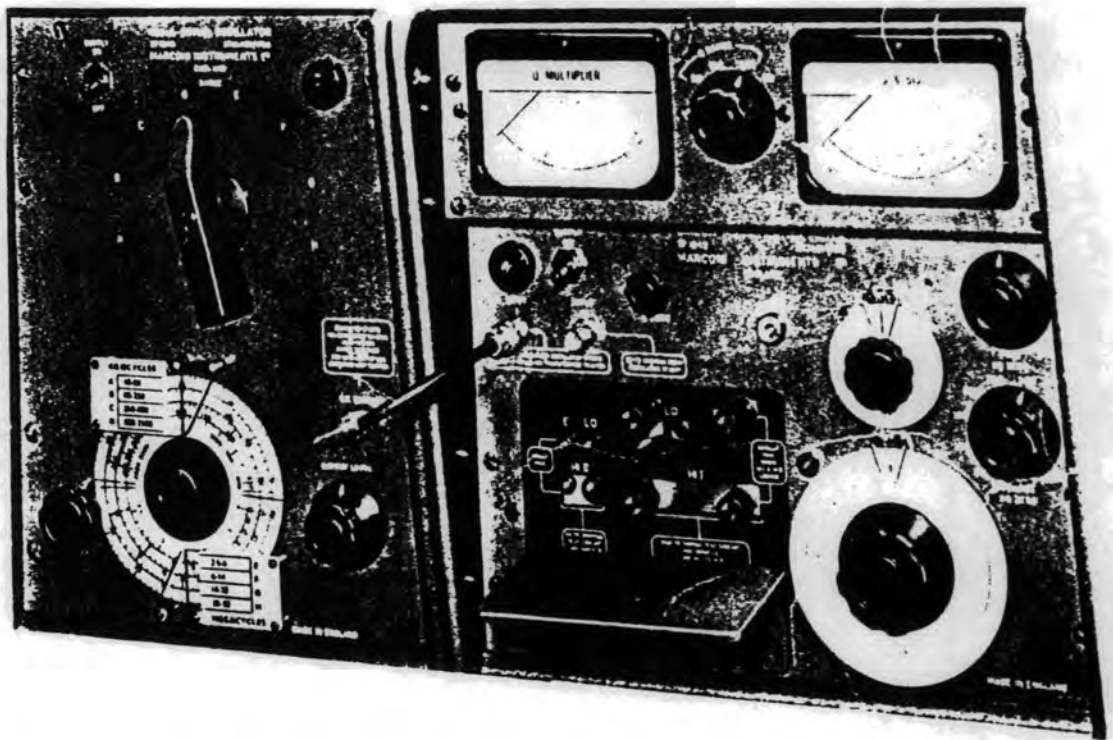


FIG 6.6: Indicators and Connectors of Marconi Q-meter TF 1245

ance dial readjusted. Let this time, the new tuning-capacitor setting at resonance be  $C_1$  and the indicated Q reading be  $Q_1$ .

The absolute values of  $\epsilon'$  and  $\tan\delta$  can now be calculated from eqns. (6.15) & (6.16) since the difference in the capacitance is a function of the dielectric constant and the change in the quality factor is a function of the loss tangent.

#### 6.4 Reflected Power Method

This method is based on determining the quality factor Q, and the resonance frequency of a cavity without and with the sample. The dielectric properties of the sample can then be obtained using the perturbation formulas.

The measurement of the quality factor in this method is basically described by Sucher and Fox [18]. The method depends on the determination of the voltage reflection coefficient magnitude  $|\rho|$  at resonance ( $f_0$ ) and at the two frequencies  $f_1, f_2$ , chosen to be symmetrically located on either side of resonance. From this data the loaded Q ( $Q_L$ ) may be computed.

The measurement is based on the equation

$$|\rho|^2 = \frac{|\rho_0|^2 + \xi^2 |\rho_1|^2}{1 + \xi^2} \quad (6.18)$$

with the bandwidth parameter  $\xi$  given by

$$\xi = \left( \frac{\Delta f}{f_0} \right) Q_L \quad (6.19)$$

where,

$|\rho_0|$  = reflection coefficient magnitude at resonance,

$|\rho_1|$  = reflection coefficient magnitude far off resonance,

$|\rho|$  = reflection coefficient magnitude at  $f_1, f_2$ .

If one desires to work with  $\xi = 1$  (corresponding to the 3dB bandwidth) the corresponding value of  $|\rho|^2$  is

$$|\rho|^2 = \frac{|\rho_0|^2 + |\rho_1|^2}{2} \quad (6.20)$$

#### 6.4.1 Measurement Procedure

The set up for this type of measurement is shown in Fig.6.7 . The system should be calibrated before taking the measurements. The repeller and the beam voltage of the Klystron was adjusted to obtain a smooth power versus frequency display from  $X_1$ . The short circuit was placed at position B-B and an adjustment of attenuator 2 was made so that the incident and the reflected tracing were in coincidence.

With the cavity in the test position and the shorting



plate out of the circuit, the cavity was tuned to the resonant frequency ( $f_0$ ). Now  $|\rho_0|^2$  and  $|\rho_1|^2$  can be measured by lowering the incident power trace in order to touch the top and the bottom of the reflected power trace respectively. These traces are shown in Fig.6.8.

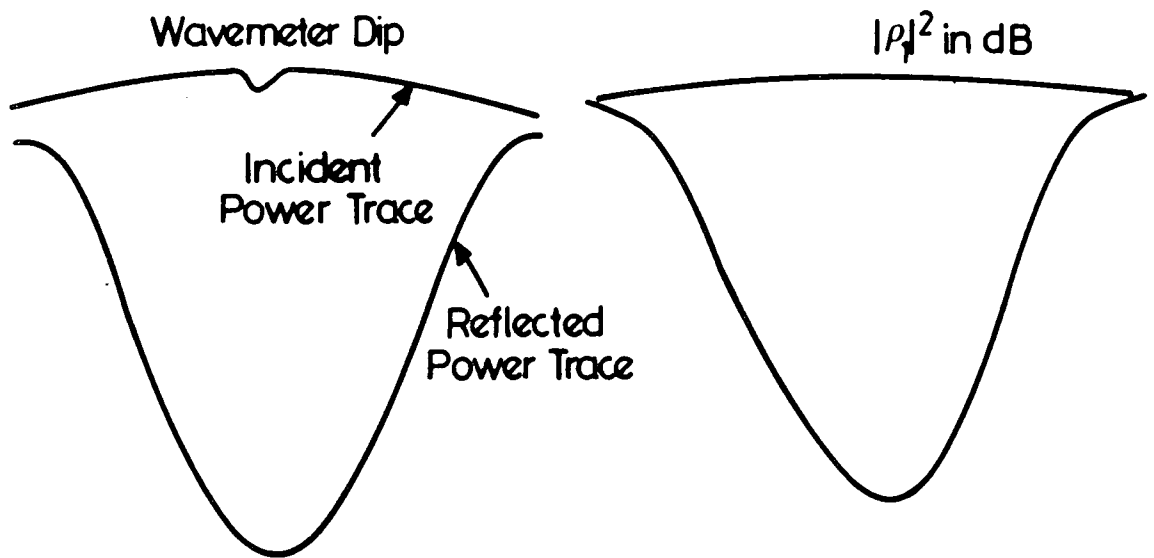
We can either choose the value of  $\xi$  to be 1, i.e. 3dB point and calculate the corresponding value of  $|\rho|^2$  from equation (6.20), or choose a convenient dB value of  $|\rho|^2$  arbitrarily, leaving the computation of  $\xi$  for later.

In both cases  $f_1$  and  $f_2$  may be determined by means of the wavemeter provided and  $Q_L$  found from eqn. (6.19).

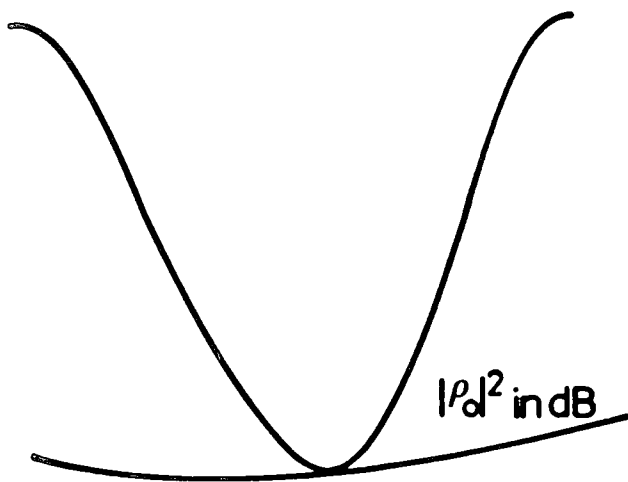
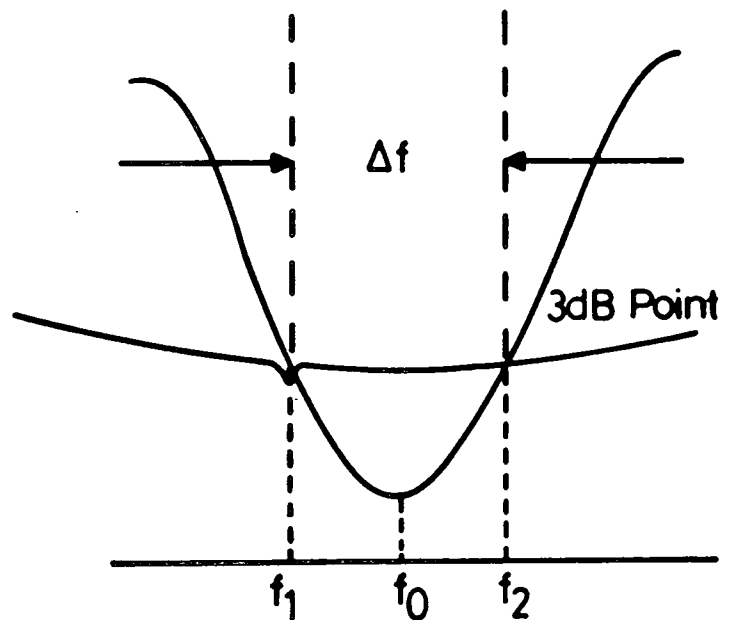
#### 6.5 Sweep Generator/Spectrum Analyzer Method (SG/SA)

The method is based on measurements of very small changes in cavity  $Q$  and its resonant frequency when the sample under test is inserted. The position of the sample in the cavity is so chosen as to produce a maximum frequency shift from which the value of the permittivity,  $\epsilon'$ , is determined. The loss tangent can be determined from the changes in the quality factor  $Q$ .

In this method a spectrum analyzer was used as a monitor for frequency shift and quality factor determination. The basic set up consists of a sweep oscillator, a spectrum analyzer, two attenuators for matching purposes and the cavity under test. Typical test circuit is shown in Fig.6.9.



(a) Incident and Reflected Traces

(b) Position of Determining  $|\rho_1|^2$ (c) Position of Determining  $|\rho_d|^2$ 

(d) 3dB Points Measurement

FIG 6.8: Oscilloscope Displays During Q Measurements

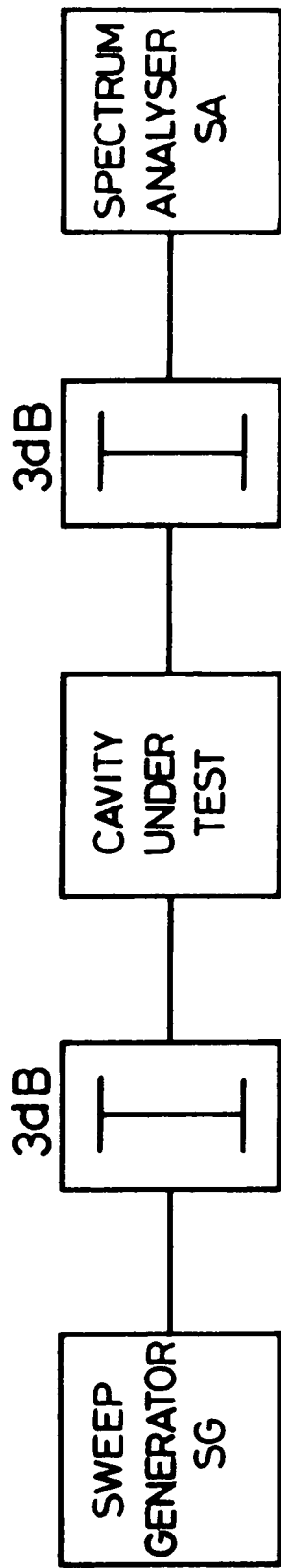


FIG 6.9: Arrangement for Measuring Q by the Spectrum Analyser Method

### Horizontal Position and Center Frequency Calibration

The spectrum analyzer should be calibrated [51] before taking the measurements. Initially the TUNING was adjusted to 2GHz. The CAL OUT was connected to RF IN, using a coaxial cable and adapter. This should produce a display on the screen. It may be necessary to adjust the TUNING slightly to center the display on the screen. The PEAKING control was adjusted to maximize the calibrator signal amplitude. The DEGAUSS button was pushed and then the CENTER FREQUENCY TUNING was adjusted for minimum calibrator signal shift as the frequency SPAN/DIV was switched between 10MHz and 100KHz positions.

Next the SPAN/DIV was returned to 10MHz and the signal was positioned to center on the screen with the HORIZ POSITION control. Finally the CENTER FREQUENCY CAL was adjusted for a center frequency readout of 2GHz. (Fig.6.10).

### AMPLITUDE and LOG CAL Adjustment

The AMPLITUDE CAL adjustment sets an input signal of the correct amplitude to the reference level (top graticule line). The LOG CAL adjustment calibrates the display for dB/DIV.

For the adjustment of the AMPLITUDE and LOG CAL, the display mode was selected to be 2dB/DIV and the FREQUENCY SPAN/DIV was set to 1MHz. Then the CENTER FREQUENCY was tuned to 2GHz. Next, the display baseline at the bottom

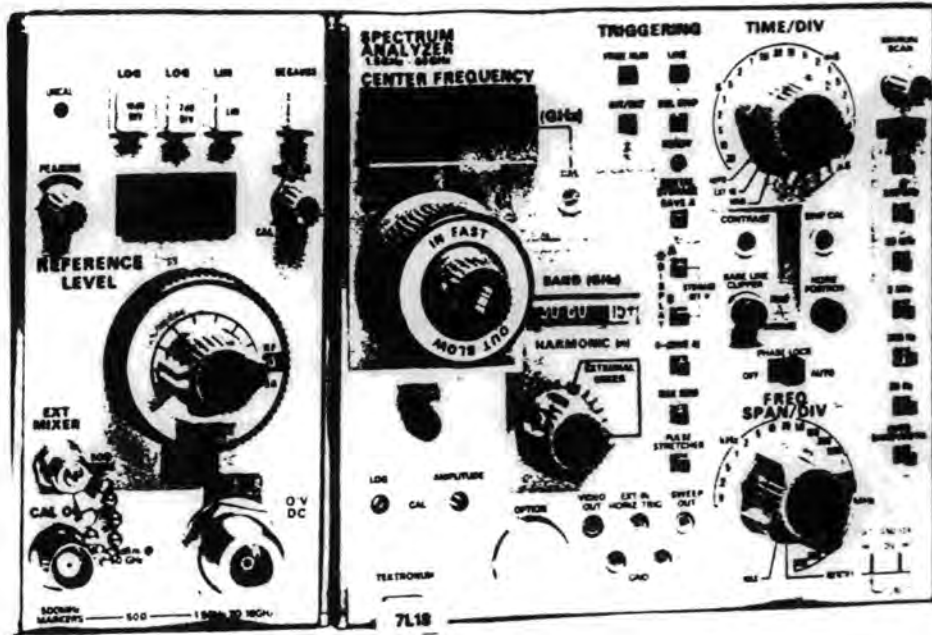


FIG 6.10 (a): Front Panel Controls, Indicators, and Connectors of 7L18 Spectrum Analyser

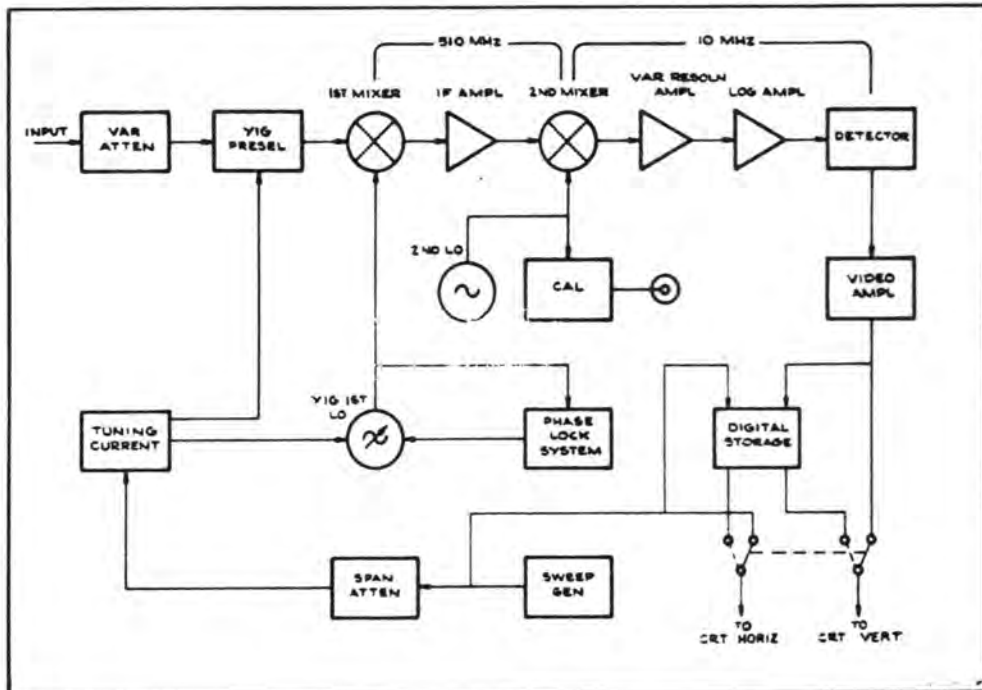


FIG 6.10 (b): Simplified Block Diagram of 7L18 Spectrum Analyser

graticule line was set with the VERTICAL POSITION control and the PEAKING was adjusted for maximum signal amplitude. Then the AMPLITUDE CAL was adjusted while alternately switching between 2dB/DIV and 10dB/DIV so that the signal amplitude was the same for both modes. Finally LOG CAL was adjusted in the 10dB/DIV mode, for a full screen signal (top graticule line).

#### 6.5.1 Measurement Procedure

Initially, the CENTER FREQUENCY of the spectrum analyzer is tuned to the desired resonant frequency ( $f_0$ ). Then the display is generated by tuning the sweeping oscillator and the cavity to that frequency ( $f_0$ ) through the spectrum analyzer span. Next, the REFERENCE LEVEL of the analyzer and the POWER LEVEL of the sweeper are adjusted for a full screen signal (top graticule line).

The response of the cavity is held in the MAX HOLD memory of the analyzer after sweeping on both sides of the resonant frequency. The sweep rate can be controlled by the speed time knob of the sweeper. Finally the bandwidth ( $\Delta f$ ) can be measured after determining the half-power points (3dB) and hence the loaded quality factor ( $Q_L$ ) can be calculated from equation (2.3). The above procedure was implemented in establishing the loaded Q-value of the cavity, firstly with the silica rod alone and secondly with the silica and the test sample. Fig.6.11 illustrates the response of the cavity with and

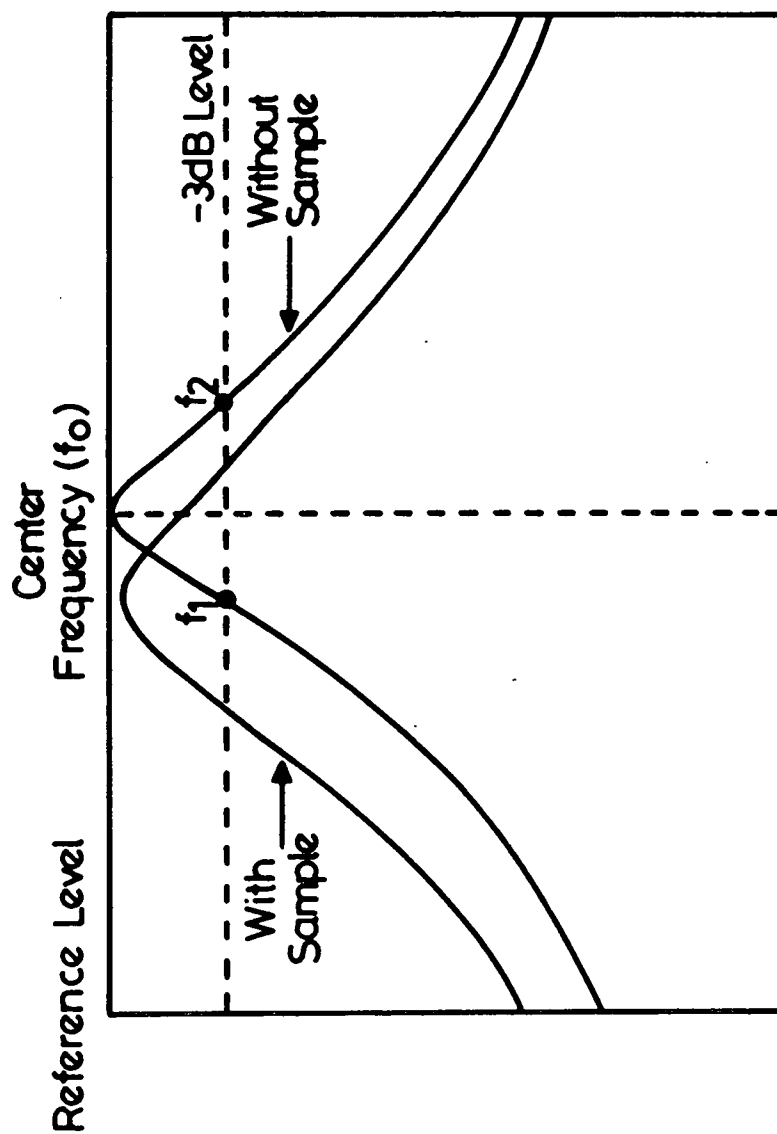


FIG 6.11: Illustration of the Cavity Response With and Without Sample as Displayed by the Spectrum Analyser

without the sample, using the spectrum analyzer method. To avoid dismantling the cavity, the sample and the silica rod were inserted through a suitably placed hole built on the end plate wall of the coaxial cavity. Vacuum grease was used to stick the sample onto the silica rod. It was found that only a thin layer was needed and moreover the vacuum grease were claimed by the manufacturers to be lossless. A micrometer was also used to lower the silica rod and the sample inside the cavity. This to ensure that the sample under study was placed at the right position in the cavity and to avoid touching the cavity while taking the measurements. From the above information and by solving eqns. (3.51) & (3.52), the dielectric properties of the test sample can now be found.

## CHAPTER 7

### RESULTS

#### 7.1 Introduction

Measurements were carried out at low frequencies, with and without gold contacts, on various types of ceramics supplied by Hirst Research Centre GEC. The measured results for these ceramics are presented in this chapter and were obtained on an experimental set up using the Wayne Kerr Universal Bridge (Type-B224), and the Standard Q-meter (Marconi TF 1245).

High frequency results, for the same materials are presented in this chapter. These were obtained by using the coaxial cavity perturbation method (CPM) and SG/SA assembly.

#### 7.2 Low Frequency Assessment

The measured dielectric constant and the loss tangent of various types of ceramics are summarized in tables (1) to (15). The values given represent the averages of several measurements on each sample .

It was found that both techniques , the bridge and the Q-meter, were of adequate precision for determining the dielectric constants of the materials. The determination of the loss tangent was found to be critical in both techniques . In the bridge method the least reading error of the conductance ,  $G$  , due to the instrument was

TABLES (1-15):  
DIELECTRIC PROPERTIES OF VARIOUS  
CERAMICS OBTAINED AT LOW FREQUENCY

Table (1): Coors ADS 995

Frequency (MHz)	Direct Contact		Gold Contact		Technique
	$\epsilon'$	$\tan\delta$ $\times 10^4$	$\epsilon'$	$\tan\delta$ $\times 10^4$	
0.001	8.24	7.16	9.71	4.55	
0.010	8.21	1.44	9.69	4.56	Bridge
0.015	8.10	5.21	9.66	4.57	Method
0.020	8.00	5.76	9.63	4.81	
1.0	8.24	2.63	9.88	4.39	
2.0	8.22	3.12	9.60	5.01	Bridge
5.0	8.31	2.92	9.74	4.80	Method
10.0	8.41	3.44	9.60	4.60	

Table (2): Coors ADS 96R

Frequency (MHz)	Direct Contact		Gold Contact		Technique
	$\epsilon'$	$\tan\delta$ $\times 10^4$	$\epsilon'$	$\tan\delta$ $\times 10^4$	
0.001	7.24	2.63	9.30	2.05	
0.010	7.21	1.11	9.26	1.23	Bridge
0.015	7.19	0.88	9.23	1.51	Method
0.020	7.15	0.77	9.20	1.65	
1.0	7.18	3.89	9.12	2.34	
2.0	7.22	1.61	9.18	2.75	Q-meter
5.0	7.16	4.89	9.12	2.16	Method
10.0	7.15	4.56	9.24	2.42	

Table (3): Coors ADO 9D

Frequency (MHz)	Direct Contact		Gold Contact		Technique
	$\epsilon'$	$\tan\delta$ $\times 10^2$	$\epsilon'$	$\tan\delta$ $\times 10^2$	
0.001	8.68	unreliable	unreliable		
0.010	8.23	2.25	9.94	2.61	Bridge
0.015	8.15	1.86	9.85	2.20	Method
0.020	8.05	2.24	9.63	2.02	
1.0	8.15	0.68	9.75	0.58	
2.0	8.15	1.00	9.75	0.75	Q-meter
5.0	8.12	1.99	9.63	0.75	Method
10.0	8.12	2.16	9.75	0.61	

Table (4): Vitox

Frequency (MHz)	Direct Contact		Gold Contact		Technique
	$\epsilon'$	$\tan\delta$ $\times 10^4$	$\epsilon'$	$\tan\delta$ $\times 10^4$	
0.001	8.28	14.50	10.29	8.75	
0.010	8.23	6.77	10.25	9.66	Bridge
0.015	8.20	4.51	10.23	8.40	Method
0.020	8.16	5.22	10.19	8.54	
1.0	8.26	4.96	10.15	9.78	
2.0	8.13	4.41	10.05	10.74	Q-meter
5.0	8.26	5.17	10.19	8.97	Method
10.0	8.13	4.98	10.10	9.32	

Table (5): MRC

Frequency (MHz)	Direct Contact		Gold Contact		Technique
	$\epsilon'$	$\tan\delta$ $\times 10^4$	$\epsilon'$	$\tan\delta$ $\times 10^4$	
0.001	8.31	6.53	9.98	unreliable	
0.010	8.28	5.89	9.95	6.60	Bridge
0.015	8.24	readings	9.91	6.36	Method
0.020	8.21	unreliable	9.87	6.25	
1.0	8.32	5.72	9.91	8.63	Q-meter
2.0	8.15	6.02	9.86	7.75	Method
5.0	8.15	7.39	9.89	7.33	
10.0	8.15	6.94	9.94	8.99	

Table (6): NTK

Frequency (MHz)	Direct Contact		Gold Contact		Technique
	$\epsilon'$	$\tan\delta$ $\times 10^3$	$\epsilon'$	$\tan\delta$ $\times 10^3$	
0.001	7.77	1.12	9.49	8.00	Bridge Method
0.010	7.75	5.85	9.39	3.37	
0.015	7.72	3.01	9.36	2.98	
0.020	7.70	4.10	9.32	2.46	
1.0	7.79	0.48	9.36	4.96	Q-meter Method
2.0	7.79	0.51	9.36	8.63	
5.0	7.57	0.61	9.28	7.27	
10.0	7.79	0.45	9.34	6.54	

Table (7): Alsimag

Frequency (MHz)	Direct Contact		Gold Contact		Technique
	$\epsilon'$	$\tan\delta$ $\times 10^3$	$\epsilon'$	$\tan\delta$ $\times 10^3$	
0.001	8.34	4.53	Bidge unbalanced		
0.010	8.32	3.18	9.95	4.97	Bridge
0.015	8.29	readings	9.91	4.03	Method
0.020	8.25	unreliable	9.87	4.27	
1.0	8.35	3.88	9.89	5.21	
2.0	8.12	4.42	9.90	4.99	Q-meter
5.0	8.35	4.89	9.86	6.01	Method
10.0	8.23	5.50	9.92	5.50	

Table (8): Rosenthal

Frequency (MHz)	Direct Contact		Gold Contact		Technique
	$\epsilon'$	$\tan\delta$ $\times 10^4$	$\epsilon'$	$\tan\delta$ $\times 10^4$	
0.001	6.03	8.72	7.03	unreliable	
0.010	6.02	6.74	6.99	6.56	Bridge
0.015	6.00	7.01	6.80	5.79	Method
0.020	5.98	7.52	6.66	5.18	
1.0	6.05	7.97	7.07	5.32	
2.0	5.86	6.66	6.89	6.76	Q-meter
5.0	6.00	7.39	6.95	5.19	Method
10.0	5.91	7.03	6.69	5.67	

Table (9): Thomson

Frequency (MHz)	Direct Contact		Gold Contact		Technique
	$\epsilon'$	$\tan\delta$ $\times 10^3$	$\epsilon'$	$\tan\delta$ $\times 10^3$	
0.001	7.15	4.51	9.93	3.23	
0.010	7.10	2.27	9.87	2.15	Bridge
0.015	7.08	2.08	9.83	2.27	Method
0.020	7.05	1.67	9.79	2.08	
1.0	7.16	2.33	9.83	2.12	
2.0	7.08	2.62	9.75	2.22	Q-meter
5.0	7.20	3.19	9.67	2.63	Method
10.0	7.24	4.00	9.75	2.94	

Table (10): Deranox

Frequency (MHz)	Direct Contact		Gold Contact		Technique
	$\epsilon'$	$\tan\delta$ $\times 10^{-3}$	$\epsilon'$	$\tan\delta$ $\times 10^{-3}$	
0.001	7.50	2.10	9.84	8.79	
0.010	7.46	1.58	9.73	3.85	Bridge
0.015	7.44	1.43	9.69	3.43	Method
0.020	7.41	1.33	9.65	2.92	
1.0	7.51	2.67	9.56	3.34	
2.0	7.34	3.07	9.61	4.71	Q-meter
5.0	7.42	3.14	9.52	3.33	Method
10.0	7.34	2.45	9.61	4.04	

Table (11): Hoechst

Frequency (MHz)	Direct Contact		Gold Contact		Technique
	$\epsilon'$	$\tan\delta$ $\times 10^3$	$\epsilon'$	$\tan\delta$ $\times 10^4$	
0.001	7.45	unreliable	9.41	11.30	
0.010	7.40	2.94	9.38	8.77	Bridge
0.015	7.38	2.23	9.36	4.73	Method
0.020	7.35	2.35	9.32	4.27	
1.0	7.34	2.53	9.34	5.88	
2.0	7.26	2.79	9.26	4.91	Q-meter
5.0	7.42	3.13	9.30	7.22	Method
10.0	7.34	2.88	9.17	7.05	

Table (12): Glass Ceramics

Frequency (MHz)	Direct Contact		Gold Contact		Technique
	$\epsilon'$	$\tan\delta$ $\times 10^3$	$\epsilon'$	$\tan\delta$ $\times 10^3$	
0.001	5.38	unreliable	6.07	unreliable	
0.010	5.25	8.43	5.96	6.18	Bridge
0.015	5.22	6.96	5.93	5.38	Method
0.020	5.20	6.02	5.90	4.99	
1.0	5.17	5.21	6.09	7.20	
2.0	5.28	6.86	5.86	5.80	Q-meter
5.0	5.40	5.47	5.98	6.76	Method
10.0	5.17	6.53	5.98	5.98	

Table (13): Kyocera

Frequency (MHz)	Direct Contact		Gold Contact		Technique
	$\epsilon'$	$\tan\delta$ $\times 10^4$	$\epsilon'$	$\tan\delta$ $\times 10^3$	
0.001	7.34	7.13	9.53	2.74	
0.010	7.32	6.44	9.48	1.96	Bridge
0.015	7.30	4.78	9.45	1.98	Method
0.020	7.27	5.65	9.41	1.88	
1.0	7.18	5.56	9.39	2.56	
2.0	7.25	6.24	9.22	2.45	Q-meter
5.0	7.33	6.74	9.26	2.20	Method
10.0	7.24	5.65	9.34	1.92	

Table (14): NK2/3447

Frequency (MHz)	Direct Contact		Gold Contact		Technique
	$\epsilon'$	$\tan\delta$ $\times 10^3$	$\epsilon'$	$\tan\delta$ $\times 10^3$	
0.001	4.50	unreliable	5.65	4.64	
0.010	4.43	6.07	5.59	4.75	Bridge
0.015	4.42	5.34	5.56	5.00	Method
0.020	4.39	5.35	5.54	5.09	
1.0	4.41	5.36	5.55	5.00	
2.0	4.39	5.40	5.58	5.10	Q-meter
5.0	4.38	5.55	5.53	5.19	Method
10.0	4.40	5.50	5.60	5.07	

Table (15): NK2/3802

Frequency (MHZ)	Direct Contact		Gold Contact		Technique
	$\epsilon'$	$\tan\delta$ $\times 10^3$	$\epsilon'$	$\tan\delta$ $\times 10^3$	
0.001	5.29	unreliable	6.46	unreliable	
0.010	5.14	5.89	6.35	5.07	Bridge
0.015	5.11	6.03	6.32	4.96	Method
0.020	5.09	6.08	6.30	4.99	
1.0	5.15	6.10	6.29	5.00	
2.0	5.05	6.05	6.35	4.99	Q-meter
5.0	5.11	6.12	6.33	5.05	Method
10.0	5.05	6.10	6.31	5.02	

$\pm 0.01$  nmhos. The measured conductance for some ceramics was found to be comparable to that value resulting in an approximate loss tangent calculation.

The smallest reading error of the quality factor possible on the Q-meter instrument was  $\pm 1$ . It is, therefore, difficult to determine the loss tangent accurately since it was found that, for many ceramics the difference between the two readings  $Q_1 - Q_2$  was less than unity.

Errors in the measurements of the unknown capacitance and conductance carried out on the Universal Bridge arise both, from the inaccuracies in the standard arms, and from the parasitic components of the bridge circuit. The latter are associated with losses of the circuit, and stray capacitances to ground.

In the Q-meter technique, there are two kinds of error. First, those related to the original calibration of the Q-meter giving rise to a fixed error and second, errors in the actual readings of  $C_1$  and  $C_2$  which may be reduced by taking several measurements on each sample and then averaging.

Re-positioning of the specimen can lead to some changes in the readings. The electrode contact defects and the surface conductivity might also introduce additional errors.

The overall accuracy of  $\epsilon'$  was estimated to be about  $\pm 5\%$  in both techniques. The error in the loss

tangent was somewhat higher than the error in  $\epsilon'$  and its estimation was more difficult, as contributions arise mainly from the errors of capacitance and Q-value readings.

### 7.3 High Frequency Results using CPM

The permittivities, the dielectric losses, and loss tangents for the samples in para. 7.2 were next determined at high frequencies covering the range from 3 to 8 GHz. The results are presented in this chapter as well as the calculated values of attenuation ( $\alpha$ ) and phase ( $\beta$ ) constants, in dB/m and radians/m, respectively, for a wave propagating in a medium of such dielectrics.

In the case of the CPM using coaxial resonator the size and position of the sample in the cavity are most critical. The best size was found to be between 0.6 and 1 mm<sup>3</sup>. The sample should be inserted through a small hole into the cavity to a place creating a maximum frequency shift. In order to eliminate any errors caused by the uneven geometry of the sample, measurements were taken at a number of silica-rod, rotational-positions and the final values were then calculated by averaging. This was an important step for the frequency shift measurements from which the value of the relative permittivity was determined. The change of position of the sample does not alter the Q significantly, and therefore the losses in

the cavity, once the sample is inserted. In addition, other precautions had to be taken into account. For example, the mode inside the cavity might not be a true TEM, which affects the function  $F(x,y,z)$  in the perturbation formulas. To overcome this problem a calibration of the system, using a material of known dielectric properties (Coors 995), was made.

Although the coaxial cavity operates in the frequency range between 2.5 GHz to 11.5 GHz, the measurements were taken covering only the band from 3 to 8 GHz. It was found that at higher frequencies, above 8 GHz, the loaded  $Q$  begins to drop ( Fig.4.9 ) because the inner conductor of the cavity was too close to the regions of the coupling loops. Consequently, the perturbation formula<sup>s</sup> did not apply because the theory is based on the assumption of high  $Q$ -value (see chapter 3). At the lower frequency of 2.5 GHz the gap between the inner conductor and the end plate was very small (0.1 mm) presenting very high capacitance, which predominated , leading to an error in the frequency shift when the sample was inserted.

It is known that the universal law (chapter 5) of dielectric response applies very widely to many materials, particularly to ceramics and glasses in which hopping is the dominant conduction mechanism.

In the present investigation, an attempt has also been made to justify the validity of the universal law on

the various types of ceramics. It was found that  $n_1$  obtained from the relation

$$[\epsilon'(\omega) - \epsilon'_\infty(\omega)] \propto \omega^{(n_1 - 1)}$$

was very close to unity for all the ceramics used, i.e. a frequency independent permittivity. On the other hand, the value of  $n_2$  obtained from

$$\epsilon''(\omega) \propto \omega^{(n_2 - 1)}$$

was less than  $n_1$ , less than unity.

Theory predicts that if the hopping model is strictly applicable  $n_1$  should be equal to  $n_2$ . This equivalence has been found for some pure materials (e.g. MgO). It implies that the loss should continue to decrease with increasing frequency.

In practice, however, very few materials (particularly sintered ceramics such as those used here) are sufficiently pure and the impurities contribute a degree of Debye type behaviour which is particularly evident on the  $\epsilon''(\omega)$  plot. In this situation  $n_2$  is generally less than  $n_1$ . The impurities may also generate Debye type loss peaks which are superimposed on the "universal law" behaviour. In this case the frequency dependence may become:

$$\epsilon''(\omega) \propto \omega^{-(n_2 - 1)}$$

This is thought to be the basis for the observed increase in loss at higher frequencies.

The graphs, shown in Fig.7.1 to Fig.7.15, give the data for  $\epsilon'$ ,  $\epsilon''$  and  $\tan\delta$  for the various ceramics at high frequencies, together with the values of  $\alpha$ ,  $\beta$  and  $n$  (universal law) obtained from the respective variations of  $\epsilon'$  and  $\epsilon''$  with frequency; all the data refers to ambient temperature measurements.

For comparison purposes Fig.7.16 to Fig.7.20 show the response of the dielectric properties of chosen samples obtained from low and high frequency measurement methods, i.e. the Bridge, the Q-meter and the SG/SA methods.

the various types of ceramics. It was found that  $n_1$  obtained from the relation

$$[\epsilon'(\omega) - \epsilon'_0(\omega)] \propto \omega^{(n_1 - 1)}$$

was very close to unity for all the ceramics used, i.e. a frequency independent permittivity. On the other hand, the value of  $n_2$  obtained from

$$\epsilon''(\omega) \propto \omega^{(n_2 - 1)}$$

was less than  $n_1$ , less than unity.

The graphs, shown in Fig.1 to Fig.15, give the data for  $\epsilon'$ ,  $\epsilon''$  and  $\tan\delta$  for the various ceramics at high frequencies, together with the values of  $\alpha$ ,  $\beta$  and  $n$  (universal law) obtained from the respective variations of  $\epsilon'$  and  $\epsilon''$  with frequency; all the data refers to ambient temperature measurements.

For comparison purposes Fig.7.16 to Fig.7.20 show the response of the dielectric properties of chosen samples obtained from low and high frequency measurement methods, i.e. the Bridge, the Q-meter and the SG/SA methods.

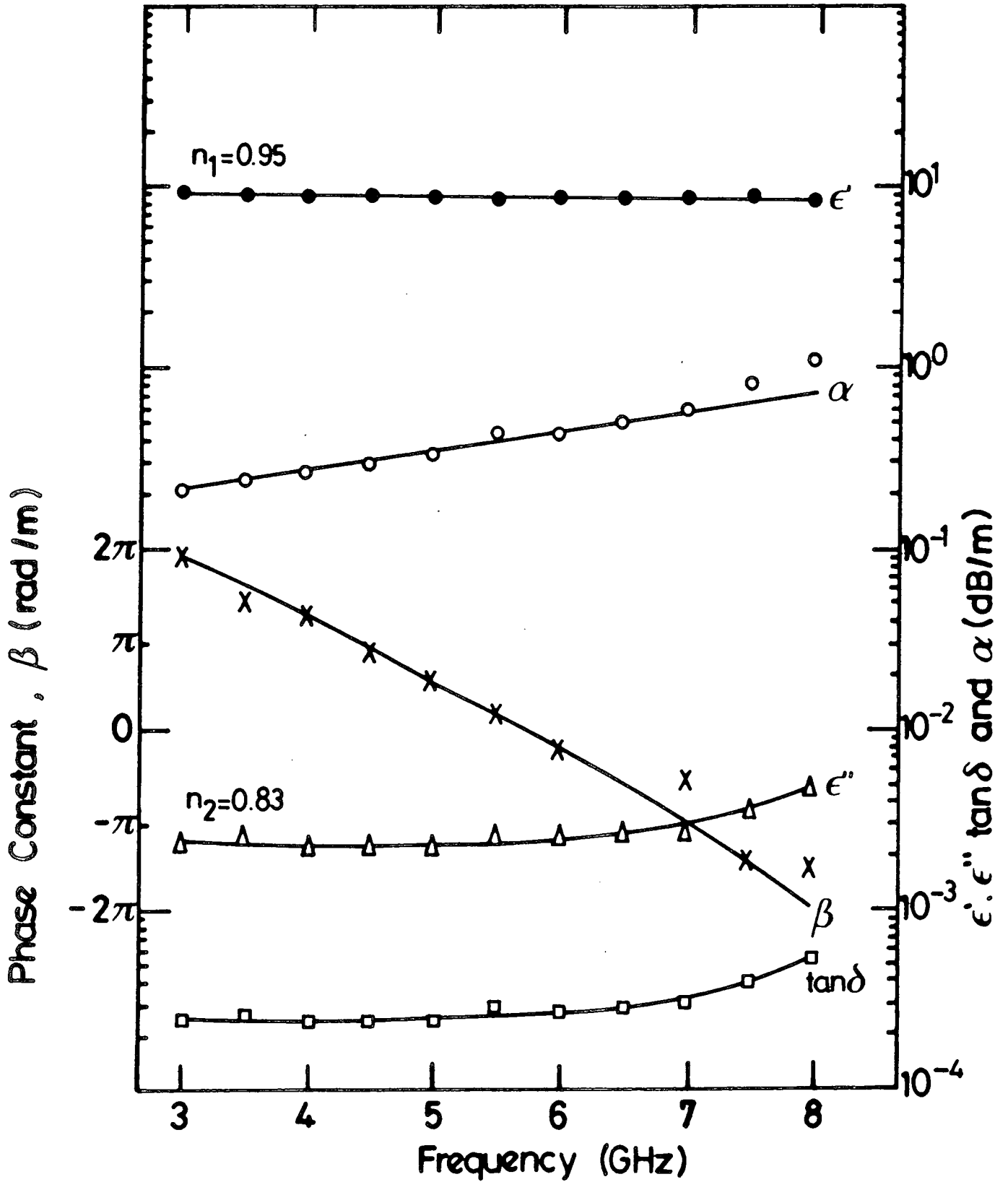


FIG. 7.1: Dielectric and Related Properties of Coors 995

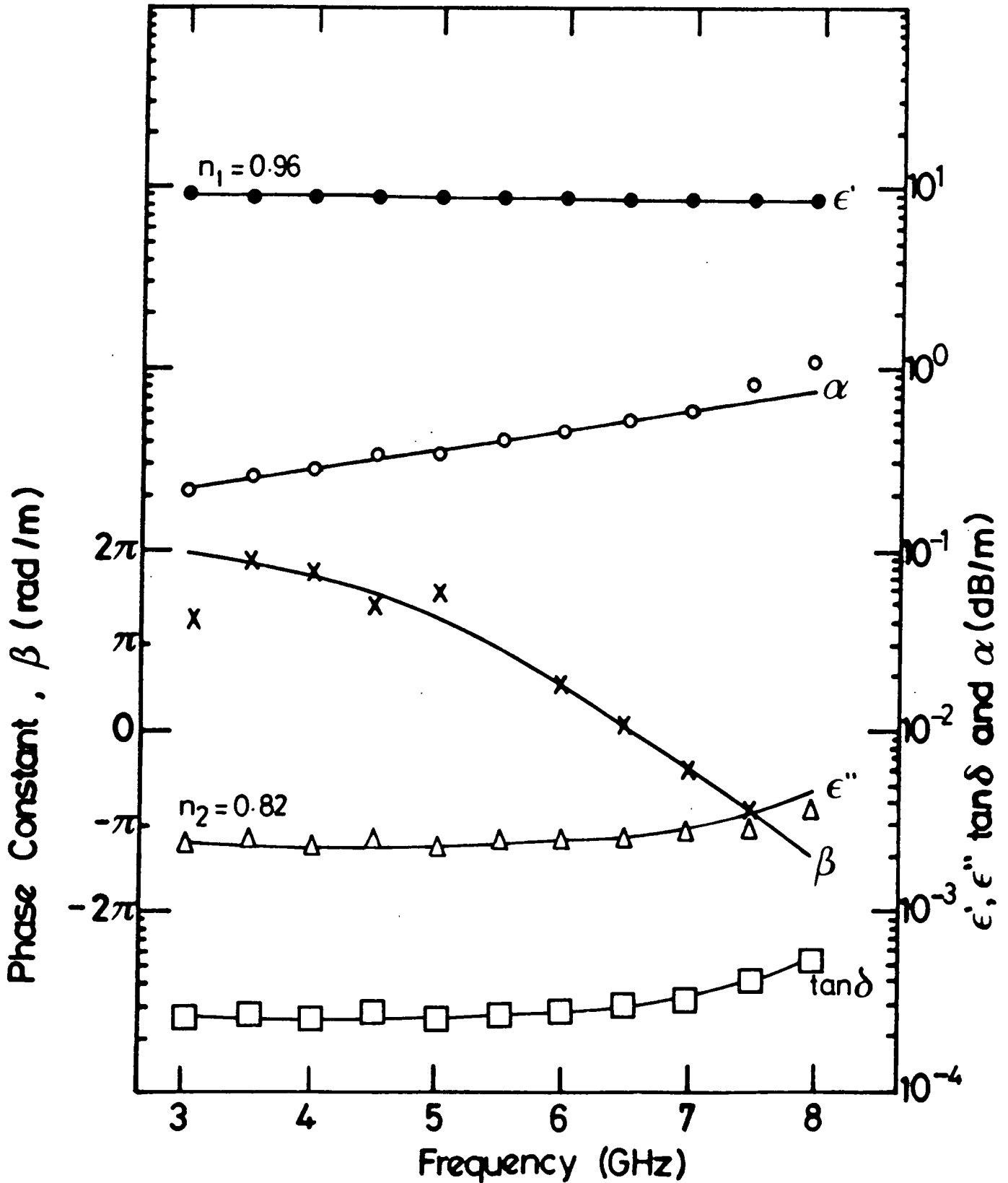


FIG. 7.2: Dielectric and Related Properties of Coors ADS 96R

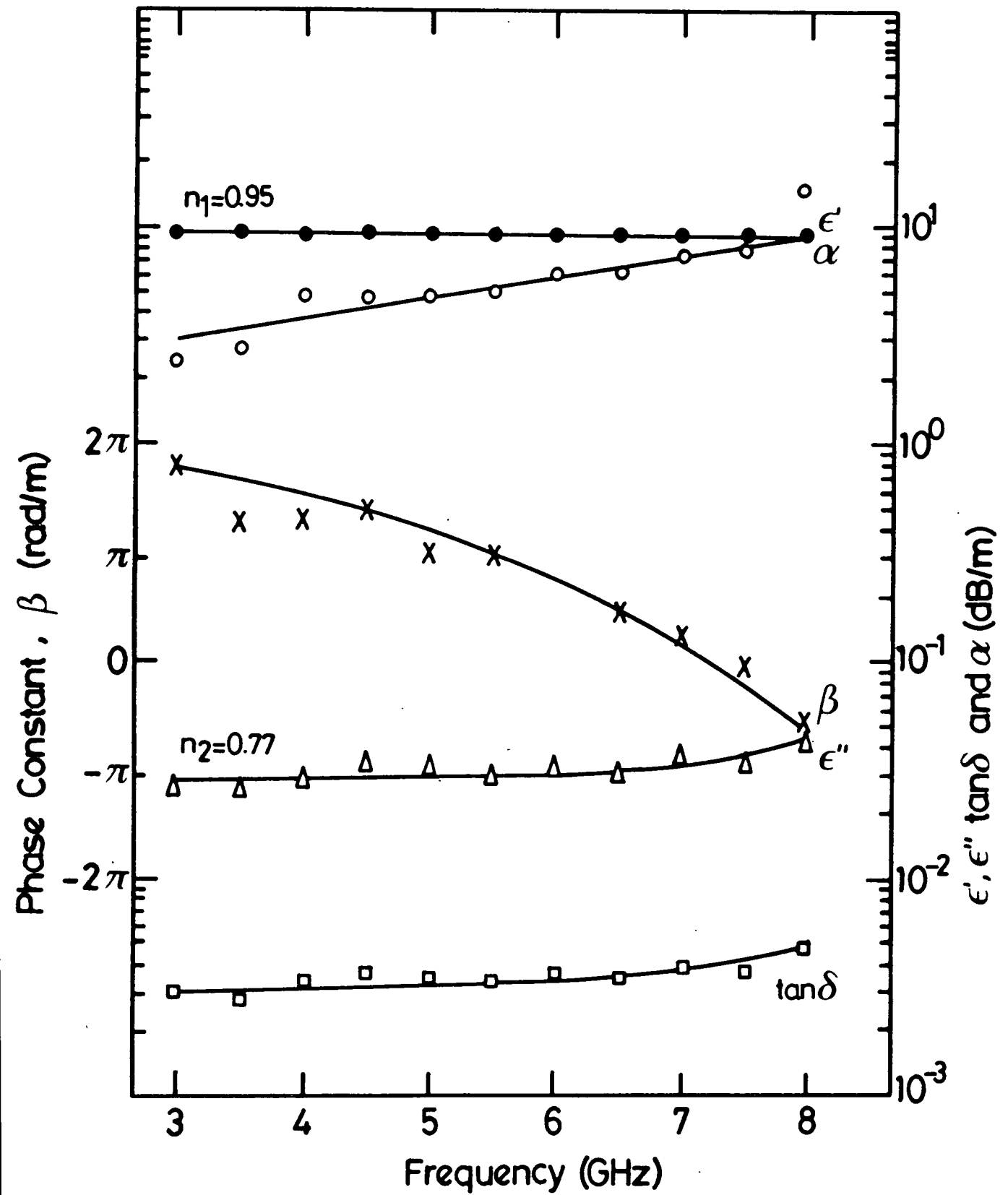


FIG 7.3: Dielectric and Related Properties of Coor ADO 9D

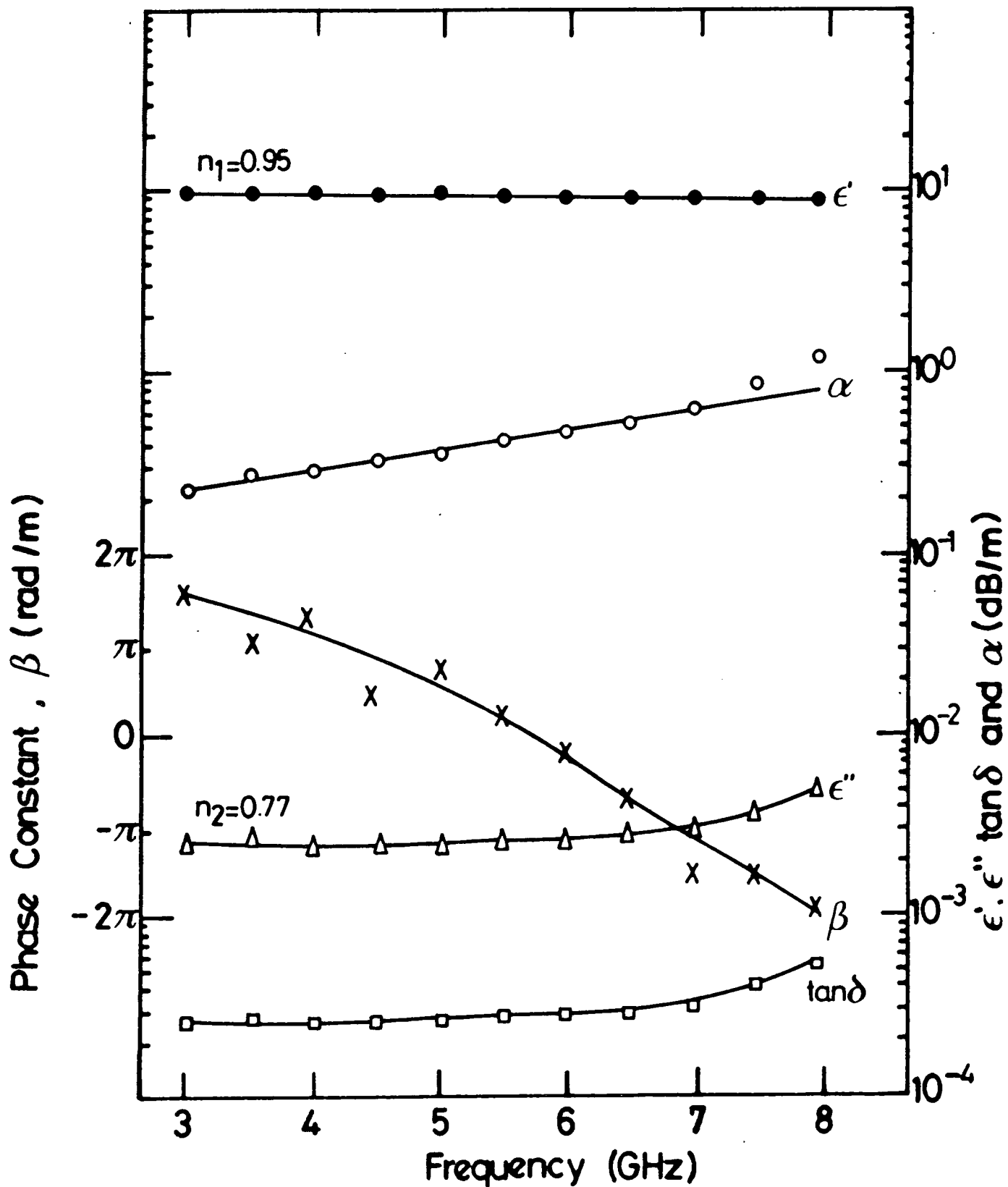


FIG. 7.4: Dielectric and Related Properties of Vitox

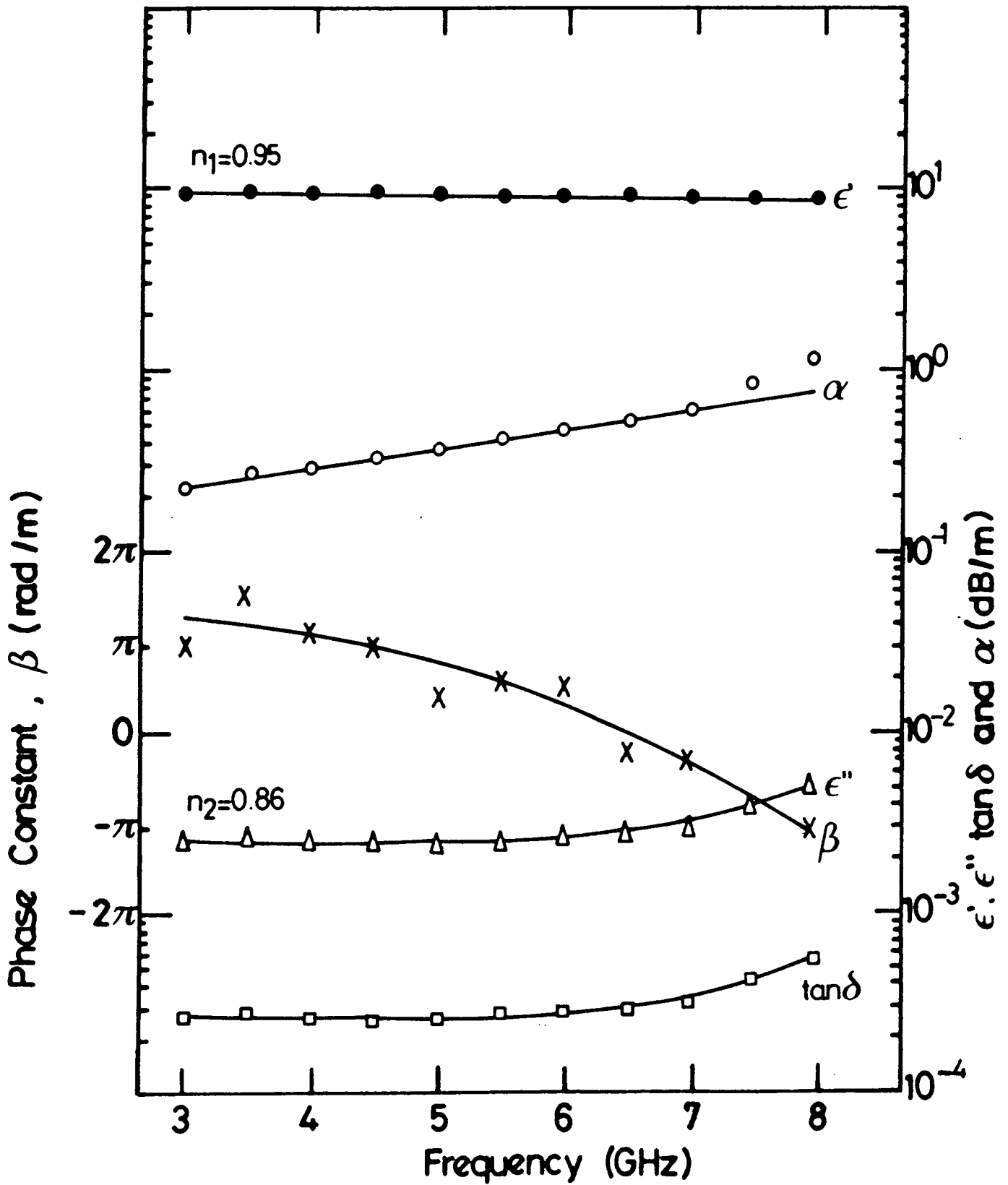


FIG. 7.5: Dielectric and Related Properties of MRC

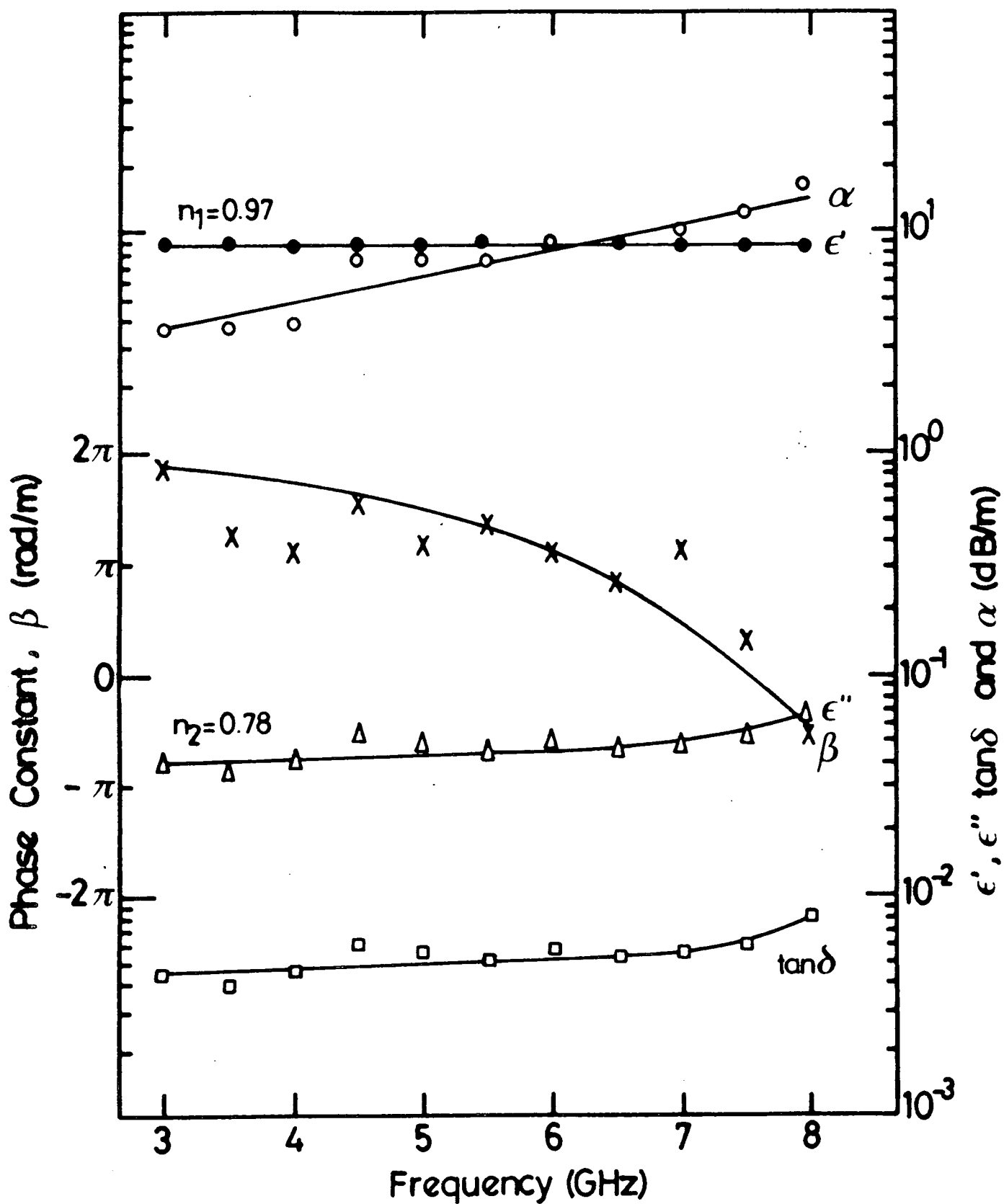


FIG 7.6: Dielectric and Related Properties of NTK

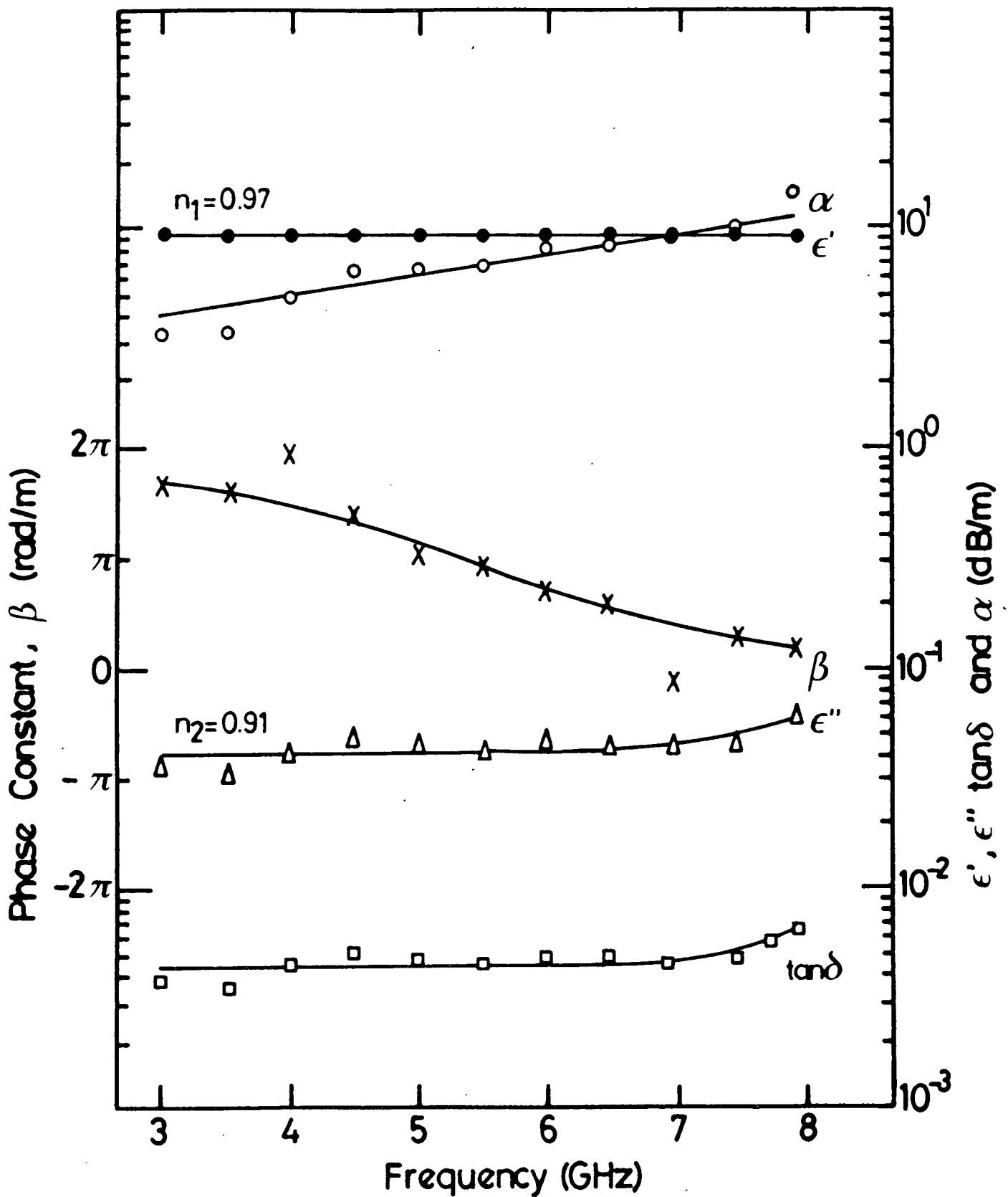


FIG 7.7: Dielectric and Related Properties of Alsimag

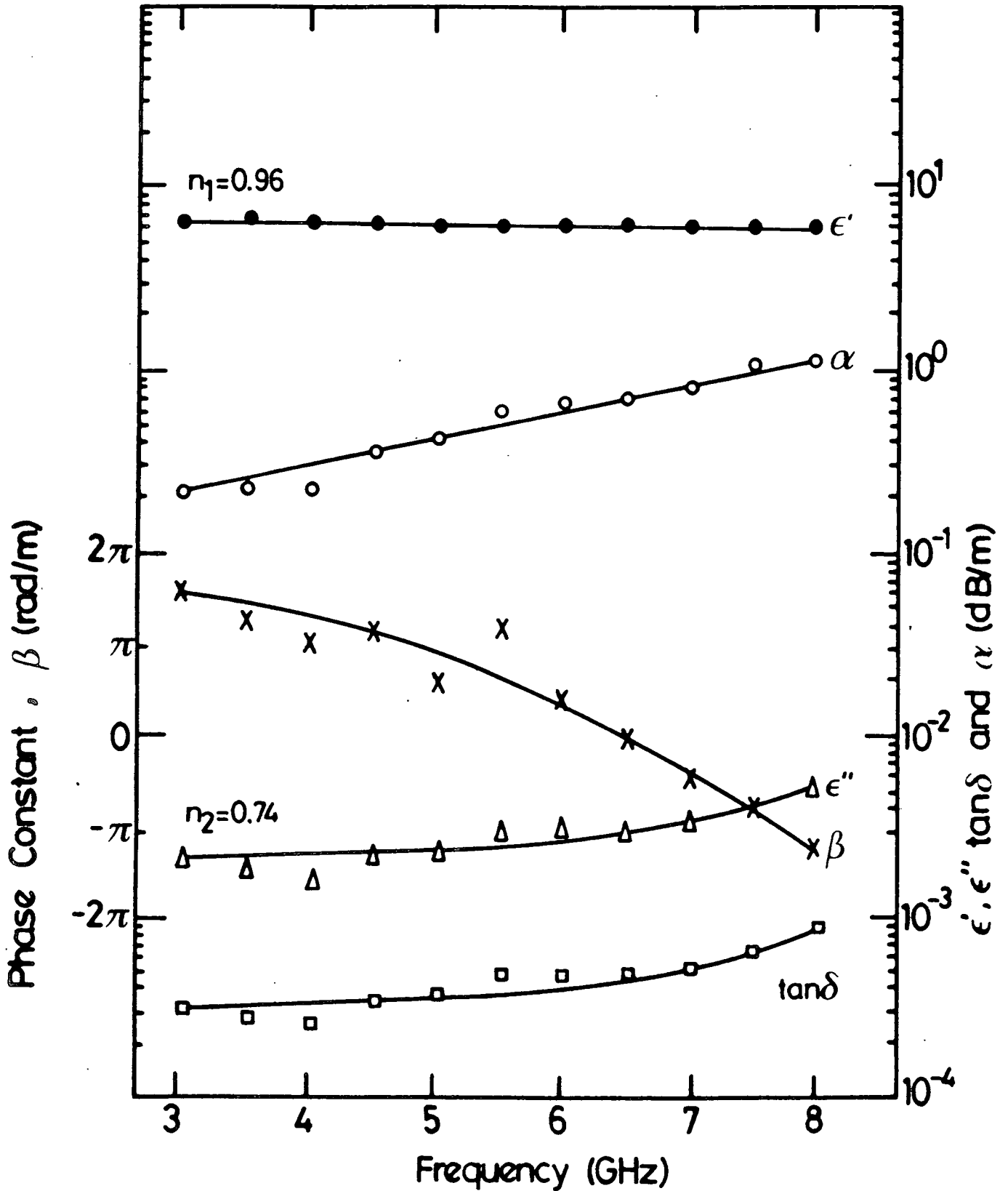


FIG 7.8: Dielectric and Related Properties of Rosenthal

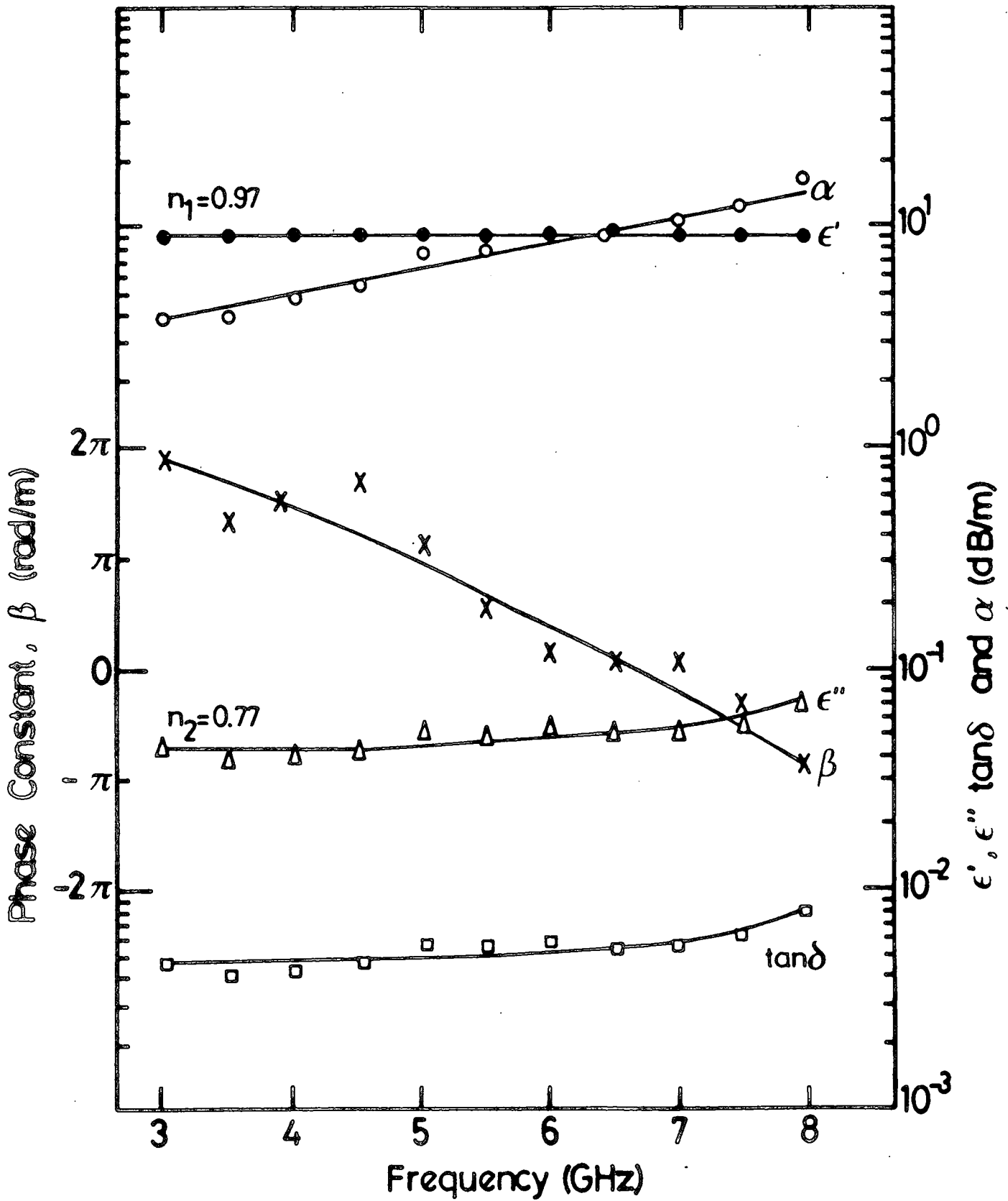


FIG 7.9: Dielectric and Related Properties of Thomson

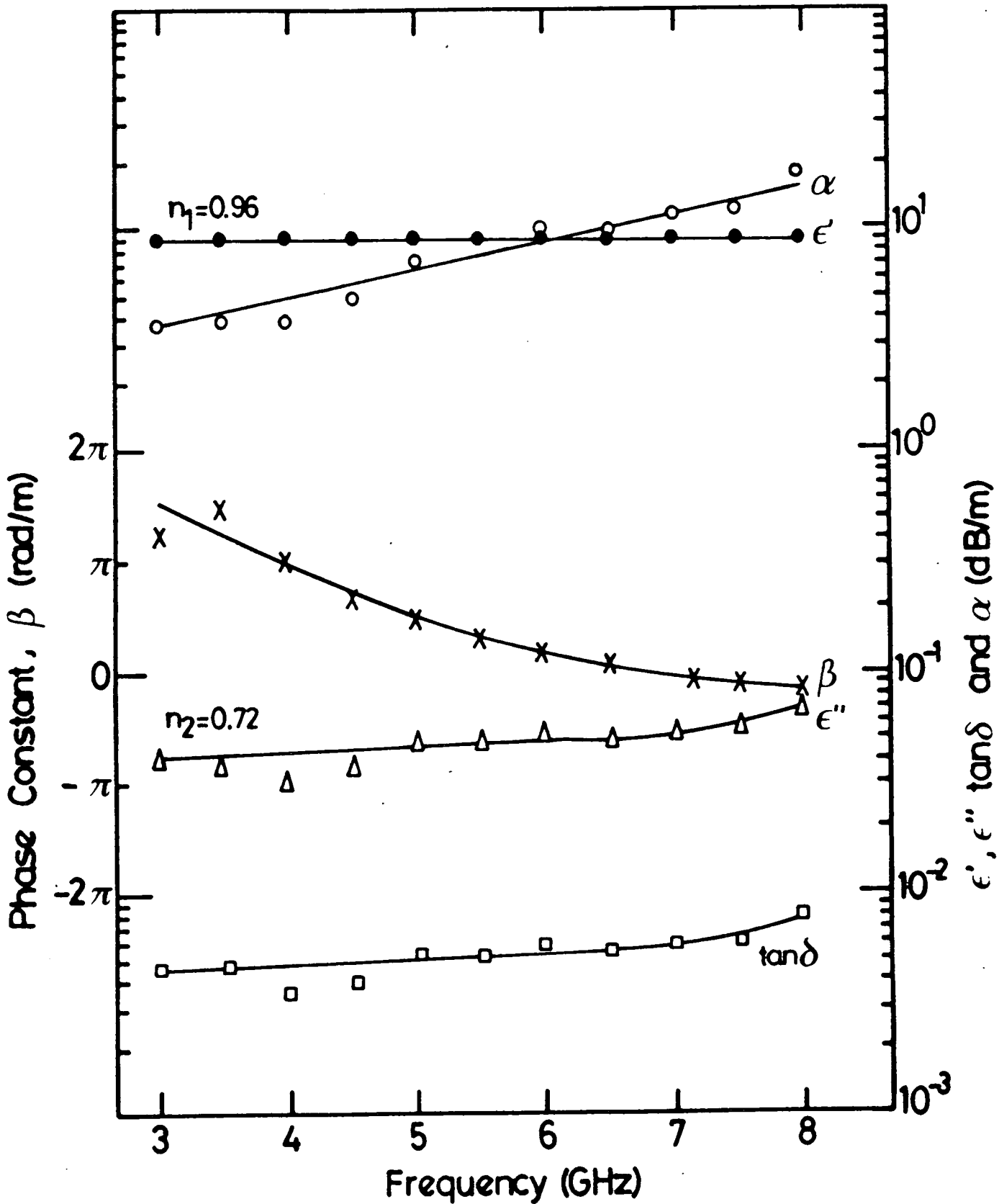


FIG 7.10: Dielectric and Related Properties of Deranox

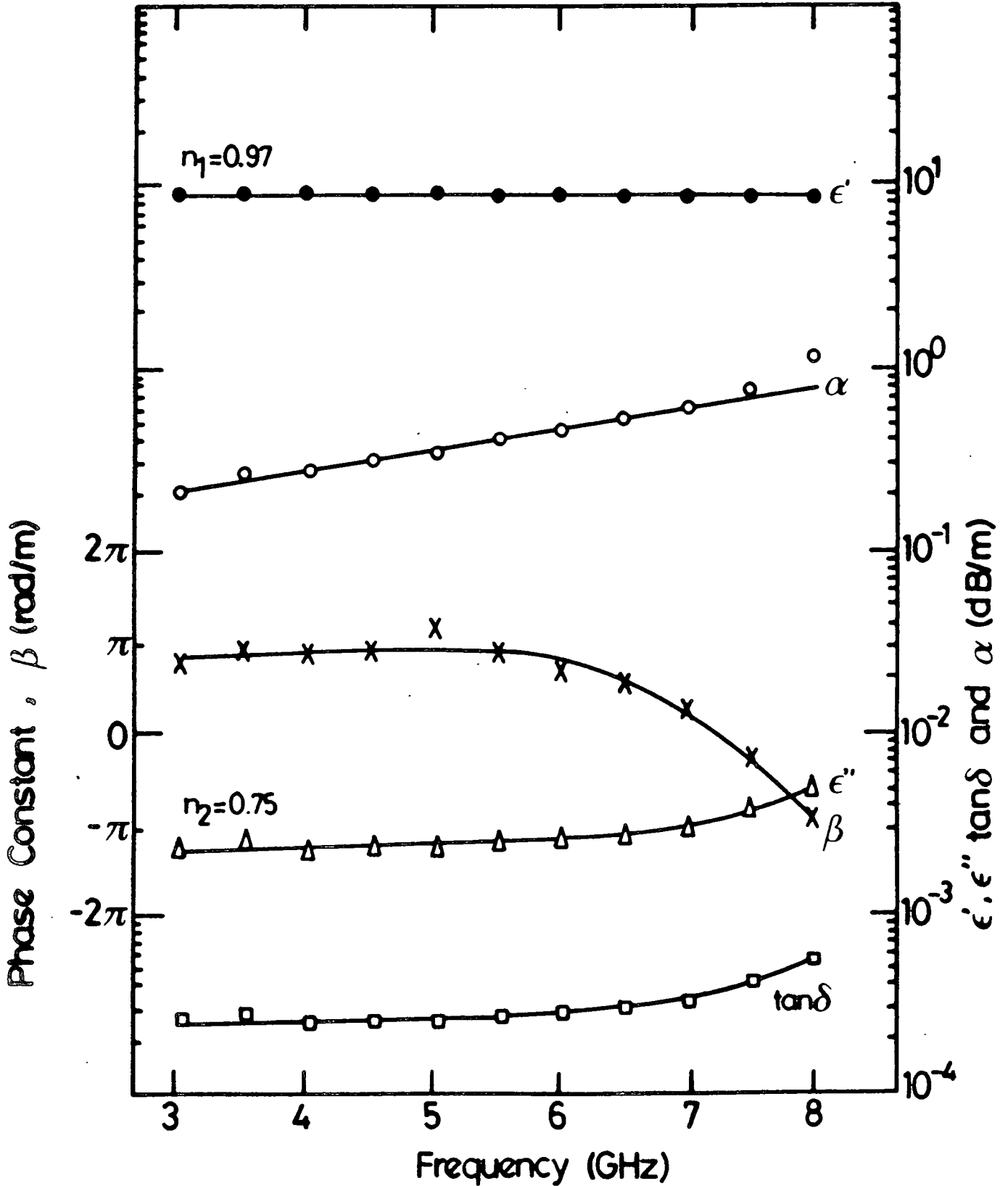


FIG 7.11: Dielectric and Related Properties of Hoechst

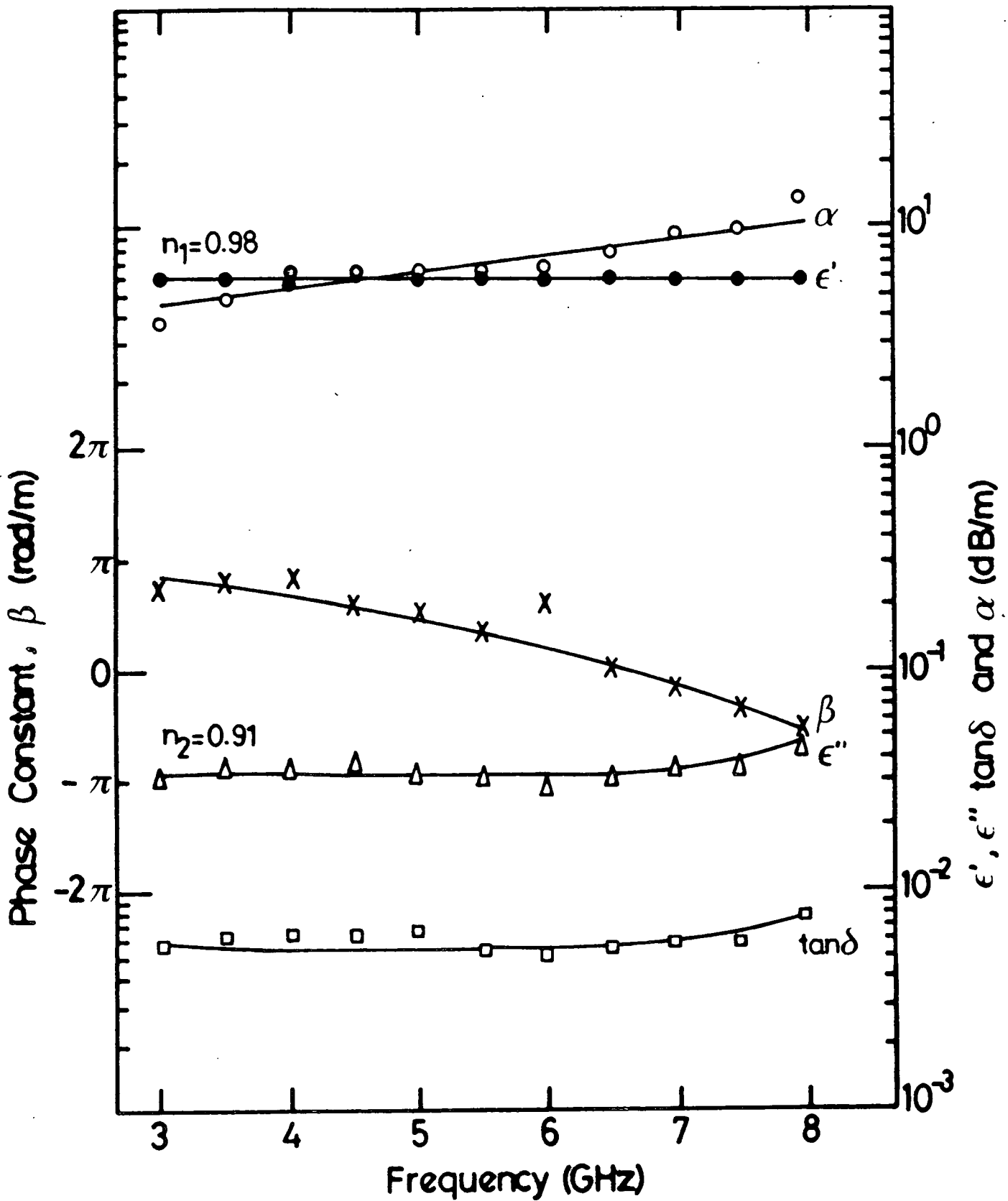


FIG 7.12: Dielectric and Related Properties of Glass Ceramics

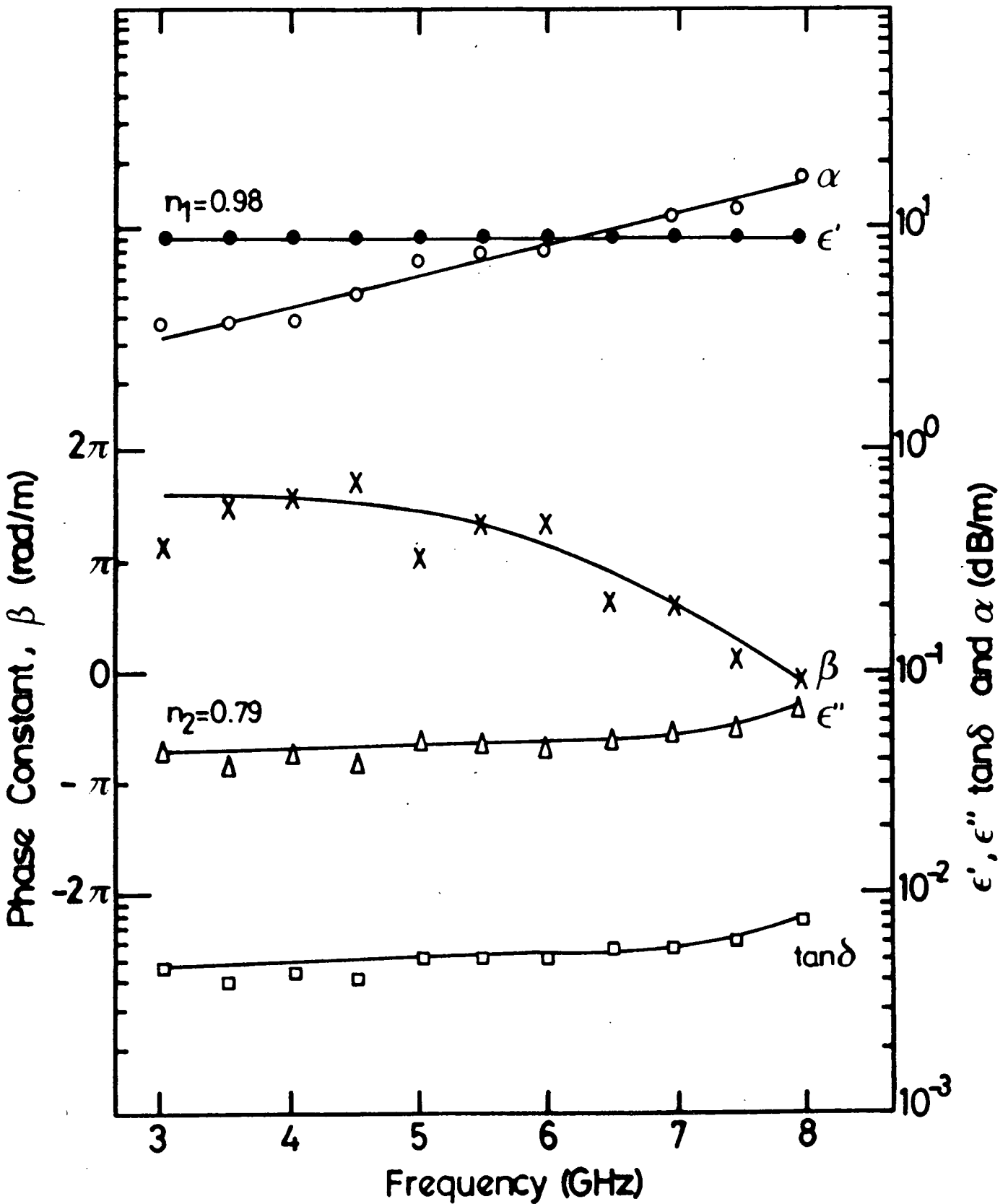


FIG 7.13: Dielectric and Related Properties of Kyocera

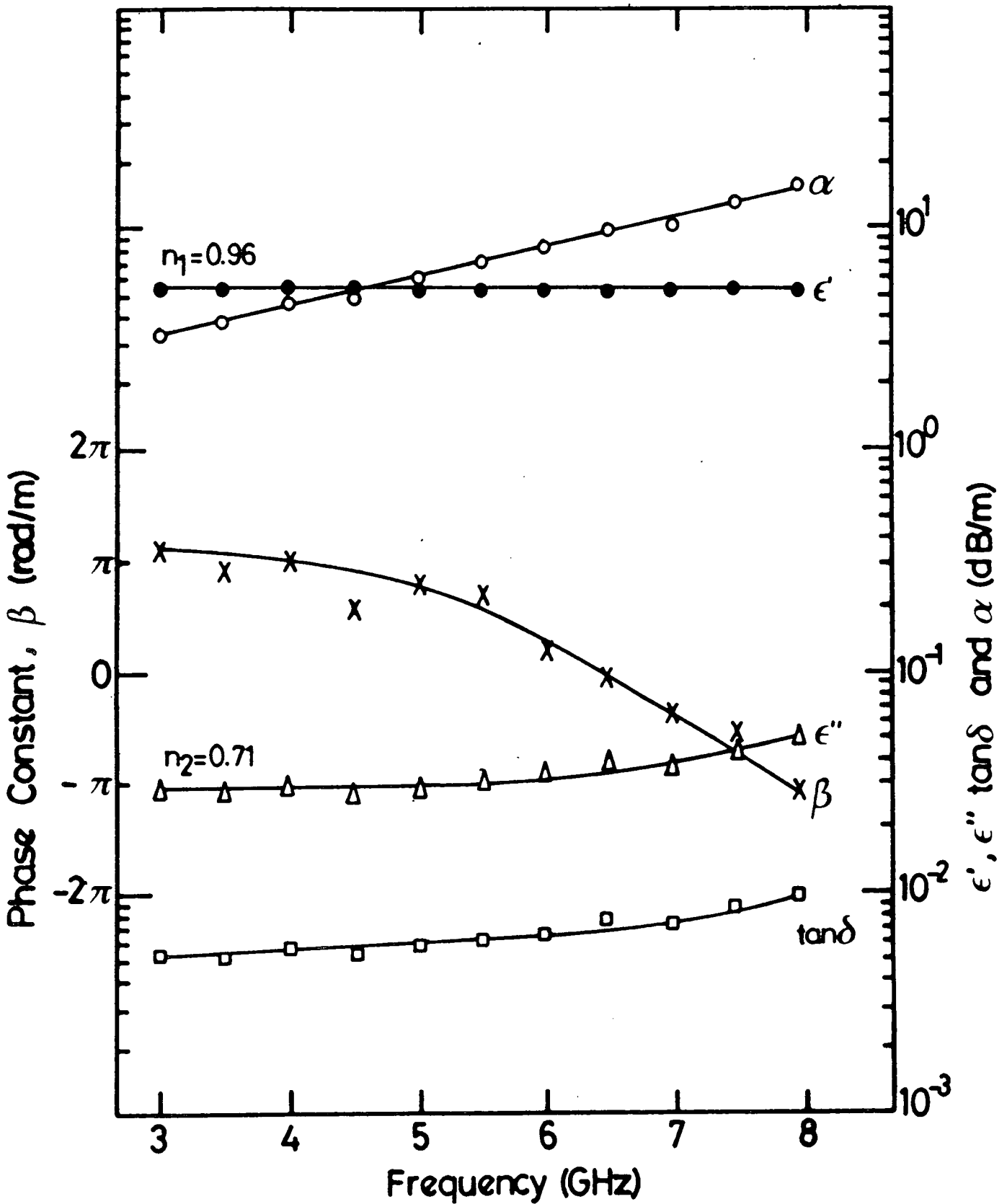


FIG 7.14: Dielectric and Related Properties of NK<sub>2</sub>/3447

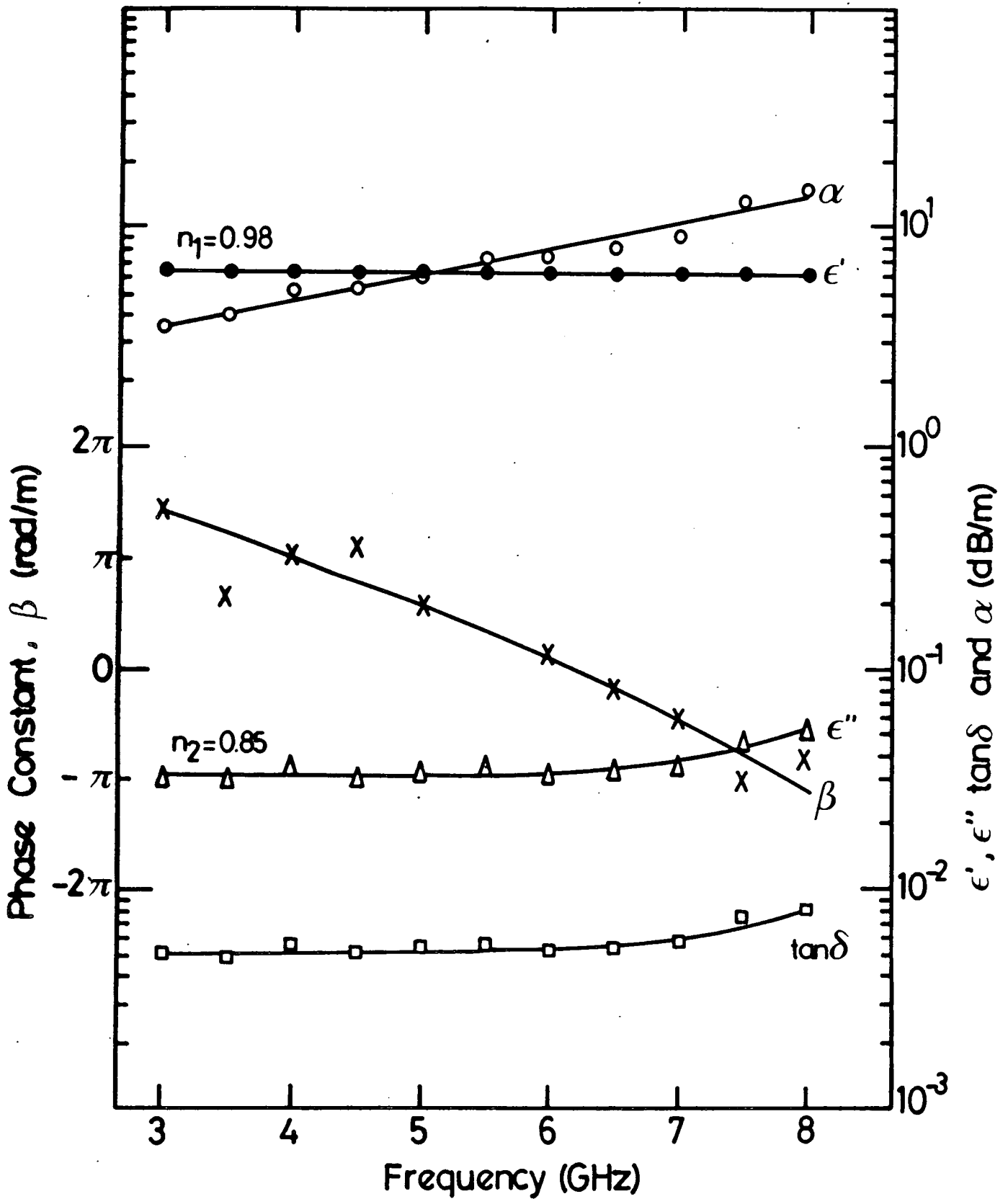


FIG 7.15: Dielectric and Related Properties of NK<sub>2</sub>/3805

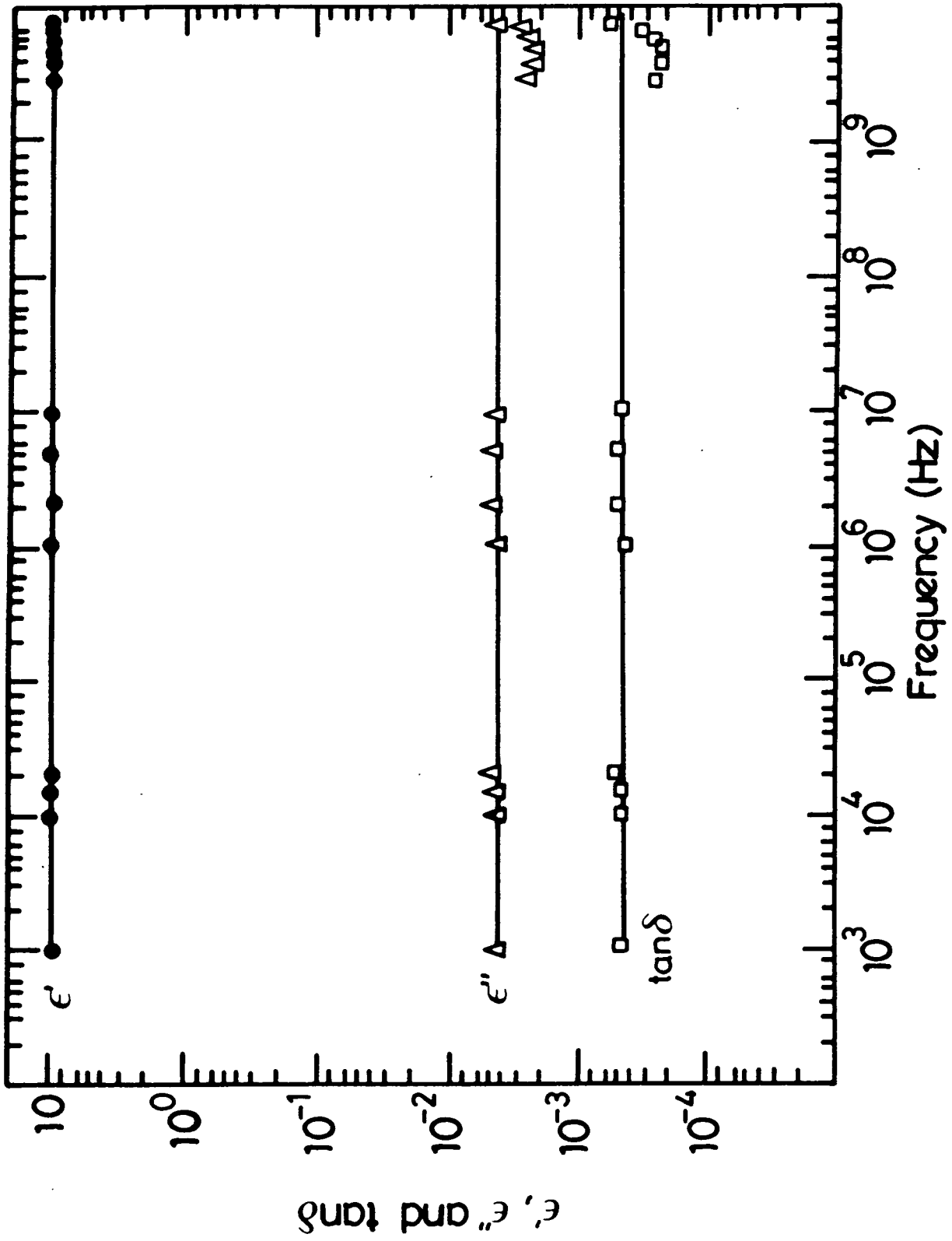


FIG 7.16: Variation of Dielectric Properties of Coors 995 as Obtained From Low and High Frequency Measurement Methods

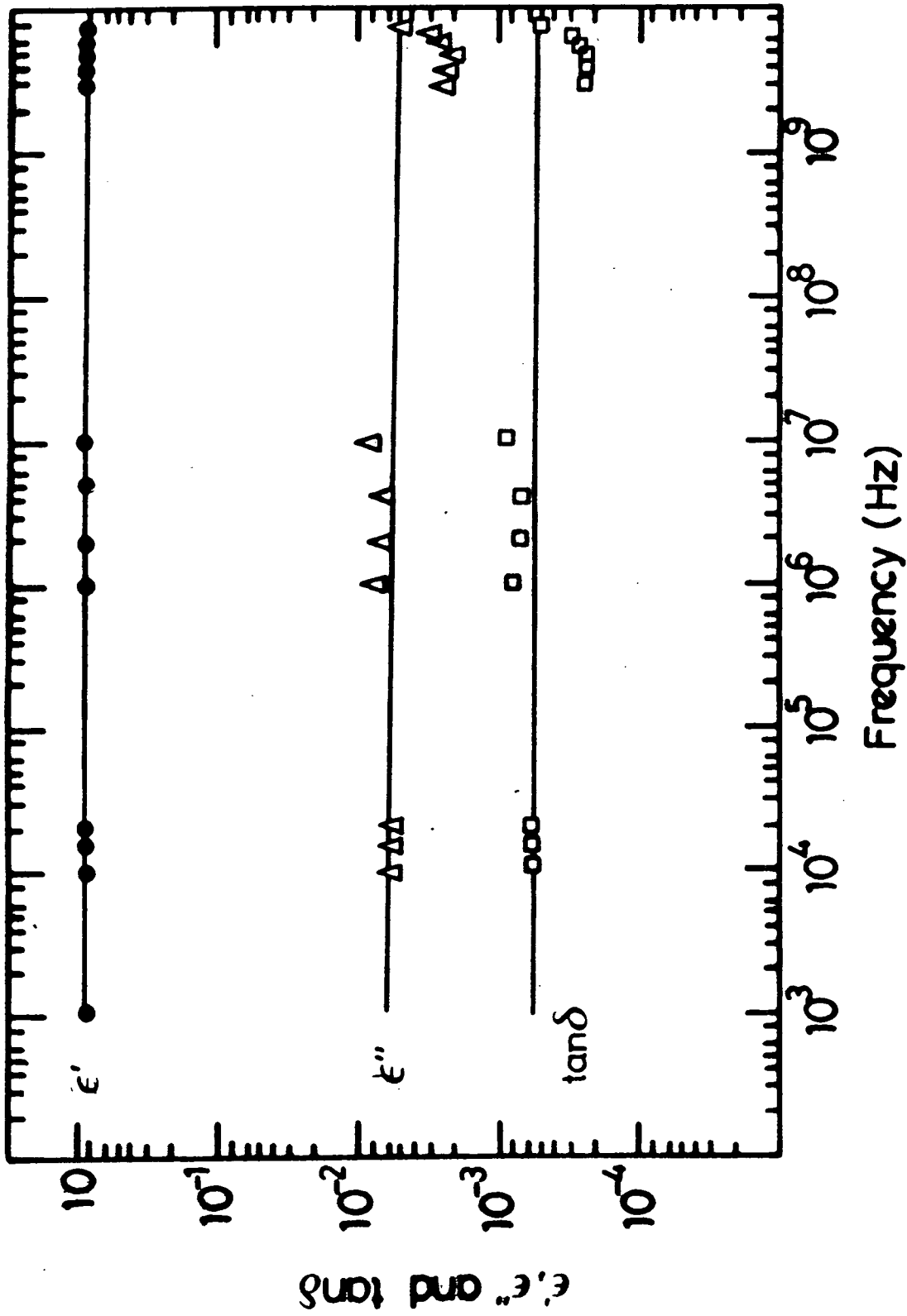


FIG 7.17: Variation of Dielectric Properties of MRC as Obtained From Low and High Frequency Measurement Methods

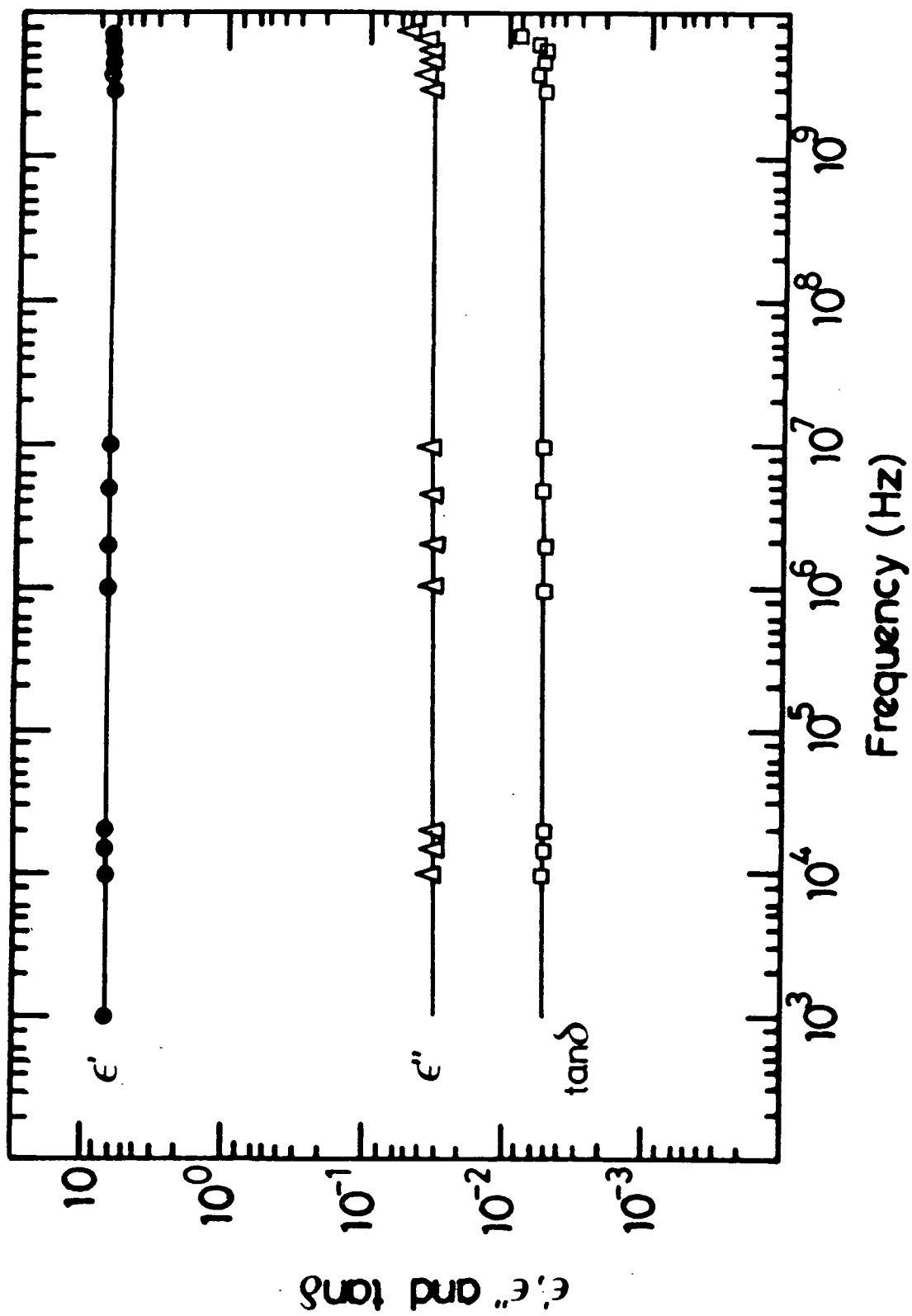


FIG 7.18: Variation of Dielectric Properties of NK<sub>2</sub>/3802 as Obtained From Low and High Frequency Measurement Methods

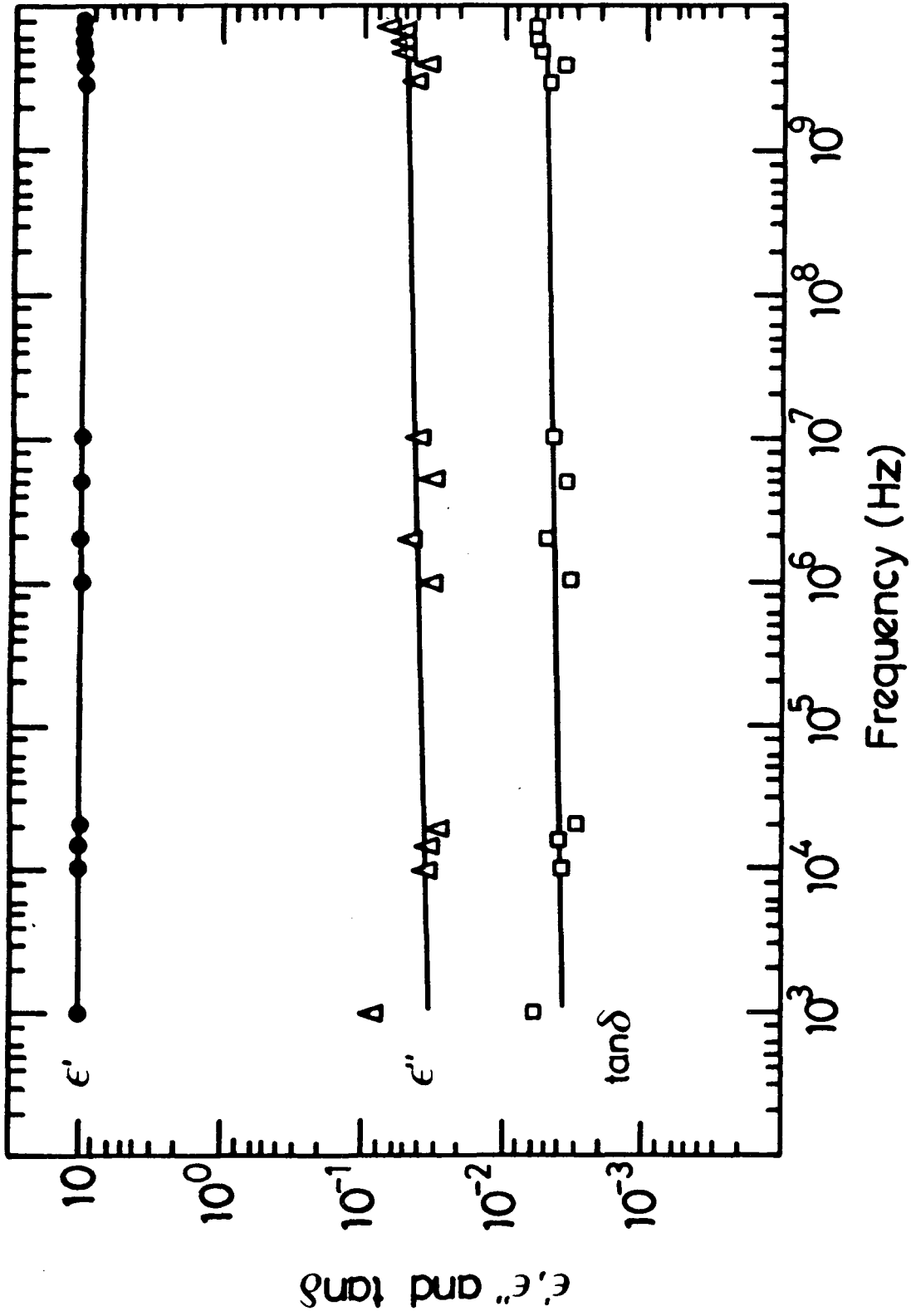


FIG 7.19: Variation of Dielectric Properties of Deranox as Obtained From Low and High Frequency Measurement Methods

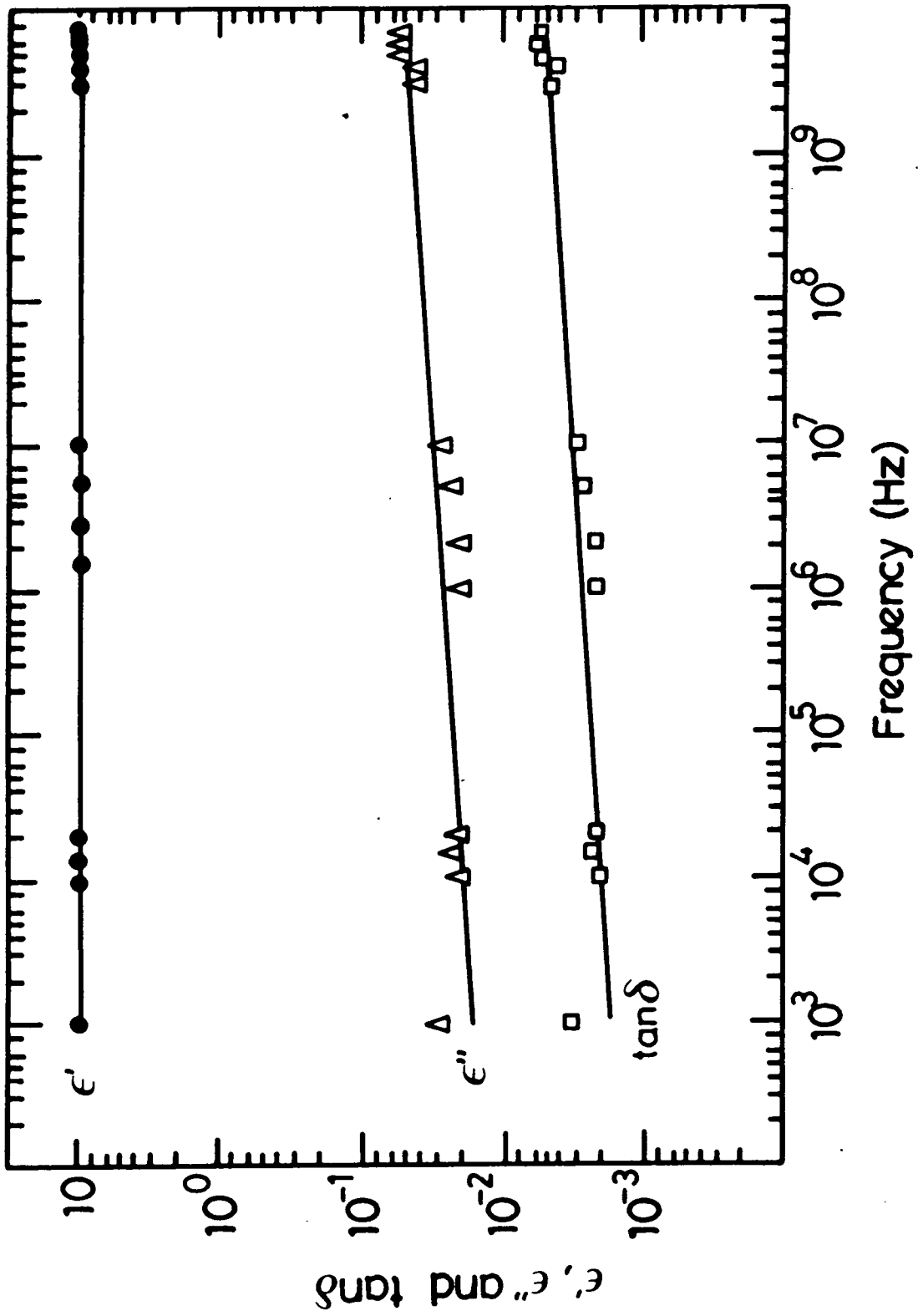


FIG 7.20: Variation of Dielectric Properties of Thomson as Obtained From Low and High Frequency Measurement Methods

CHAPTER 8CONCLUSIONS AND COMMENTS8.1 Coaxial Cavities

One of the main objectives in this project was to construct a high frequency broadband cavity and ensure that it was of sufficient accuracy to be used as a necessary measuring device in subsequent research application.

From among various types of resonators that may be used over a wideband microwave range, the coaxial resonator offered the most suitable electrical and mechanical properties.

A short-circuited coaxial line section forms an excellent resonator, for the following electrical reasons:

- (i) it is enclosed and therefore does not radiate energy.
- (ii) it operates in a TEM mode, which by proper selection of conductors' diameters may be adequately separated in frequency from most of the higher order parasitic resonances that may occur.
- (iii) it is suitable for many applications because of its circular, symmetrical construction.

Furthermore, obvious mechanical advantages of a coaxial resonator are its simplicity and the ease with

which circularly symmetrical parts may be produced on a machine lathe.

## 8.2 Cavity Perturbation Formulae

Initially, in chapter 3, cavity perturbation theory was reviewed together with its application to resonant cavities of different shapes, namely,  $TE_{101}$  rectangular cavity,  $TE_{011}$  cylindrical cavity and TEM coaxial cavity.

Cavity perturbation measurements can be highly sensitive and are particularly advantageous in the determination of small loss tangent ( $\tan \delta$ ). The perturbation approach makes it unnecessary to account for many of the details of the cavity, since these are the same for the cavity with and without the sample, and therefore gives rise to the effects which "cancel out".

It is well-known that the location of the sample material, its volume, geometry, and dielectric properties in the cavity working in a particular mode of operation affect both resonant frequency and the Q factor of the system. Eqns. (3.30) and (3.31) give the frequency shift and a change in a Q-value of a resonant cavity due to perturbation. The use of these formulae enables the dielectric properties of a material to be calculated by measuring the frequency shift and drop in Q when the material sample is placed in the cavity.

The possibility of using the perturbation theory for any different shapes of cavity depends on the ease of

evaluating  $E_0$  and  $E_1$  in eqn. ( 3.29).

Cavity perturbation methods are highly sensitive and quite versatile. It is this very sensitivity which needs stable frequency sources and accurate frequency detecting equipment to carry out precision measurement. The perturbation formulas were found to be valid for the system under consideration and the limitations on accuracy obtained in the experiment were imposed by the apparatus used (i.e sweep generator and spectrum analyzer). The sweep generator was very stable and the spectrum analyzer was capable of resolving 50 KHz at 8 GHz. The use of better quality equipment produced an improvement in the accuracy of the results.

The perturbation formulas have been derived for specific specimen shape and the validity of calculation will also depend if the sample is placed in a suitable place in the cavity for maximum effect. In addition, it is required that the sample volume must be small enough to produce a definite perturbation without upsetting the complete field distribution in the cavity. The frequency shift must be adequate to measure, otherwise large relative errors are introduced. The use of larger samples will also disturb the fringing fields which upsets the basic assumptions on which the derivation of the working formulas was based.

### 8.3 Assessment of the Measurements

As it has already been mentioned, measurements were carried out on a number of materials over low and high frequencies using the Bridge, Q-meter and Cavity Perturbation methods.

The known Bridge and Q-meter methods were employed initially in the investigations to provide the low frequency values for the materials as reference. The principal advantage of these two methods is that the measurements of dielectric constants and loss tangents of materials at low frequencies can be easily carried out. Throughout this range of frequencies the sensitivity and the accuracy of the techniques are affected by either stray capacitance or non-ideal characteristics of the system. To minimize the residual and external effects and to improve the accuracy of the results, strict procedures for calibration and balancing the test jig, developed over the years were followed.

In chapter 6, two methods for the measurements at high frequency are described, namely, the reflected power method and sweep generator/spectrum analyzer method. To achieve high accuracy in the first method (i.e. the reflectometer method), the two directional couplers in the set up should normally be of high directivity in the frequency range of interest. The wavemeter should be of high Q to give a good resolution. Although the wavemeter may give a very sharp peak of resonance, its accuracy is

still limited by the scale of the calibration chart. To improve this, a linear approximation was made for <sup>the</sup> small portion of the curve and <sup>an</sup> enlarged graph was produced. It was also found that a slight movement of the wavemeter caused a change in frequency and consequently made the measurement of the quality factor difficult. To improve the accuracy of the measurements further, the attenuator 3 in Fig.6.7 should be a calibrated precision component. The crystal detector  $X_1$  and  $X_2$  should be matched to the line and must be selected to give identical responses over the required frequency and power ranges.

For high accuracy in the second method (i.e. SG/SA), the system should be allowed to warm up for at least 30 minutes before <sup>the</sup> use. The sweep rate of the sweeping generator should be slower than the actual scanning rate of the analyzer to ensure a true production of the actual response of the cavity. This method beside its accuracy has other advantages. Firstly, the sweep generator frequency setting not only controls the span but also determines uniquely the centre frequency. Secondly, it is possible to generate a signal whose frequency is equal to the instantaneous frequency of the spectrum analyzer. Thirdly, the spectrum analyzer is more sensitive (-110 dBm), thereby permitting testing of components which can not stand <sup>a</sup> high voltages normally needed in the detector oscilloscope system of measurements.

The agreement on the order of magnitude for the loss

tangent values between low and high frequency measurements was reasonable. The effect of the contact in low frequency measurements was apparent. As expected, at low frequencies, there is a significant difference between readings obtained by a direct contact and using gold contact deposited on the samples. It is logical that the latter results will agree with those recorded at microwave frequencies using Cavity Perturbation Method (CPM) since no contacts are involved in the latter case. The errors for high permittivity values between direct and gold contact measurements were found to be high for most materials. This emphasises the need for gold deposition for low frequency measurements and hence smoother surfaces and lower contact resistance in the measuring setup.

Confirmation of the results already obtained with the coaxial cavity and perturbation technique is now in progress by other researchers in <sup>the</sup> H.F. Measurements and Application Research Group. A high precision coaxial slotted-line with a especially designed dielectric sample holder system is employed. Some of the results have already been confirmed.

#### 8.4 Future Work

An important investigation into dielectric properties of powders was not carried out using broadband coaxial cavity because of the lack of time. This would have

involved packing the powder in a thin-walled capillary tube and lowering it into the cavity through a small hole. Examination of the field will be necessary in order to place the sample in the right position. Care should be taken to ensure that the powder is finely ground so that tight and uniform packing could be achieved.

Investigations and relevant work have been reported in the literature and comparison were made between dielectric parameters of powder and bulk materials [52] - [57]. The theory relating the dielectric properties of the material in powder form to those of the equivalent solid is given by Looyenga [52] and Böttcher [53]. The two models were studied by Dube [54,55] at radio and microwave frequencies for a number of materials and various particle sizes, shapes and packing fractions. It was found that Looyenga's formula gives good accuracy (about 3%) of dielectric constant for particle size of less than 50 $\mu\text{m}$ . For fine powders (particle size less than 30 $\mu\text{m}$ ) the measured dielectric constant was low by about 3-8%. Dielectric loss determination from the formula was, however, less accurate; the calculated values being always lower by about 10-20%. The experimental results using Böttcher's formula showed that good accuracy was obtained for low permittivities ( $\leq 7$ ) but deviations occurred at high permittivities with low packing fractions ( $< 0.5$ ). The errors for  $\tan\delta$  were even higher between 10 to 30%. It was concluded that the formula was

satisfactory for the powders having particle sizes in the range 50-150 $\mu$ m.

Additional work has been carried out with the main project on Curie temperature measurements. The object was to develop a simple and reliable method, using <sup>2</sup>Gouy balance technique, which may in future correlate the Curie temperatures of materials with their dielectric properties. The results of the measurements for single crystal chippings of MgO containing iron in concentrations from 310 to 12900 ppm, and of MgFe<sub>2</sub>O<sub>4</sub> (99%) in form of powders using this method are presented and discussed in Appendix A.

There is a scope for extending frequency measurements by suitably adapting a circular waveguide cavity to operate from 8.5 to 12GHz. There will be a need to investigate that appropriate equations are developed to allow for the varying modes excited as a result of the frequency variations. Furthermore, an examination of the field pattern within such a cavity will be necessary to establish the correct positioning of the perturbing sample.

Overall, the perturbation method together with the coaxial cavity proved to be a reliable combination for obtaining accurate and repeatable measurements of dielectric properties of materials at microwave frequencies.

APPENDIX AA Gouy Balance Technique For CurieTemperature MeasurementIntroduction

Several techniques have been developed and devised for determining the Curie temperature of materials. Blackman [58] used the oscillation method described by Bates, Gibbs and Pantulu [59] for determining the Curie temperature of MgO in magnesium ferrite. Wirtz and Fine [60] used the technique of a vibrating sample magnetometer for determining Curie temperature of a magnesio-ferrite precipitates from dilute solutions of iron in MgO. At a later date, Inglis, Russell, and Thorp [61] published a paper on magnesio-ferrite formation in low-concentration Fe/MgO single crystal in which the Curie temperature was determined from linewidth measurements obtained using the electron spin resonance technique (E.S.R.).

The purpose of this Appendix is to present an alternative simple method for determining the Curie temperature of materials in form of powders.

The Gouy balance method (Crangle [62], Williams, Hoon and Thorp [63]) in which the magnetic force exerted on a small sample suspended between the poles of an electromagnet is measured, is widely used for the determination of magnetic susceptibilities. Here the

Gouy balance technique has been adapted and used to obtain direct estimates of the Curie temperatures of some magnesio-ferrites for comparison with the data quoted above.

#### Measurement Procedure

The high temperature modification of the Gouy balance technique is shown in Fig.1 . A furnace was located between the poles of the electromagnet with its centre on the pole axis. The sample, in powder form, was placed in a silica tube suspended in the furnace in such a way that the bottom of the powder column was at the furnace centre. This was to ensure that the sample was positioned in the region where the magnetic field gradient was maximum, as is customary in the Gouy method. The choice of furnace dimensions represents a compromise between two conflicting demands. One is that the temperature available at the centre of the furnace should be maximised although the furnace outer wall must remain cool in order to prevent damage to the pole faces; this favours increasing the furnace diameter. The other is that the magnetic field should be as high as possible, (to increase the accuracy of measurements); this points to reducing the pole gap. In the present apparatus the Newport Type A electro-magnet gives a maximum field of 470 mT over the 7.8 cm wide gap and the furnace, (which had a bore of 19mm and outside diameter of 6.3 cm) could

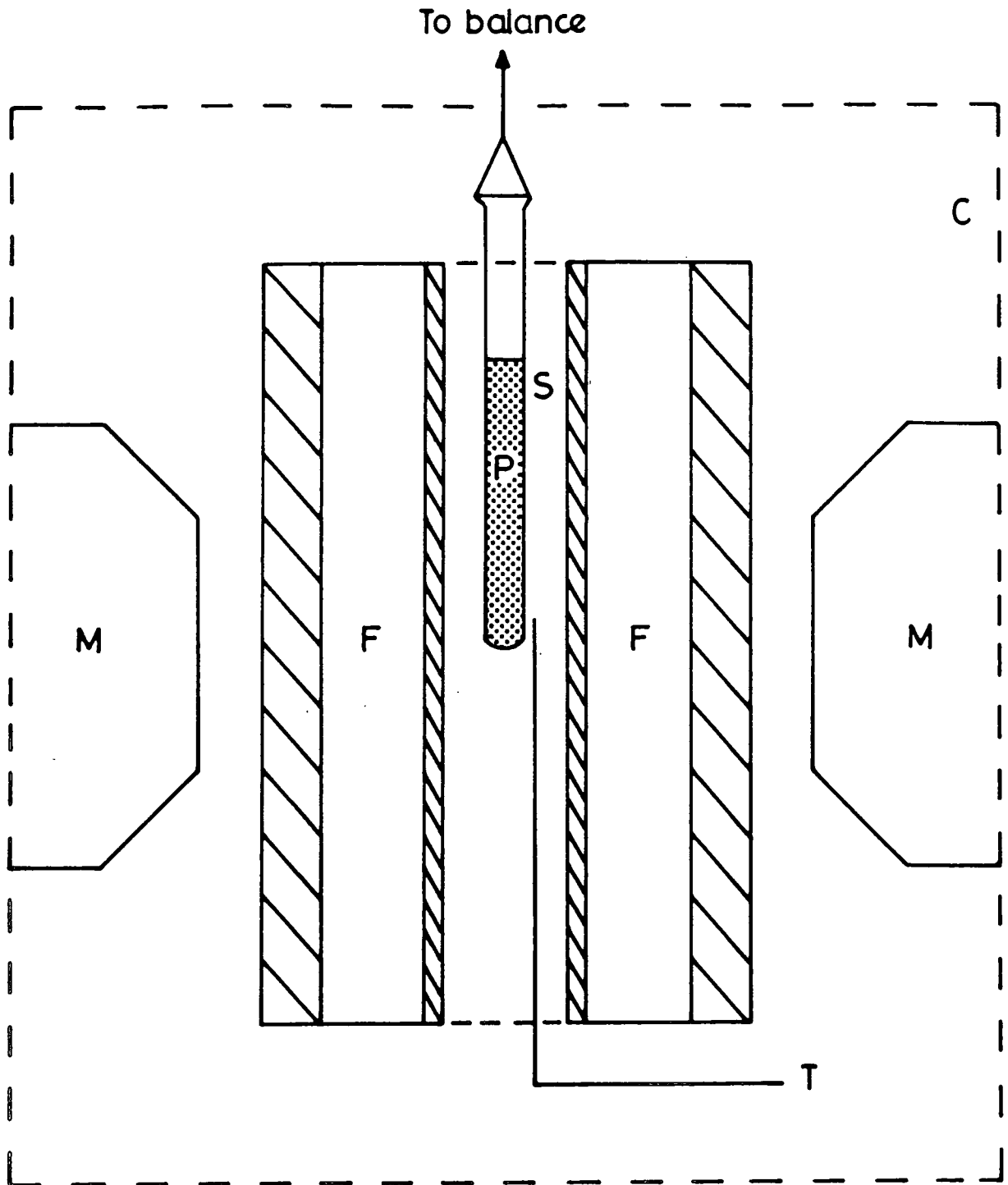


Fig 1. Schematic arrangement of modified Gouy balance.  
(M, electromagnet; F, furnace; T, thermocouple and temperature controller; S, silica specimen tube; P, specimen; C, cover.

reach 900°C.

#### Preparation of the Samples

The single crystal chippings of Fe/MgO which were used in this experiment had iron concentrations ranging from 310 to 12900 parts per million. The nominal dopant concentrations were determined (using x-ray fluorescence techniques) by W & C.Spicer Ltd. and were claimed by the manufacturers to be accurate to within 2%. These samples ranged in colour from cloudy white through progressively darker shades of green to olive green as the iron concentration increased.

Powder samples were prepared by first crushing the single crystal chippings in an agate pestle and mortar. The powders were sieved through a 185  $\mu\text{m}$  mesh in order to control the upper limit of the particle size and to form powders suitable for Gouy magnetometer. Magnesio-ferrite precipitation was induced in these powder samples by means of heat treatment in an auxiliary furnace. The samples were loaded in "Thermalox" recrystallised alumina combustion boats and placed in the centre of the furnace where the temperature profile was almost flat. A thermocouple, placed as close to the sample boat as possible, was connected to a temperature controller and this arrangement enabled the required temperature to be set and maintained. A steady flow of oxygen gas through the furnace ensured that the precipitation occurred in an

oxidizing atmosphere and a temperature of 800°C was chosen, (over a period of 3.5 hours), to ensure that all the available iron had been converted (Thorp, Johnson and Savage [64]) to magnesio-ferrite. The samples were then gradually cooled down from the chosen temperature of 800°C (at which, in most cases, they were held for 24 hours) to room temperature. Then the samples were ready for Curie temperature measurements.

#### Operating Details

When the electromagnet was switched on, the sample becomes magnetized in the field and experiences a force in regions of the field gradient. In this case, towards the centre of the field. This force (F) exerted on a volume susceptibility ( $\chi_v$ ) was derived from the relation [62]

$$F = \frac{1}{2} \chi_v \alpha (H_A^2 - H_B^2) (\rho_1 / \rho_2)$$

where  $H_A$  and  $H_B$  refer to the field values at the ends of the sample,  $\alpha$  is the cross-sectional area of the specimen and  $\rho_1$  and  $\rho_2$  represent the packing density of the powder and the density of magnesium oxide respectively. Care should be taken in packing the powder to ensure homogeneity both in packing density and concentration of the various components of the powder mixtures. The

maximum field used here was 360mT which corresponds to a current of 7 amperes. In order to avoid disturbances produced by convection currents, a water cooling system was used. For accurate measurement of temperature a wooden shield has been made to isolate the electromagnet and the furnace from the ambient draught, vibrations and air currents so as to keep the temperature steady and uniform. A digital monitor was used for accurate reading of the temperature. The length of the powder column should be such that it does not exceed the limits of the uniform region of the furnace; this was found to be 5 cm in this case.

The forces measured were small (i.e 1 - 260 mg) and therefore a high sensitivity balance was required. The order of accuracy depends also on the uniformity of packing in the silica tube, so a very finely ground powder is necessary. A thin column of sample was needed in order to eliminate all forces other than the vertical force. The silica tube was of 0.2 cm bore and 20 cm length.

By measuring the force with an electronic balance before and after the magnetic field was applied and making allowances in the calculation for the force on the silica tube, the net force due to magnetization can be determined. This procedure was followed for successively increasing temperatures until the force tends to zero, which indicates the transition to paramagnetic behaviour

occurring at or near the Curie point.

In order to confirm the validity of the Gouy balance technique the Curie temperature of nickel was measured. To prevent lateral displacement, the specimen tube was filled with a thoroughly homogenised mixture of 1% nickel powder diluted in 99% high purity magnesium oxide. The experimental results are shown in Fig.2. Taking the Curie temperature as the intersection on the temperature axis of the tangent to this curve at its point of maximum slope (Wirtz and Fine [60]), we find  $\theta_c = 360 \pm 5^\circ\text{C}$ ; this was in close agreement with the accepted value of  $358^\circ\text{C}$  (Weast, [65]) and indicated that the technique provides a simple and reasonably accurate method for Curie temperature measurement.

#### Results and Discussion

The temperature dependence of magnetisation (expressed as the forces measured on the Gouy balance) was measured for a series of heat-treated Fe/MgO crushed single crystal powders which had iron concentrations ranging from 2300 ppm to 12900 ppm. The data is shown in Fig.3. It is evident firstly that the curves for all the different compositions converge towards the same Curie point; this common Curie temperature was  $310 \pm 5^\circ\text{C}$ . Furthermore, it may be noted that the different specimens (each containing a different amount of iron) were all heat-treated in the same way so that they contained

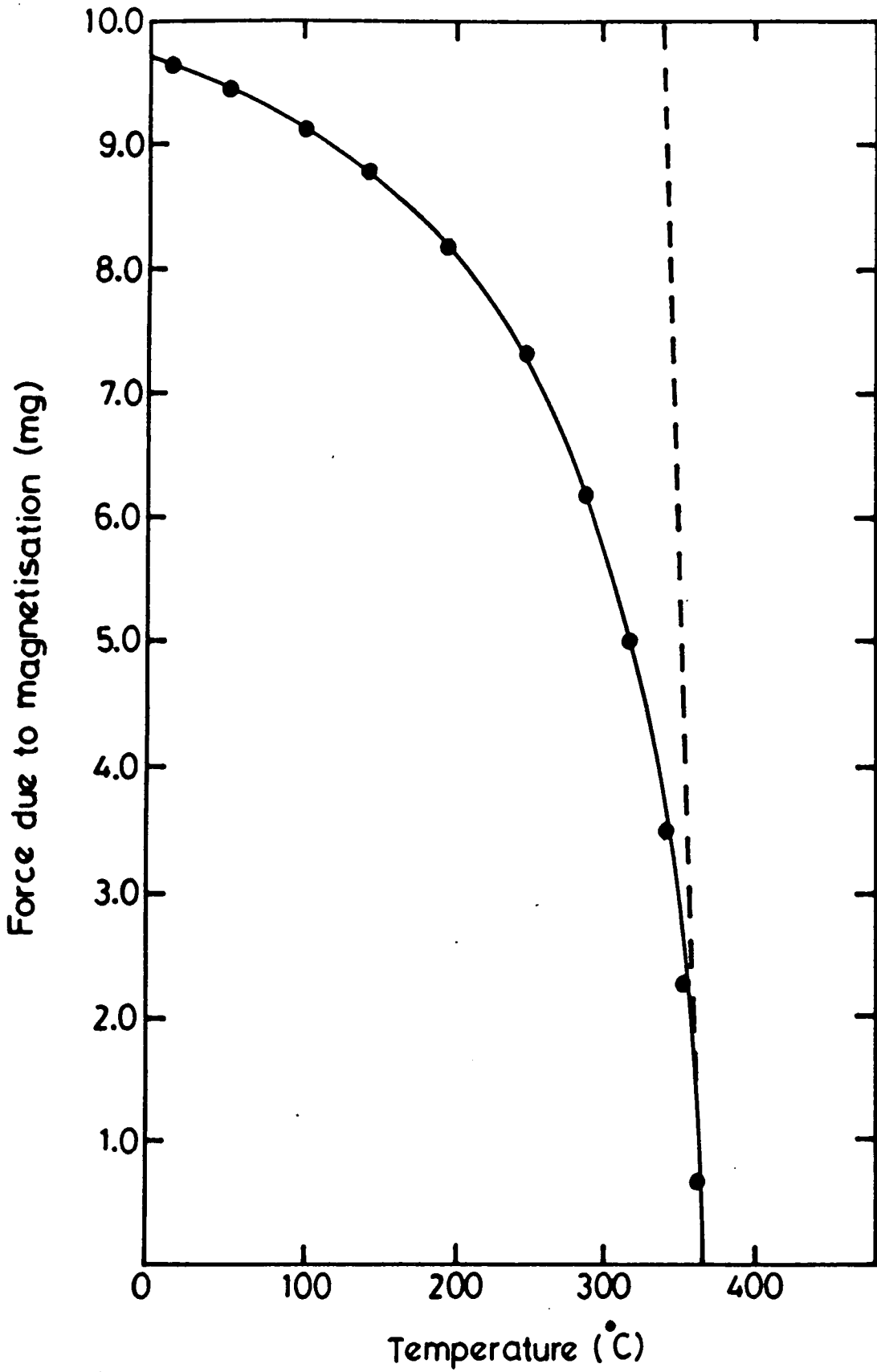


Fig 2. Force - temperature variation for nickel powder

different amounts of magnesio-ferrite precipitate, as evidenced by the susceptibility measurements reported earlier (Thorp., Johnson and Savage [64]). Thus Fig.3 also confirms Wirtz and Fine's [60] statement that the Curie temperature of the magnesio-ferrite precipitate phase is independent of the volume fraction of the precipitate. The measured Curie temperature ( $\sim 310^\circ\text{C}$ ) is very close to the value of  $307^\circ\text{C}$  reported by Blackman [58] for MgO-saturated magnesio-ferrite and this suggests a precipitate composition near  $\text{Mg}_{1.05} \text{Fe}_{1.95} \text{O}_{3.97}$ .

It is interesting to compare the present determination with the values obtained for other compositions within the magnesio-ferrite phase since it is known that  $\theta_c$  is sensitive to small changes in composition and cation distribution (Epstein and Frackiewicz [66]), especially to the number of iron ions on tetrahedral sites. Here we may note that, with a lower proportion of iron, Wirtz and Fine [60] reported  $\theta_c = 217^\circ\text{C}$  for magnesio-ferrite particles of composition  $\text{Mg}_{1.2} \text{Fe}_{1.8} \text{O}_{3.9}$ . At the other extreme of the range we have found (Fig.4) that for the composition  $\text{Mg}_{1.0} \text{Fe}_{2.0} \text{O}_{4.0}$ , (supplied as powder by Ventron GMBH Karlsruhe) the Curie temperature is  $(430 \pm 10)^\circ\text{C}$ , in close agreement with the value of  $440^\circ\text{C}$  quoted by Tebble and Craik [67]. Both the magnetic and dielectric properties of magnesio-ferrite phases are of considerable importance in the production of high quality electrical grade magnesia for refractory insulator applications

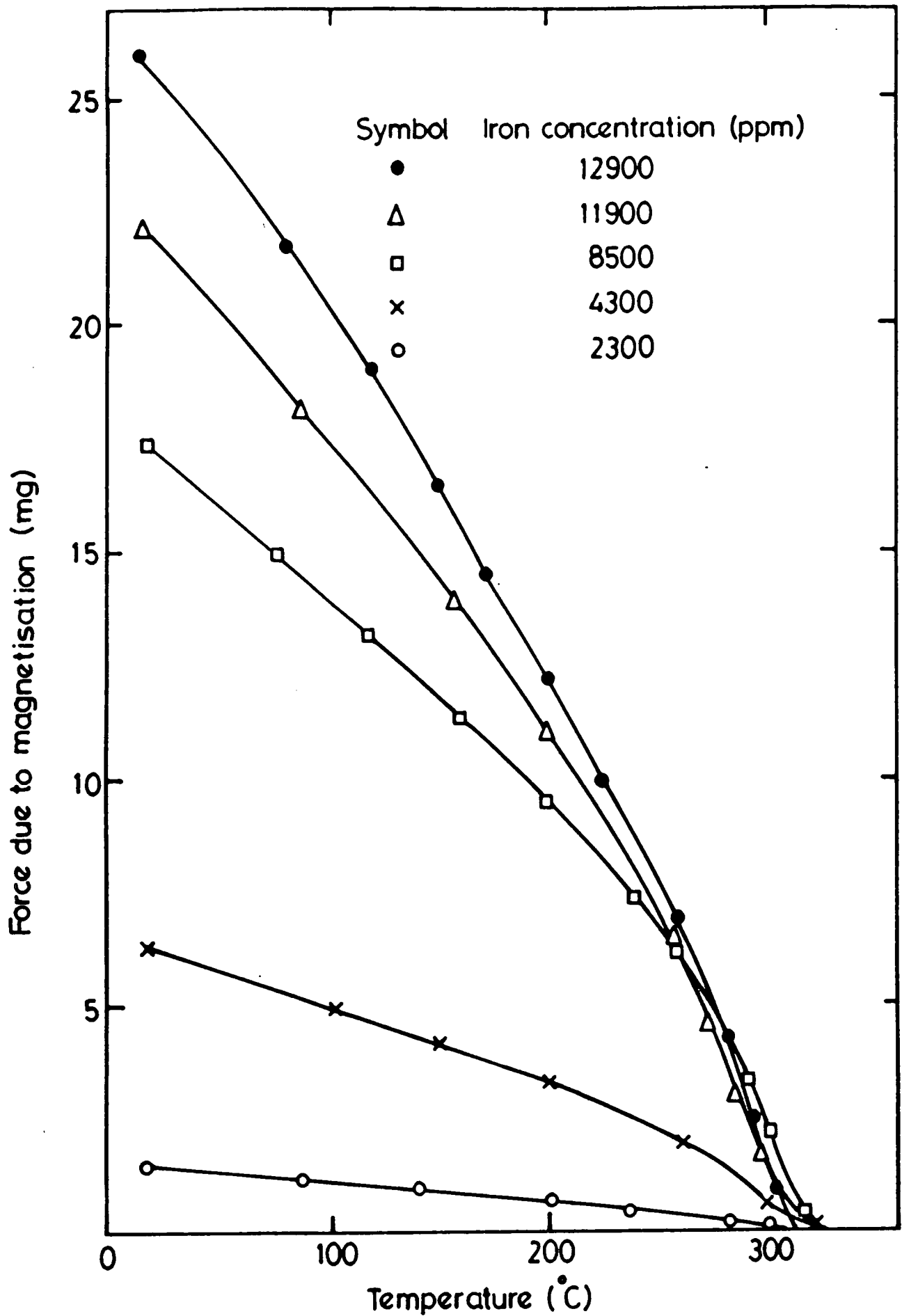


Fig 3. Force - temperature variation for Fe/MgO samples samples aged at 800°C for 3½ hours

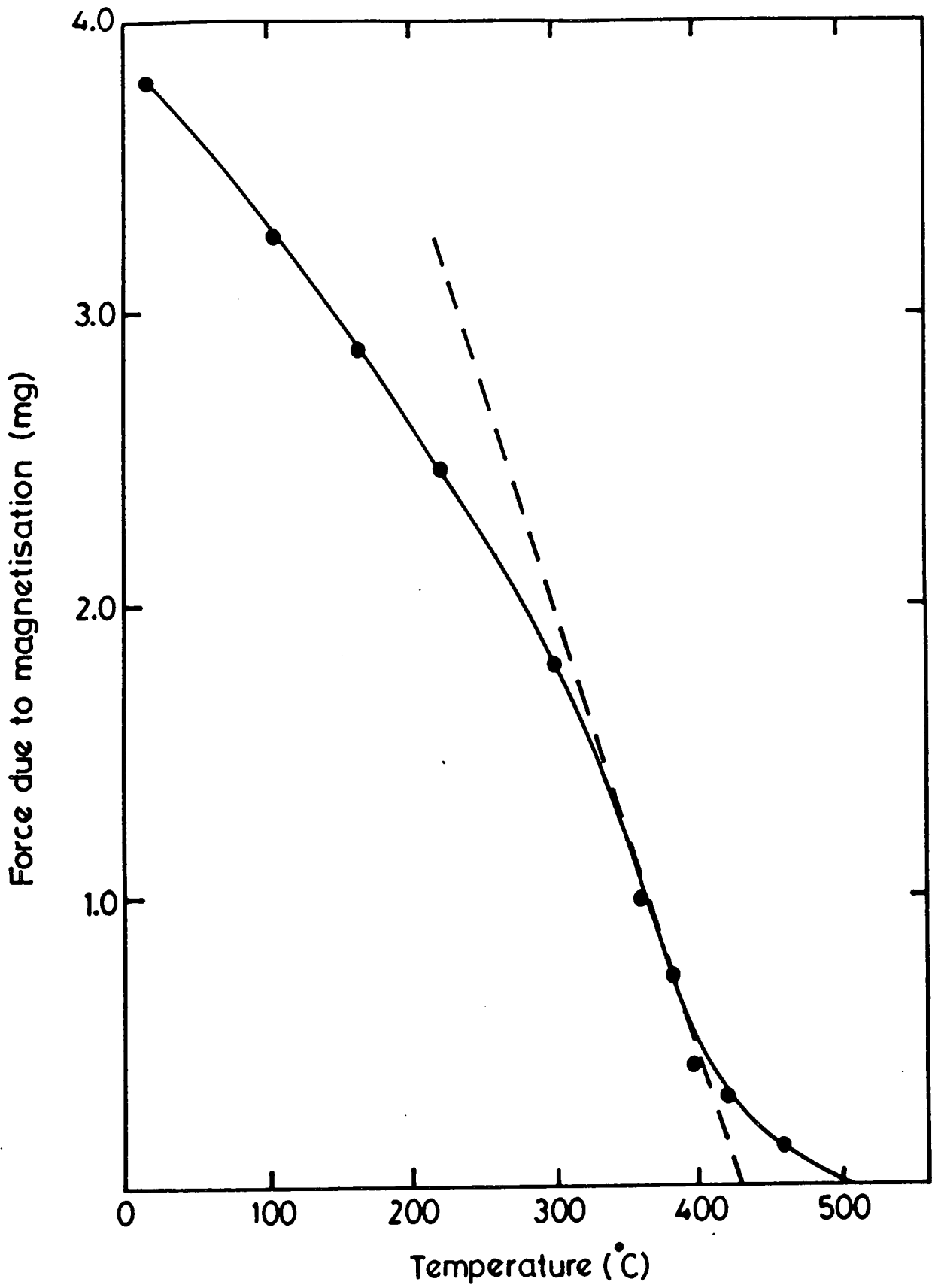


Fig 4. Force - temperature variation for magnesium di-iron oxide, ( $\text{Mg Fe}_2 \text{O}_4$ , Ventron)

(e.g. Neidhardt and Schneider [68]); work is now in progress to ascertain whether the dielectric properties of similar magnesio-ferrite phases, some of which are notable for their high loss, are subject to corresponding variations.

REFERENCES

1. ELDUMIATI, I.I. & HADAD, I.G., "Cavity Perturbation Techniques for Measurement of the Microwave Conductivity and Dielectric Constant of a Bulk Semiconductor Material", IEEE Trans. on Microwave Theory and Techniques, Vol. MTT-20, NO.2, 126, Feb. 1972.
2. KACZOWSKI, A. & MILEWSKI, A., "High-Accuracy Wide-Range Measurement Method for Determination of Complex Permittivity in Reentrant Cavity", part A and B, IEEE, Trans. on Micro. Theory and Techniques, Vol. MTT-28, No.3, 225, March 1980.
3. SUSANTA SEN, SAHA, P.K. & NAG, B.R., "New Cavity Perturbation Technique for Microwave measurement of Dielectric Constant", Rev. Sci. Instrum., Vol. 50, No. 12, 1594, December 1979.
4. ROSENBERG, C.B., HERMIZ, N.A. & COOK, R.J., "Cavity Resonator Measurements of the Complex Permittivity of Low-Loss Liquids", IEE Proc., Vol. 129, Pt.H, No.2, 71, April 1982.
5. PARKASH, A., VAID, J.K., & MANSINGH, A., "Measurement of Dielectric Parameters at Microwave Frequencies By Cavity Perturbation Technique" IEEE Trans. on Micro. Theory and Tech., Vol. MTT-27, No.9, 791, September 1979.

6. MANSINGH, A. & PARKASH, A., "Microwave Measurement of Conductivity and Permittivity of Semiconductor Sphere by Cavity Perturbation Technique", IEEE Trans. on Micro. Theory and Tech., Vol. MTT-29, No.1, 62, Jan, 1981.
7. HONG, K.H. & ROBERTS, J.A., "Microwave Properties of Liquids and Solids using a Resonant Microwave Cavity as a Probe", J. of App. Phy., Vol. 45, No. 6, 2452, June 1974.
8. LAKSHMINARAYANA, M., PARTAIN, L. & ALLAN COOK, W., "Simple Microwave Technique for Independent Measurement of Sample Size and Dielectric Constant with Results for a Gunn Oscillator System", IEEE on Micro. Theory and Tech., Vol. MTT-17, No. 7, 661, July 1979.
9. LI, S., AKYEL, C. & BOSISIO, R. "Precise Calculations and Measurements on the Complex Dielectric Constant of Lossy Materials Using  $TM_{010}$  Cavity Perturbation Techniques", IEEE Trans. on Micro. Theory and Tech., Vol. MTT-29, No. 10, 1041, October 1981.
10. VON HIPPEL, A., "Dielectric Materials and Applications" The Technology Press of MIT and Wiley, New York, Chapman and Hall, London, April 1958.
11. KULESZA, B.L.J., THORP, J.S., & BAKAR-AHMAD, A., "Coaxial Line Methods for Measuring Permittivity and Dielectric Loss", J. of Material

Science, 19, 915, 1984.

12. NELSON, S., STETSON, L., & SCHLAPHOFF, C., " A General Computer Program for Precise Calculation of Dielectric Properties From Short-Circuited-Waveguide Measurements", IEEE Trans. on Ins. and Meas., Vol. IM-23, No.4, 455, Dec. 1974.
13. GEMERT, M.J.C., "High Frequency Time Domain Methods in Dielectric Spectroscopy", Philips Res. Repts. 28, 530, 1973.
14. BUCCI, O., CORTUCCI, G., FRANCESCHETTI, G., SAVARESE, C. TIBERIE, R., " Time-Domain Techniques for Measuring the Conductivity and Permittivity Spectrum of Materials", IEEE Trans. on Ins. and Meas., Vol. IM-21, No.3, 237, Aug. 1972.
15. COLE, R., "Time-Domain Spectroscopy of Dielectric Materials", IEEE Trans. on Ins. and Meas. Vol. IM-25, No. 4, 371, December 1976.
16. RZEPECKA, M., & STUCHLY, S., "A Lumped Capacitance Method for Measurement of the Permittivity and Conductivity in the Frequency and Time-Domain - A Further Analysis", IEEE Trans. on Ins. and Meas., Vol. IM-24, No. 1, 27, March 1975.
17. NICOLSON, A.M. & ROSS, G.F., "Measurement of the Intrinsic Properties of Materials by Time-Domain Techniques", IEEE Trans. on Ins. and Meas., Vol. IM-19, No. 4, 377, November 1970.

18. SUCHER, M. & FOX, J., "Microwave Measurements", Vol. II  
John Wiley & Sons, Inc., New York, London,  
1963.
19. CHOU, C. & GUY, A., "Effects of Electromagnetic Fields  
on Isolated Nerve and Muscle Preparations",  
IEEE on Micro. Theory and Tech. Vol. MTT-26,  
No. 3, 141, March 1978.
20. BIANCO, B., DRAGO, G., MARCHESI, M., MARTINI, C., MELA, G.  
& RIDELLA, S., "Measurements of Complex Dielectric  
Constant of Human Sera and Erythro-  
cytes", IEEE Trans. on Ins. and Meas., Vol.  
IM-28, No. 4, December 1979.
21. STUCHLY, M., STUCHLY, S., "Coaxial Line Reflection  
Methods for Measuring Dielectric Properties  
of Biological Substances at Radio and Micro-  
wave Frequencies - A Review", IEEE Trans. on  
Ins. and Meas., Vol. IM-29, No. 3, 176, Sep.  
1980.
22. STUCHLY, M., ATHEY, T., SAMARAS, G., & TAYLOR, G., "Mea-  
surement of Radio Frequency Permittivity of  
Biological Tissues with an Open-Ended Coax-  
ial Line", IEEE Trans. on Micro. Theory and  
Tech., Vol. MTT-30, No. 1, 87, January 1982.
23. NELSON, S. & STETSON, L. "Possibilities for Controlling  
Insects with Microwaves and Lower Frequency  
RF Energy", IEEE Trans. on Micro. Theory and  
Tech., Vol. 22, 1303, December 1974.

24. RAD, N.E., "The Radio Frequency and Microwave Properties of Doped Magnesium Oxide", Ph.D thesis, Durham Univ., England, June 1980.
25. KULESZA, B.L.J., "Microwave Measurements and Experiments", Rank Precision Industries Ltd., Hertfordshire, England, October 1983.
26. GARDIOL, F.E., "Introduction to Microwaves", Artech House Inc., Dedham 1984.
27. GLAZIER, E.V.D. & LAMONT, H.R.L., "Transmission and Propagation", Vol.5, Wireless World, London, 1958.
28. MONTGOMERY, C.G., "Techniques of Microwave Measurements", McGraw-Hill Book Comp., London, 1947.
29. MATTHAEI, YOUNG & JONES, "Microwave Filters, Impedance Matching Networks of Coupling Structures," McGraw-Hill Book Comp., London, 1964.
30. HARVEY, A.F., "Microwave Engineering", Academic Press, London and New York, 1963.
31. BETHE, H.A. & SCHWINGER, J., "Perturbation Theory for Cavities", N.R.D.C., Cornell Univ., March 1943.
32. CASIMIR, H.B.G., "On the Theory of Electromagnetic Waves in Resonant Cavities", Philips Research Reports, 6, 162, 1951.
33. WALDRON, R.A., "Theory of the Measurement of the Elements of the Permeability Tensor of a Ferrite by means of a Resonant Cavity", IEE

Proc., No. 2225R, October 1956.

34. KORN & KORN, "Mathematical Handbook for Scientist and Engineers", McGraw-Hill Book Comp., London, 1961.
35. SANDER, K.F. & REED, G.A.L., "Transmission and Propagation of Electromagnetic Waves", Cambridge Univ. Press, London, 1978.
36. HANSEN, W.W., "On the Resonant Frequency of Closed Concentric Lines", J. of App. Phys., Vol. 10, Jan. 1939.
37. CHIPMAN, R.A. "Theory and Problems of Transmission Lines", Schaum's Outline Series, McGraw-Hill, Book Comp., 1968.
38. RAGAN, G.L., "Microwave Transmission Circuits", Dover Publications, 1965.
39. SINNEMMA, W., "Electronic Transmission Technology" Prentice-Hall, 1979.
40. BLAKE, L.V., "Transmission Lines and Waveguides", John Wiley & Sons, 1969.
41. Compiled by the Staff of the Radio Research Laboratory, Harvard Univ., "Very High Frequency Techniques", Vols. 1 & 2, McGraw-Hill Book Comp., 1947.
42. ISKANDER, M. & STUCHLY, S., "Fringing Field Effect in the Lumped Capacitance Method for Permittivity Measurement", IEEE Trans. on Ins. and Meas., Vol. IM-27, No. 1, 107, 1978.

43. CHAMBERLAIN, J. & CHANTRY, G.W. (eds.), "Introduction - The Propagation Factor", Proc. of a Tut. Conf. on Meas. of HF Dielectric Properties of Materials, NPL, Teddington, UK, March 1972.
44. HARRIS, B. & BUNSELL, A.R., "Structure and Properties of Engineering Materials", Longman, London and New York, 1977.
45. JONSCHER, A.K., "Low-Frequency Dispersion in Carrier-Dominated Dielectrics", Philos. Mag. B, Vol. 38, No. 6, 587, 1978.
46. TERMAN, F.E., "Radio Engineers' Handbook", McGraw-Hill Company Limited, London, 1950.
47. WAYNE KER UNIVERSAL BRIDGE, "Operating Instruction Handbook No. B224", England, 1975.
48. SCOTT, A.H., & CURTIS, H.L., "Edge Correction in the Determination of Dielectric Constant", J. of Res. of the N.B.S., Vol. 22, 747, 1939.
49. GOUGH, E.R., & ISARD, J.O., "Errors due to Electrode Effects in Dielectric Measurements on Glass", IEE Proc., Vol. 116, 471, 1969.
50. MARCONI INS. LTD, "Instruction Handbook for Type TF1245", England, 1961.
51. TEKTRONIX, "Instruction Manual of 7L18 Spectrum Analyzer" USA, 1977.
52. LOOYENGA, H., "Dielectric Constant of Heterogeneous Mixtures", Physica 31, 401, 1965.

53. BOTTCHER, C.J.F., "Theory of Electric Polarization" p.419, Elsevier, Amsterdam 1952.
54. DUBE, D.C., "Study of Landau-lifshitz-Looyenga's Formula for Dielectric Correlation between Powder and Bulk", J. of App. Phys. Vol. 3., 1648, 1970.
55. DUBE, D.C., & PARSHAD, R., "Study of Bottcher's Formula Correlation between Powder and Bulk", J. of App. Phys. Vol. 3, 677, 1970.
56. ARUNA, R., & BEHARI, J., "Dielectric Loss in Biogenic Steroids at Microwave Frequencies", IEEE Trans. on Micro. Theory and Tech., Vol. MTT-29, No. 11, 1209, November 1981.
57. THORP, J.S. & RAD, N.E., "The RF Permittivity and Dielectric Loss of Calcium, Iron and Magnesium Silicides" J. of Mat. Sc. lett. 157, 1986.
58. BLACKMAN, L.C.F, Trans. Faraday Soc. 55, 391, 1959.
59. BATES, L.F, GIBBS, R.E. & PANTALU, D.V.R., Proc. of Phys. Soc. 48, 665, 1936.
60. WIRTZ, G.P., & FINE, M.E., J. App. Physics , 38, 3729, 1967.
61. INGLIS, A.D., RUSSELL, G.J., & THORP, J.S., "Magnesio-Ferrite Formation in Low-Concentration Fe/MgO Single Crystal", J. Mater. Sci. 16, 1887, 1981.
62. CRANGLE, J., "The magnetic Properties of Solids",

- Edward Arnold, London, 1977.
63. WILLIAMS, C.D.H., HOON, S.R., & THORP J.S., Jour. Mat. Sci. Lett. 5, 221, 1985.
  64. THORP, J.S., JOHNSON, A.P., & SAVAGE, C., "Magnesio-Ferrite Formation in Heat-Treatment Fe/MgO Powders", J.Mater., Sci.Lett. 4, 221, 1985.
  65. WEAST, R.C., "Handbook of Chemistry and Physics", CRC Press 57th edition, E120, 1976 - 1977.
  66. EPSTEIN, D.J., & FRACKIEWICZ, B., J. Appl. Phys. 28, 329, 1958.
  67. TEBBLE, R.S., & CRAIK, D.J., "Magnetic Materials", John Wiley and Sons Ltd., London, 1969.
  68. NEIDHARDT, M. & SCHNEIDER, J. United States Patent, 3621204, 1971.
  69. OXFORD, D.F., "Series-Tuned Cavity Frequency Multiplier", Ph.D thesis, Durham Univ., U.K., December 1983.
  70. EMMETT, J.R., "Microwave Lattice Mixers at 4.5 GHz", Ph.D thesis, Durham Univ., U.K., 1974.
  71. LAVERGHETTA, T.A., "Microwave Materials and Fabrication Techniques" Artech House Inc., USA, 1984.
  72. KALPAKJIAN, S., "Manufacturing Processes for Engineering Materials", Addison-Wesley Publishing Co. Inc. 1984.
  73. COELHO, R. "Physics of Dielectrics", Elseier Sc. Pub. Comp., Amsterdam-Oxford-New York, 1979.

74. MORRELL, R. "Handbook of Properties of Technical and Engineering Ceramics", NPL, London, 1985.
75. VON HIPPEL, R., "Dielectrics and Waves", John Wiley and Sons, London, 1954.
76. AMMAR, E.A.E., Ph.D thesis, Durham Univ., U.K, 1976.
77. EVANGELINOS, E., "Dielectric Filled 1 to 18 GHz Coaxial Slotted Line", M.Sc thesis, Durham Univ. U.K., 1986.

